

**DEVELOPMENT OF PARAQUAT DETECTION
SYSTEM BASED ON GOLD NANOPARTICLES AND
DNA APTAMERS**



Pakawat Kongpreecha

**A Thesis Submitted in Partial Fulfillment of the Requirements for the
Degree of Master of Science in Environmental Biology
Suranaree University of Technology**

Academic Year 2020

การพัฒนาระบบตรวจวัดพาราควอทโดยอาศัยอนุภาคนาโนทอง
และดีเอ็นเอแอปทาเมอร์



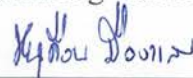
นายภควัต คงปรีชา

วิทยานิพนธ์นี้เป็นส่วนหนึ่งของการศึกษาตามหลักสูตรปริญญาวิทยาศาสตรมหาบัณฑิต
สาขาวิชาชีววิทยาลิ่งแวดล้อม
มหาวิทยาลัยเทคโนโลยีสุรนารี
ปีการศึกษา 2563

**DEVELOPMENT OF PARAQUAT DETECTION SYSTEM
BASED ON GOLD NANOPARTICLES AND DNA APTAMERS**

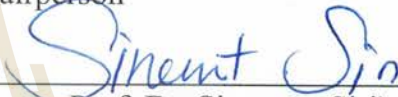
Suranaree University of Technology has approved this thesis submitted in partial fulfillment of the requirements for a Master's Degree.

Thesis Examining Committee



(Assoc. Prof. Dr. Nooduan Muangsan)

Chairperson



(Assoc. Prof. Dr. Sineenat Siri)

Member (Thesis Advisor)



(Assoc. Prof. Dr. Sanchai Prayoonpokarach)

Member



(Asst. Prof. Dr. Kiattisak Batsungnoen)

Member



(Assoc. Prof. Flt. Lt. Dr. Kontorn Chamniprasart)

Vice Rector for Academic Affairs

and Internationalization



(Assoc. Prof. Dr. Worawat Meevasana)

Dean of Institute of Science

ภควัด คงปรีชา : การพัฒนาระบบตรวจวัดพาราควอทโดยอาศัยอนุภาคนาโนทองและดีเอ็นเอแอปตามอร์ (DEVELOPMENT OF PARAQUAT DETECTION SYSTEM BASED ON GOLD NANOPARTICLES AND DNA APTAMERS) อาจารย์ที่ปรึกษา : รองศาสตราจารย์ ดร.สินีนานู ศิริ, 112 หน้า.

พาราควอทเป็นสารเคมีกำจัดวัชพืชชนิดหนึ่งที่ใช้กันอย่างแพร่หลายในหลายประเทศเพื่อควบคุมวัชพืชในทางการเกษตร เนื่องจากพาราควอททำให้เกิดพิษร้ายแรงถึงขั้นเสียชีวิตได้ จึงเกิดความกังวลถึงความเสี่ยงต่อสุขภาพของมนุษย์จากการปนเปื้อนของพาราควอทในอาหารและสิ่งแวดล้อม ดังนั้นวิธีการตรวจวัดพาราควอทที่ง่าย รวดเร็ว และมีความไวจึงเป็นที่ต้องการ งานวิจัยนี้จึงสนใจที่จะพัฒนาระบบตรวจวัดพาราควอทแบบสีถึงสองระบบ ระบบแรกคือระบบที่ใช้อนุภาคนาโนทองหุ้มด้วยซิเตรตและอีกระบบหนึ่งเป็นการใช้แอปตามอร์ร่วมกับอนุภาคนาโนทอง หรือเรียกว่าแอปตาเซนเซอร์ การสังเคราะห์อนุภาคนาโนทองใช้วิธีซิเตรตรีดักชัน ซึ่งได้อนุภาคนาโนรูปร่างกลมและมีขนาดเส้นผ่านศูนย์กลางเฉลี่ยประมาณ 13 นาโนเมตร โดยยืนยันเอกลักษณ์ของอนุภาคนาโนทองจากการวิเคราะห์ฟิสิกส์เซอร์เฟสพลาสมอนรีโซแนนซ์และโครงสร้างผลึกจากค่าเลี้ยวเบนของอิเล็กตรอน โดยหลักการ ทั้งสองระบบจะมีสีแดง และเปลี่ยนเป็นสีน้ำเงินในสภาวะที่มีพาราควอท ในระบบแรกซึ่งคือระบบที่ใช้อนุภาคนาโนทองหุ้มด้วยซิเตรต อาศัยการที่พาราควอทชักนำให้เกิดการเกาะกลุ่มของอนุภาคนาโนทองในสภาวะที่มีไซเดียมคลอไรด์และพาราควอท ซึ่งพบมีค่าขีดจำกัดของการตรวจวัดพาราควอทที่ 1.59 ไมโครโมลาร์ ในระบบที่สอง เป็นแอปตาเซนเซอร์ซึ่งพัฒนาขึ้นเพื่อเพิ่มความไวและความจำเพาะในการตรวจวัดพาราควอท ในระบบนี้อาศัยแอปตามอร์ชนิดใหม่ร่วมกับอนุภาคนาโนทอง โดยแอปตามอร์นี้มีการออกแบบโครงสร้างใหม่โดยอาศัยการเพิ่มจำนวนซ้ำของดีเอ็นเอเป้าหมาย ในบรรดาแอปตาเซนเซอร์ที่พัฒนาขึ้น แอปตาเซนเซอร์ชนิด P3-L3 เป็นระบบที่ดีที่สุด เนื่องจากตรวจวัดพาราควอทได้ในช่วง 0.5-10 นาโนโมลาร์ และมีค่าขีดจำกัดของการตรวจวัดพาราควอทที่ 0.11 นาโนโมลาร์ ระบบแอปตาเซนเซอร์นี้มีความจำเพาะต่อการตรวจวัดพาราควอท นอกจากนี้ยังมีค่าร้อยละการคืนกลับของพาราควอทในตัวอย่างน้ำประปาและน้ำบ่อผสมพาราควอทในร้อยละ 97.0-108.5 และมีค่าเบี่ยงเบนมาตรฐาน

Association of Official Agricultural Chemists (AOAC) ผลการวิจัยนี้ได้แสดงถึงความสำเร็จในการสร้างระบบตรวจวัดพาราควอดที่มีค่าความแม่นยำและความน่าเชื่อถือ ดังนั้นระบบดังกล่าวจึงมีศักยภาพในการประยุกต์เพื่อใช้เป็นระบบตรวจวัดพาราควอดเชิงพื้นที่แบบง่าย รวดเร็ว และมีความไวสูง



สาขาวิชาชีววิทยา

ปีการศึกษา 2563

ลายมือชื่อนักศึกษา

ภาคิน อภิชาติ

ลายมือชื่ออาจารย์ที่ปรึกษา

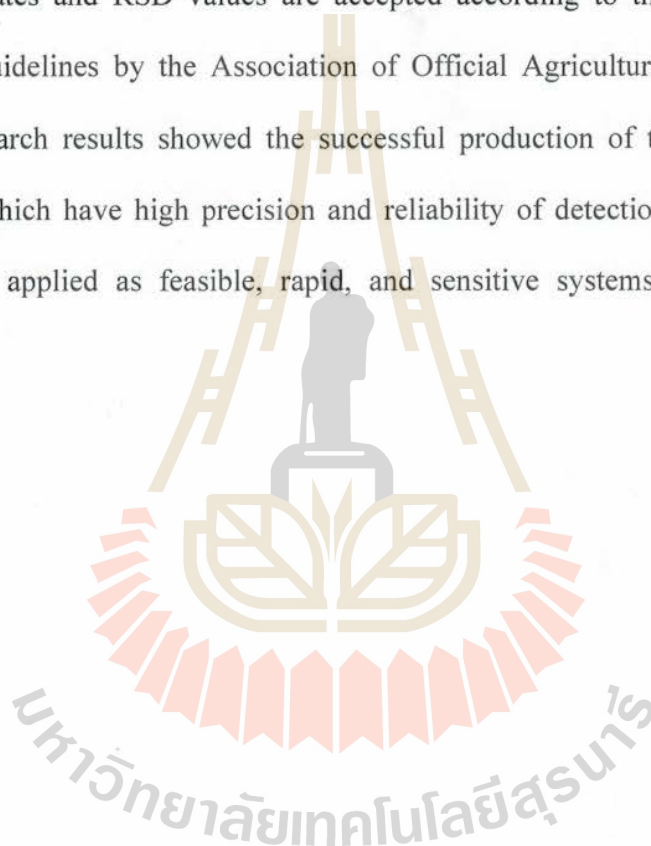
อ.อ.อ.

PAKAWAT KONGPREECHA : DEVELOPMENT OF PARAQUAT
DETECTION SYSTEM BASED ON GOLD NANOPARTICLES AND DNA
APTAMER. THESIS ADVISOR : ASSOC. PROF. SINEENAT SIRI, Ph.D.
112 PP.

APTAMER/APTASENSOR/DETECTION/GOLD NANOPARTICLES/PARAQUAT

Paraquat is one of the widely used herbicides for controlling weeds in agriculture in many countries. As paraquat ingestion can lead to fatal poisoning, the contamination of paraquat residues in food and the environment has increasingly concerned with the human health risk. Therefore, a simple, rapid, and sensitive method for paraquat detection is still needed. This research aimed to develop two optical sensing systems for paraquat detection. One system is the citrate-capped AuNP system and another is an aptamer-AuNP system referred to as aptasensor. AuNPs were synthesized by a citrate reduction method and the obtained AuNPs were spherical with an average diameter of approximately 13 nm. The identity of AuNPs was confirmed by the characteristic surface plasmon resonance peak and crystalline structure based on selected area electron diffraction analysis. In principles of both systems, the systems appear in red and turn into a blue color by paraquat induction. In the first system, a citrate-capped AuNP system was based on the paraquat-induced aggregation of AuNPs under a NaCl condition that its limit of detection (LOD) for paraquat was 1.59 μM . The second system, the aptasensor, was developed to improve the sensitivity and specificity of paraquat detection. This system was based on new aptamers and AuNPs. The new

Among several developed aptasensors, the P3-L3 aptasensor was the best system, which could detect paraquat in ranges of 0.5-10 nM with a limit of detection as low as 0.11 nM. This aptamer was selective to paraquat detection. It also showed high recovery rates of paraquat detection in the paraquat-spiked tap water and pond water in a range of 97.0-108.5% and the relative standard deviation values of less than 5.0%. These recovery rates and RSD values are accepted according to the official methods of analysis guidelines by the Association of Official Agricultural Chemists (AOAC). These research results showed the successful production of the paraquat detection systems, which have high precision and reliability of detection. Therefore, they are potentially applied as feasible, rapid, and sensitive systems for on-site paraquat detection.



School of Biology

Academic Year 2020

Student's Signature

Parikant Kongsuech

Advisor's Signature

Sirint Sirin

ACKNOWLEDGEMENTS

My master thesis would not have been completed without the great help and support from these kind people. First of all, I would like to express my special thanks of gratitude to my advisor Assoc. Prof. Dr. Sineenat Siri for being my great mentor for 6 years since the undergraduate year. She gave me the golden opportunity and challenged me to do a new project that no one in the lab had ever done before. I am concerned and fear to initiate this project. However, her support, suggestion, and enormous knowledge helped me in doing a lot of research and I came to know about so many new things I am really thankful to her. I have not only acquired research skills, but also life skills from her. She gave me a wonderful chance to attend overseas conferences. Moreover, she also supports me when I come across discouragement or frustration.

Besides my advisor, my appreciation is also expressed to all teachers, who sharpen my scientific knowledge and staff who help me with the paperwork and instruments. I thank all SIRI lab members for their advice, support, encouragement, and for all the fun we have had in the past six years.

I also would like to thank the Development and Promotion of Science and Technology Talent Project (DPST) for financial support since my bachelor's degree.

Finally, I would like to express my sincere gratitude and appreciation to my family: my parents for supporting my life in general. Thank you for believing in me and understand the path that I chose.

Pakawat Kongpreecha

CONTENTS

	Page
ABSTRACT IN THAI	I
ABSTRACT IN ENGLISH	III
ACKNOWLEDGEMENT	V
CONTENTS	VI
LIST OF TABLES	X
LIST OF FIGURES	XI
CHAPTER	
I INTRODUCTION	1
1.1 Background	1
1.2 Significance of the study	3
1.3 Research objectives	3
1.4 Scope of the study	4
II LITERATURE REVIEWS	5
2.1 Pesticides	5
2.1.1 Insecticides	5
2.1.2 Fungicides	10
2.1.3 Rodenticides	12
2.1.4 Nematicides	14

CONTENTS (Continued)

	Page
2.1.5 Herbicides	15
2.2 Pesticide detection methods	20
2.2.1 Chromatography	21
2.2.2 Enzyme-linked immunosorbent assay	22
2.2.3 Capillary electrophoresis	22
2.2.4 Molecular imprinted polymers	22
2.2.5 Biosensors	23
2.3 Gold nanoparticles	26
2.4 Aptamers	27
2.5 Review of related studies	29
III MATERIAL AND METHODS	32
3.1 Preparation and characterization of citrate-capped AuNPs	32
3.2 Production of DNA-aptamer selective for paraquat	33
3.3 Production of paraquat detection systems	35
3.3.1 Citrate-capped AuNP system	35
3.3.2 Aptamer-AuNP system	35
3.4 Sensitivity of detection	36
3.4.1 Sensitivity of detection of citrate-capped AuNP system	36
3.4.2 Sensitivity of detection of aptamer-AuNP system	37
3.5 Selectivity of detection	37

CONTENTS (Continued)

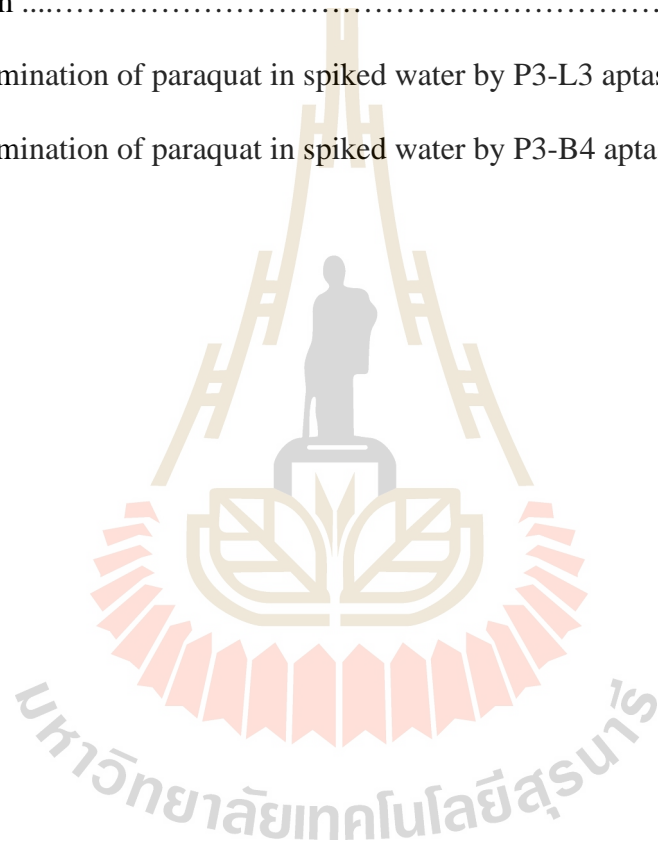
	Page
3.5.1 Selectivity of detection of citrate-capped AuNP system	37
3.5.2 Selectivity of detection of aptamer-AuNP system	38
3.6 Interference of natural water on the detection	39
3.6.1 Evaluation of spiked paraquat in tap and pond water by the citrate-capped AuNP system	39
3.6.2 Evaluation of spiked paraquat in kale sample by the citrate- capped AuNP system	39
3.6.3 Evaluation of spiked paraquat in tap and pond water by the aptamer- AuNP system	40
3.7 Statistical analysis	40
IV RESULTS AND DISCUSSION PART I	42
4.1 Synthesis and characterization of citrate-capped AuNPs	42
4.2 Optimal condition for paraquat detection by citrate-capped AuNPs	45
4.3 Sensitivity of the citrate-capped AuNP system	46
4.3.1 The citrate-capped AuNP system without NaCl	46
4.3.2 The citrate-capped AuNP system with NaCl	48
4.4 Selectivity of the citrate-capped AuNP system	50
4.5 Interference of natural water on the detection by the citrate-capped AuNP system	51

CONTENTS (Continued)

	Page
4.6 Interference of vegetable samples on the detection by the citrate-capped AuNP system	52
V RESULTS AND DISSCUSSION PART II	54
5.1 Production of DNA-aptamer selective for paraquat	54
5.2 Optimized conditions for the aptamer-AuNP system	62
5.3 Sensitivity of the aptamer-AuNP system	65
5.3.1 Sensitivity of the aptasensors based on linear aptamers	65
5.3.2 Sensitivity of the aptasensors based on linear aptamers	68
5.4 Selectivity of the aptamer-AuNP system	71
5.5 Detection of paraquat dissolved in pond and tap water by the developed aptasensors	74
VI CONCLUSION	76
REFERENCES	78
APPENDICES	95
APPENDIX A	96
APPENDIX B	98
CURRICULUM VITAE	112

LIST OF TABLES

Table	Page
4.1	Detection of paraquat-spike water using the citrate-capped AuNP system ...52
4.2	Detection of paraquat-spike vegetable using the citrate-capped AuNP system53
5.1	Determination of paraquat in spiked water by P3-L3 aptasensor75
5.2	Determination of paraquat in spiked water by P3-B4 aptasensor75



LIST OF FIGURES

Figure	Page
2.1	Classification of insecticides6
2.2	Chemical structures of common OC pesticides7
2.3	Chemical structures of commonly used OPs8
2.4	Chemical structures of main carbamate compounds9
2.5	Structures of synthetic pyrethroids10
2.6	Examples of herbicides belonging to different chemical families16
2.7	Detection system for pesticide determination modified from20
2.8	Basic layout of elements of biosensor for its construction24
2.9	Colorimetric AuNPs-based sensor for the detection of food nuisances, including heavy metals, veterinary drug residues, pesticide drug residues, toxin, and hazardous substances27
2.10	The mechanism of the colorimetric detection of acetamiprid utilizing the acetamiprid binding aptamer (ABA) and unmodified AuNPs as well as its selective performance29
3.1	The secondary structure of paraquat aptamer containing 3 small structural loops (L1, L2, and L3)33
3.2	The designed aptamers in this work34
3.3	The structures of the tested herbicides38
4.1	UV-Vis spectra of the formation of AuNPs in a time course of 15 min43

LIST OF FIGURES (Continued)

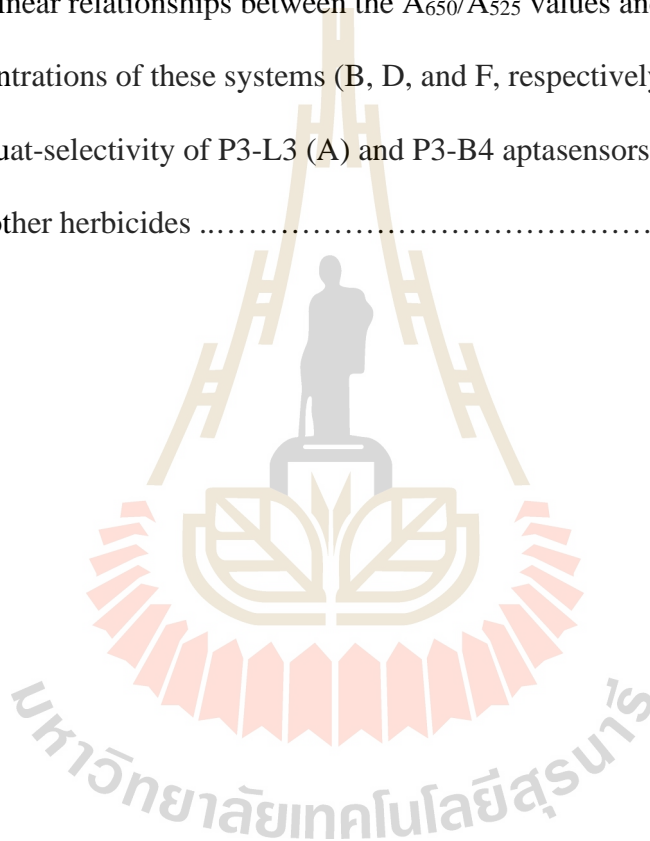
Figure	Page
4.2 TEM image (A) and SAED pattern (B) of the citrate-capped AuNPs	44
4.3 Optimal concentration of NaCl for the paraquat detection system	45
4.4 UV-Vis spectra of the citrate-capped AuNPs without NaCl in the presence of different concentrations of paraquat (A) and the linear relationship between the A_{690}/A_{525} values and paraquat concentrations (B)	47
4.5 UV-Vis spectra of the citrate-capped AuNPs with NaCl in the presence of different concentrations of paraquat (A) and the linear relationship between the A_{690}/A_{525} values and paraquat concentrations (B)	49
4.6 The selectivity of the citrate-capped AuNP system for paraquat detection	51
5.1 The predicted secondary structures of the paraquat-aptamer (A), the modified P2 aptamer (B), and the modified P3 aptamer (C)	55
5.2 The molecular dynamic simulation of P2 aptamer binding to paraquat presenting the average distance (A), the number of hydrogen bond (B), and the interaction states between paraquat and P2 aptamer (C)	57
5.3 The molecular dynamic simulation of P3 aptamer binding to paraquat presenting the average distance (A), the number of hydrogen bond (B), and the interaction states between paraquat and P3 aptamer (C)	58

LIST OF FIGURES (Continued)

Figure	Page
5.4 The designed DNA-aptamers with the linear structure with 2-5 repeated sequence (P3-L2, P3-L3, P3-L4, and P3-L5) (A) and the branched structure with 205 repeated sequence (P3-B2, P3-B3, P3-B4, and P3-B5) (B) according to the predicted secondary structures by the Mfold software	59
5.5 The efficiency of the linear form (A) and branched form (B) DNA aptamers evaluated by SYBR Green I competitive assay	61
5.6 Effect of NaCl to induce the aggregation of AuNPs	62
5.7 Effect of different concentrations of aptamers with linear structure (P3-L3, P3-L4, and P3-L5) (A) and branched structure (P3-B3, P3-B4, and P3-B5) (B) to prevent the NaCl-induced aggregation of AuNPs	64
5.8 UV-Vis-spectra of the developed aptasensor in the conditions with and without paraquat	65
5.9 UV-Vis spectra of aptasensors based on linear aptamers (P3-L3 (A), P3-L4 (C), and P3-L5 (E)) and their linear relationship plots between A_{650}/A_{525} and paraquat concentration (P3-L3 (B), P3-L4 (D), and P3-L5 (F))	67

LIST OF FIGURES (Continued)

Figure	Page
5.10 UV-Vis spectra in the presence of different paraquat concentrations of the P3-B3 (A), P3-B4 (C), and P3-B5 (E) aptamer-AuNP systems and their linear relationships between the A_{650}/A_{525} values and paraquat concentrations of these systems (B, D, and F, respectively)	70
5.11 Paraquat-selectivity of P3-L3 (A) and P3-B4 aptasensors as compared with other herbicides	73



CHAPTER I

INTRODUCTION

1.1 Background

The chemical contamination in the environment is one of the global concerning issues, especially the pesticide contamination due to the effects on organisms in the ecosystem and human health. Pesticides have been widely used in agriculture to protect crops from pests and increase the quality and quantity of agricultural products (Liu et al., 2019). Among all pesticides, paraquat is one of the most commonly used pesticides in agricultural fields in the world. Although paraquat is well-known very toxic, the agriculturists still used especially in the developing countries due to low cost and effectiveness to control weeds and grass (Sukumar et al., 2019). With the high water solubility, paraquat is readily leached into the environments, especially aquatic environments such as surface water, groundwater, and drinking water with the long half-life (Konthonbut et al., 2018). The paraquat residues can cause acute poisoning and long-term health effects depending on the intake levels. At high levels of paraquat, acute poisoning causes pulmonary fibrosis, which is usually death (Laghrib et al., 2020). With the low levels, the paraquat was adsorbed through human organs, especially liver and kidney and thus result in liver and kidney failure (Awadalla, 2012). Moreover, the exposure of paraquat harms to the neuron that induced risk of Parkinson's disease (Baltazar et al., 2014). Therefore, several analytical methods were developed to detect the paraquat residues such as gas chromatography

(Posecion et al., 2008), thin-layer chromatography (Spangenberg, 2012), liquid chromatography (Bauer et al., 2018), spectrophotometry (Siangproh et al., 2017), and electrochemistry (Tcheumi et al., 2019). Although these techniques are sensitive for detection, they require complicated process, laboratory instrument, time-consuming, high cost, experienced technician, and labor-intensive mean. Therefore, a simple, sensitive, and portable method for detecting these environmental chemicals is in need. A biosensor-based method is one of the suitable approaches to fulfill the mentioned requirements since it offers fast, straight, instant, effective, and labor-free entity (Ding et al., 2015). Biosensors are analytical devices that can convert a biological response into a signal (Mehrotra, 2016). Due to the unique optical property, gold nanoparticles (AuNPs) are commonly used as the optical biosensing system as their changed colors under the free and aggregated forms. The principle of biosensor based on AuNPs involves the electrostatic interaction between the tested chemicals and AuNPs, leading to the aggregation of AuNPs which their colors change from red to blue. This electrostatic interaction greatly depends on the surface charge of AuNPs, which attributes from the charge of the capping agent. In addition, to enhance the selectivity of the detection, the surface modification of AuNPs and the addition of specific molecules are incorporated in the biosensing system. DNA-aptamer is recently received high research attention since it can function as a biorecognition element for detection of various analysts including bacteria (Golichenari et al., 2018), biomolecules (Eivazzadeh-Keihan et al., 2017), chemicals (Nosrati et al., 2018), and cancer biomarkers (Hasanzadeh et al., 2018). DNA-aptamer is the single-stranded nucleic acid with a unique secondary structure that can specifically bind to its target (Guo and Zhao, 2016). With the high affinity and high selectivity of DNA-aptamer, thus this work is

interesting to use DNA-aptamer couple with AuNPs for developing the simple, sensitive, specific and portable system for paraquat detection.

1.2 Significance of the study

The contaminated paraquat in the environment has received increasing concerns on its potential risk on human health and the effects on organisms in the ecosystem. Although several laboratory methods are commonly used for its evaluation, these methods are not suitable for agriculturists and household users since these techniques require an advanced instrument, trained-operating technician, high analysis cost, and unpractical on-site detection. The simple, sensitive, specific, and portable system for a paraquat detection system, therefore, is still needed for the development, which is the interest of this research work. In this work, the optical sensing systems for paraquat detection will be developed. One system is based on the use of the negatively charged AuNPs for optical sensing of paraquat. The other one is based on the DNA-aptamer couple AuNPs, in which the addition of DNA-aptamer is hypothesized to enhance the sensitivity and selectivity of the detection system for paraquat.

1.3 Research objectives

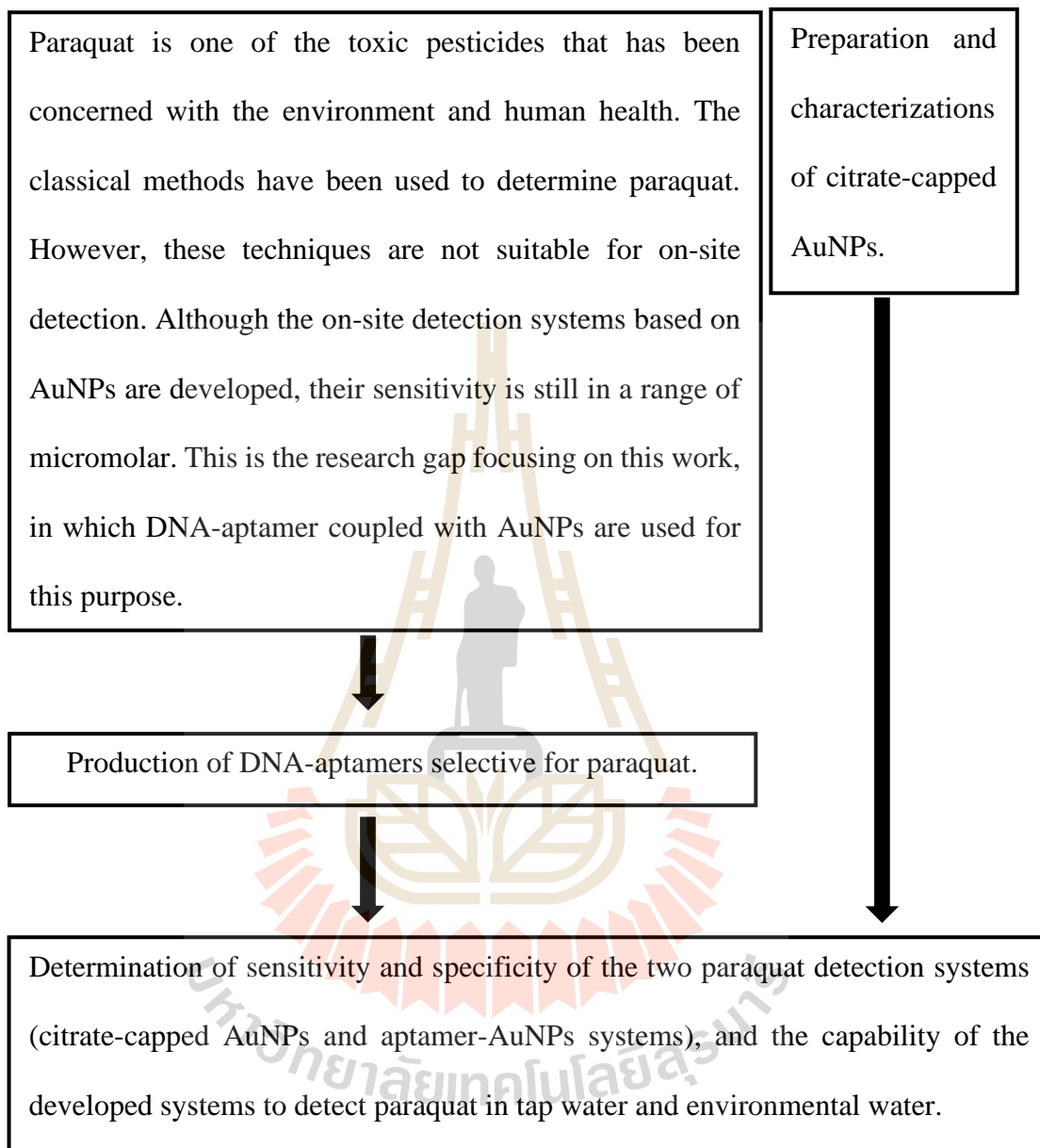
The objectives of this study are as below:

1.3.1 To synthesize and characterize citrate-capped AuNPs.

1.3.2 To design the DNA-aptamer that highly selective for paraquat

1.3.3 To develop the paraquat detection systems; citrate-capped AuNPs and aptamer-AuNPs.

1.4 Scope of the study



CHAPTER II

LITERATURE REVIEWS

2.1 Pesticides

As the world population grows so does the increasing demands for food. Crop protections become an important factor for ensuring the sufficient crop production. Pesticide is one of the regularly used chemicals in agriculture to improve the quantity of crop yields. Pesticides are natural or synthetic substances used for controlling pests such as insects, weeds, fungi, and other animals. Since their modes of actions are not specific to one pest species, they frequently execute or hurt other non-pest species, including human (Tang et al., 2015). Pesticides are classified based on their target organisms such as insecticides, fungicides, rodenticides, nematocides, and herbicides (Manahan, 2017).

2.1.1 Insecticides

Insecticides are substance or mixture of substances that are formulated to kill, harm, repel or prevent insects. The most common and useful method of classifying insecticides is based on their source and chemical composition (Figure 2.1). Insecticides can be derived from natural and synthetic sources. Most natural insecticides are derived from phytochemicals that plants produce as defense chemicals against insects, such as pyrethrum and azadirachtin. Pyrethrum, extracted from chrysanthemum flowers, is a substance in the ester group that directly affects the nervous system of insects, resulting in rapid insect-poisoning. Azadirachtin is an active ingredient in the limonoid group,

which has a structure similar to ecdysone hormones. This substance, found in neem extracts, is used for prevention and removal of pests by inhibiting growth and food-consumption of insects (Isman and Akhtar, 2007). It is low toxic to human and other mammals, and easily decompose in the environment. Although natural insecticides can control insects and low toxicity to human, they are costly in production and easily decompose in the environment. Thus, farmers mostly prefer to use the synthetic insecticides for insect controlling. The synthetic insecticides can be divided into four groups; organochlorines, organophosphorus, carbamates, and pyrethroids (Yadav and Devi, 2017).

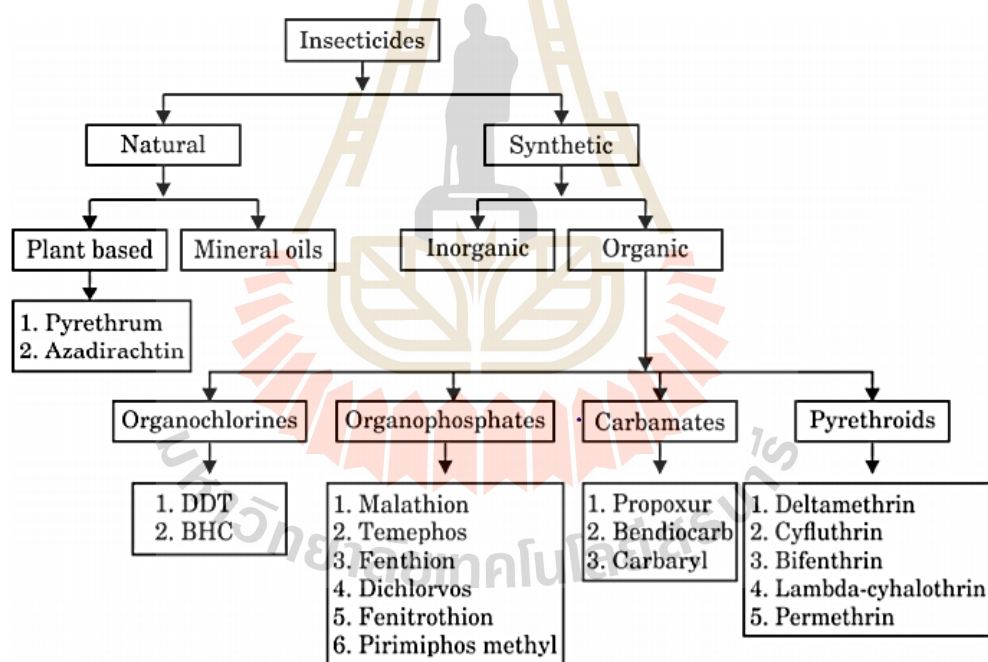


Figure 2.1 Classification of insecticides (Yadav and Devi, 2017).

Organochlorine insecticides (OCs) or chlorinated hydrocarbons are a group of chemicals consisting of hydrogen, carbon, and chlorine atoms that good soluble in fat and slowly degrade in the environment. However, the high persistence of OCs in the

environment still causes a high risk of contamination in the food chain and affects a reproductive system (e.g., eggshell thinning) in certain bird species. Therefore, OCs are banned from the market in many countries (Aktar et al., 2009). The chemical structures of the common OCs are shown in Figure 2.2. OCs can be divided into 3 groups following their structure; diphenyl aliphatic compounds, benzene hexachloride (BHC) isomers, and cyclodienes. A mechanism of diphenyl aliphatic compounds to kill insects involves the interruption of insect nervous system by increasing the amount of sodium ions in cells and blocking the release of potassium ions, leading to convulsion of insects. Examples of OCs in this group include dichlorodiphenyl-trichloroethane (DDT), methoxychlor, perthane, and dicofol. In the case of BHC isomers and cyclodienes, such as chlordane and dieldrin, their modes of action involve the interference of central nervous system (CNS) by inhibiting GABA-mediated chloride influx in the CNS (Brannen et al., 1998). Cyclodienes are the most toxic substances in the group of OCs and usually used in the soil to control termites (Doble and Kumar, 2005).

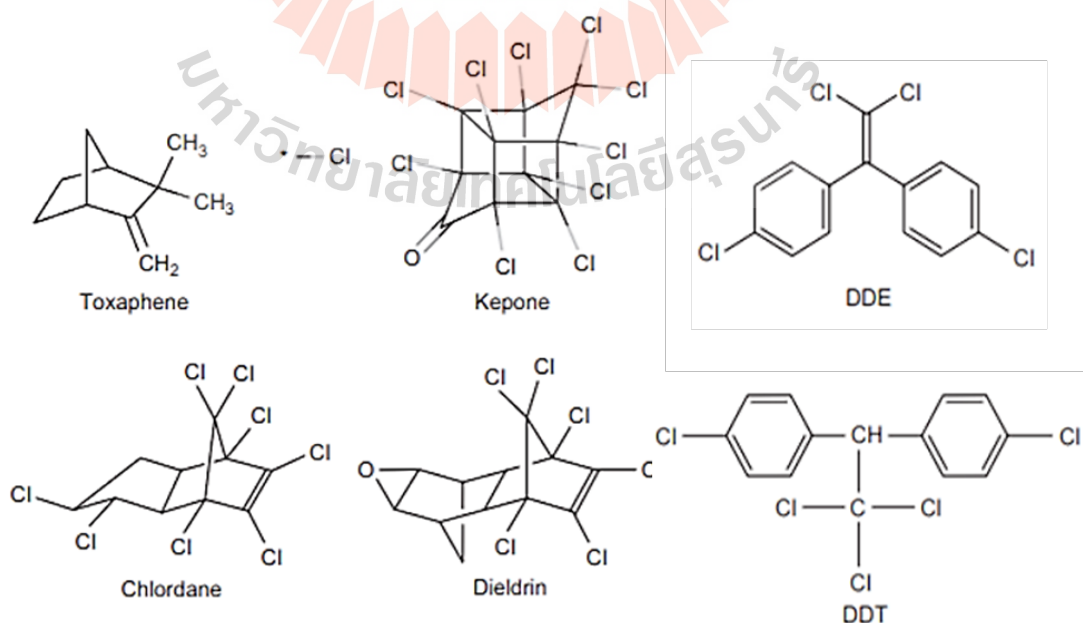


Figure 2.2 Chemical structures of common OC pesticides (Ensley, 2018).

Organophosphates (OPs) are hydrocarbon compounds that contain phosphorus as an essential component. They are usually esters, amides or thiol derivative compounds of phosphonic acid. OPs are widely applied in household and agriculture for insect controlling due to their low persistent in the environment. A common mechanism of OPs involves an inhibition of acetylcholinesterase enzyme, resulting in high accumulation of acetylcholine at the synapses, neuromuscular junction, and end organs, which causes excessive stimulation at these sites (Bajgar, 2004). Malathion, parathion, chlorpyrifos, diazinon, dichlorvos, and fenthion are the most widely used OPs to control insects in agriculture (Figure 2.3).

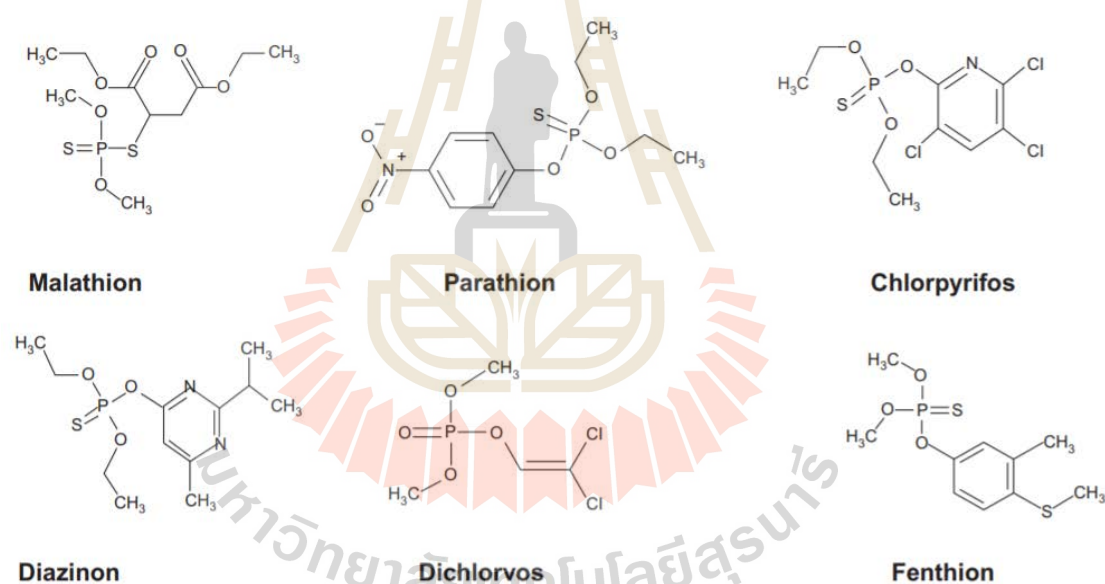


Figure 2.3 Chemical structures of commonly used OPs (Gupta et al., 2018).

Carbamate, a new class of insecticides, is derived from carbamic acid. Their toxicity is similar to OPs by inhibiting the activity of enzymes in the nervous system. Carbamate shows high efficiency to kill insects, especially bees, but they have low toxicity to mammals. The main carbamate compounds are carbaryl, carbofuran, and propoxur (Figure 2.4) (Doble and Kumar, 2005).

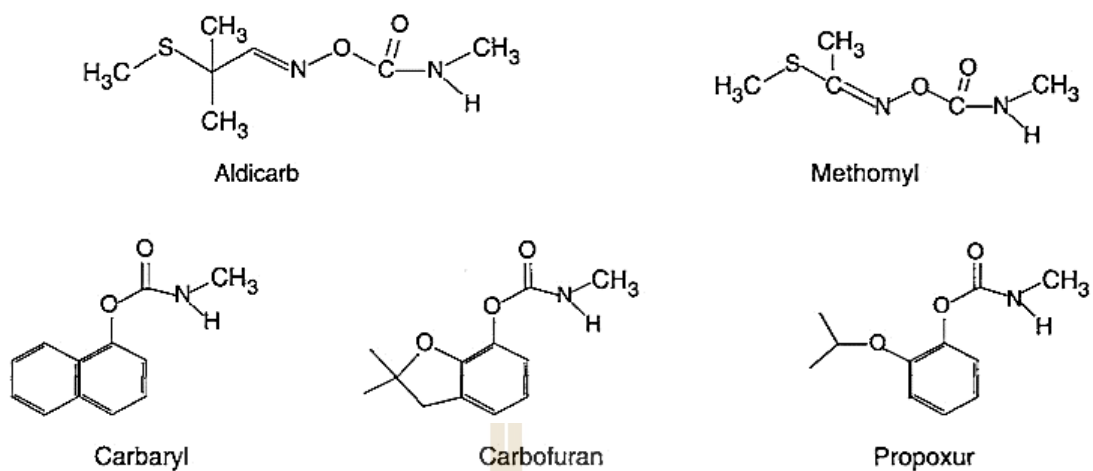


Figure 2.4 Chemical structures of main carbamate compounds (Doble and Kumar, 2005).

Pyrethroids are synthetic compounds, similar to natural pyrethrum from chrysanthemum flower, but are more stable under sunlight and heat. Their toxic mechanism is similar to OPs, but less effective, by blocking the sodium channel at the cell membrane. Pyrethroids have capability to eliminate many insect species but be relatively low toxicity to humans nor left residues in the environment, thus often applying for insect control in households. The commonly used chemicals in this subgroup, as shown in Figure 2.5, include deltamethrin, cypermethrin, and fenvalerate (Ray and Fry, 2006).

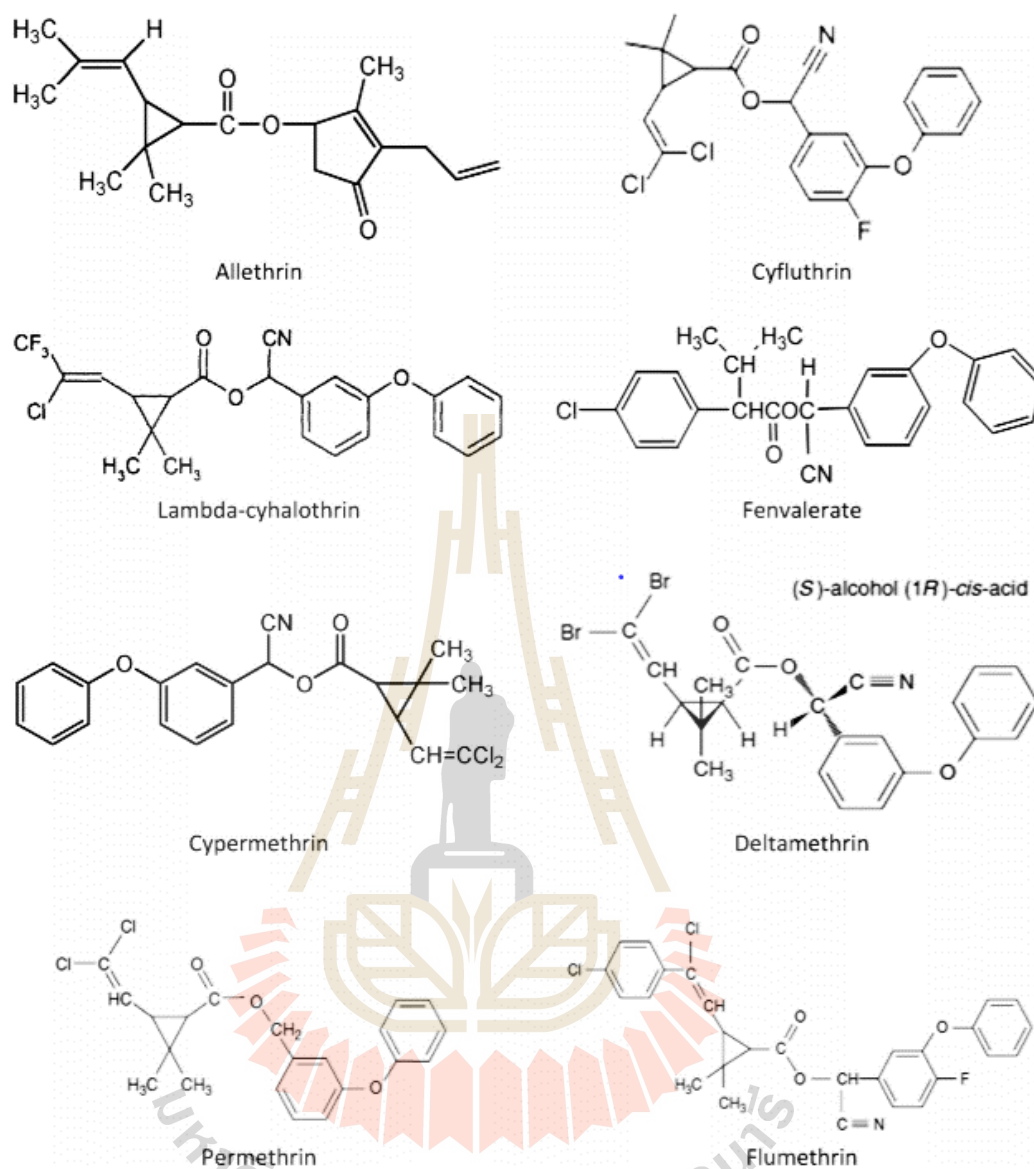


Figure 2.5 Structures of synthetic pyrethroids (Malik et al., 2017).

2.1.2 Fungicides

Fungicides are pesticides used to control or protect plants from fungal diseases, generally low toxicity to mammals. Fungicides are divided into five major groups according to their chemical groups, including azoles, benzimidazoles, dithiocarbamates, morpholines, and miscellaneous (Tadeo, 2008).

Azoles are the widely used fungicides to control cereal diseases, particularly in Europe, North America, Australia, and New Zealand (Sampson et al., 1992). The fungicides in this group often contain both imidazole ring and triazole ring. The examples are as difenoconazole, fenbuconazole, myclobutanil, propiconazole, tebuconazole, tetraconazole, triadimefon, and triticonazole. The antifungal activity of azoles is via the inhibition of key enzymes in the sterol biosynthesis, which is important for fungal cell membranes. Since the activity of azoles is at very specific site, the fungal resistance is highly concerned (Fishel, 2005).

Benzimidazoles are the group of specific fungicides, which their structures contain nitrogen heterocycle and thiabendazole and/or benzimidazole. Their mode of action involves the inhibition of β -tubulin assembly during mitosis. Later on, they were found to be ineffective for fungal control due to the resistance capability of the field pathogens. Nevertheless, since they have a broad spectrum activity, they are still used for the relating crop groups (Hirooka and Ishii, 2013).

Dithiocarbamates are the class of fungicides that are the heavy metal salts of ethylenebisdithiocarbamates. They are used to protect to control fungi during crop plantation, storage, and transport. Dithiocarbamates exhibit multi-site inhibition activities for fungal control. The well-known dithiocarbamates are mancozeb, maneb, nabam, thiram, zineb, and ziram. It is noted that dithiocarbamates is highly toxic to aquatic organisms (Medicine, 1995).

Morpholines are fungicides used to control the fungal diseases in cereals, cucumbers, and apples. The widely used morpholine fungicides are fenpropimorph and tridemorph, which their activity involves the inhibition of the sterol biosynthesis (Tadeo, 2008).

Miscellaneous fungicides are the group of aromatics hydrocarbons fungicides including captan, chlorothalonil, chloroneb, dichloran, hexachlorobenzene, pentachlorophenol, and sodium pentachlorophenate. They are used in various fruit and vegetables to control fungi. The mechanism of their antifungal activity involves the inhibition of oxidative phosphorylation and synthesis of lipids (Yang et al., 2011).

2.1.3 Rodenticides

Rodenticides are used to control rodents such as rats, squirrels, and prairie-dog. They can be grouped according to the mechanism of action; anticoagulant and non-anticoagulant.

The anticoagulant rodenticides are widely used to protect crops from rats and other rodent animals. They are divided into 2 major groups according to the chemical structure; hydroxycoumarin and indandione. In the group of hydroxycoumarin, they are also classified to the first generation and second-generation rodenticides. In the first generation, warfarin is the well-known main active ingredient for rodenticides. (Valchev et al., 2008). To improve the toxicity, the second generation has been developed, which have high efficiency to kill rats and exhibit the greater resistance than the first-generation chemicals. Commonly known chemicals in this group are brodifacoum, bromadiolone, difenacoum, difethialone and flocoumafen. The poison of anticoagulant rodenticides involves the inhibition of blood clotting. These rodenticides cause the blood flows through the capillaries and the opening of the body from the wound, resulting in death of rodents (Rattner and Mastrota, 2018).

There are several rodenticides that work differently than anticoagulants; non-anticoagulant. The currently used anticoagulants in agriculture are such as fluoroacetate, bromethalin, cholecalciferol, zinc phosphide, and strychnine. Sodium

fluoroacetate is a worldwide rodenticide of poisonous white powder. It is highly toxic to mammals because the substance has a structure similar to acetate, which involves to many cell-metabolism processes. In the cells, fluoroacetate is changed to fluorocitrate, which can inhibit the activity of aconitase enzymes in tricarboxylic acid (TCA) cycle (Proudfoot et al., 2006), leading to the inhibition of the oxidation process of citric acid. Therefore, the TCA cycle is interrupted, affecting the energy production.

Bromethalin, the diphenylamine compound exhibiting very high toxicity, is developed for controlling warfarin-resistant rodents. Bromethalin has a slow degradation in plasma, which its half-life is approximately six days. The toxic activity of bromethalin occurs in the central nervous system by causing the uncoupler of oxidative phosphorylation in the mitochondria, resulting in the decreasing of ATP synthesis (Heggem-Perry et al., 2016). As nerve cells lack ATP, they swell and put pressure on the brain, resulting in paralysis and death of rodents (Huntington et al., 2016).

Cholecalciferol, also known as vitamin D₃, is the rodenticide that has a high affinity to vitamin D receptor, 500 times greater than other vitamin D molecules. Cholecalciferol cause the elevation the levels of calcium and phosphorus in rodent plasma via two processes. First process is related to the increased amount of intestinal calcium-binding protein (calbindin) at the enterocyte and gastrointestinal tract. The level of calbindin is directly related to the absorption of calcium. Second process involves the degradation of calcium and phosphorus from bones, leading to the increasing level of calcium and phosphorus in the blood. The high calcium concentration in the blood can cause heart failure, kidney failure, and death (Gupta, 2018).

Zinc phosphide is the recommended rodenticide for agriculture because of its high specificity to rodents. Zinc phosphide can be hydrolyzed to phosphine, which is a gas that can cause irritation to the gastrointestinal tract and respiratory system. It also cause oxidative stress when diffuse to blood vessels (Nath et al., 2011).

Strychnine is an alkaloid extracted from seeds of the plant *Strychnos nux-vomica* found in South Asia, North Asia, and Australia. This substance is highly toxic to all animals. It is a competitive inhibitor that functions to inhibit the function of glycine. It acts as the inhibitory neurotransmitter at the interneuron (Renshaw cell) in the reflex arc postsynaptic in the spinal cord and medulla brain. Strychnine also increases the level of glutamic acid and amino acid, which are the neurotransmitters involved in stimulating the compression of the central nervous system muscles (Gupta, 2018).

2.1.4 Nematicides

Nematicides are the pesticides for controlling plant-parasitic nematodes, which are classified as fumigant and non-fumigant (non-volatile) nematicides. Fumigant nematicides, the halogenated aliphatic hydrocarbons, are the broad-spectrum pesticides that effectively passed through soil as gas. Fumigant nematicides are not taken up by plants nor bound by soil, so they have a short period of activity. Examples of fumigant nematicides are 1,3-dichloropropene, ethylene dibromide, methyl bromide, and 1,2-dibromo-3-chloropropane (Van Gundy and McKenry, 2012). A primary effect of halogenated hydrocarbons is to serve as alkylating agents. The sulfhydryl groups of proteins, in particular, are labile to methyl bromide-induced methylation (Bell et al., 1996). Moreover, ethylene dibromide alkylated proteins and oxidized Fe^{2+} center in the cytochrome-mediated electron transport chain, thereby blocking respiration (Wright,

1981). Unlike fumigant nematicides, non-fumigant nematicides are formulated in liquid or granular states and move through the soil by water. They have the activity against multiple pests, particularly if they contain more than one active ingredient. But generally, they have a narrower spectrum of activity than fumigant nematicides. Some, but not all, non-fumigant nematicides are systemic, meaning the active ingredient is taken up by the plant and translocated to other parts of the plant. Carbamates and organophosphates are the main compounds in non-fumigant nematicides. They are well-known reversible inhibitors of acetylcholinesterase activity that interfere with nerve transmission processes (Becker, 2014).

2.1.5 Herbicides

Herbicides are any poisonous substances that can prevent and kill undesired plants. Good herbicides should specifically control weeds and not destroy the economic crops. Herbicides are divided by chemical groups to aliphatic carboxylic, amides, benzoic and phthalic, benzonitriles, carbamates and thiocarbamates, cyclohexanediones, dinitroanilines, diphenyl ethers, imidazolinones, pyridines, ureas and sulfonylureas, and triazines (Figure 2.6) (Herrera-Herrera et al., 2016). However, as many weeds are resistant to herbicides, the appropriate herbicides to manage these weeds are greatly concerned. In the presence, the classification of herbicides is based on their toxic mechanisms, rather than the chemical family. Based on their actions, eight major groups of herbicides are classified; lipid biosynthesis inhibitors, amino acid biosynthesis inhibitors, plant growth regulators, photosynthesis inhibitors, nitrogen-metabolism inhibitors, pigment inhibitors, cell-membrane disruptors, and seedling-growth inhibitors.

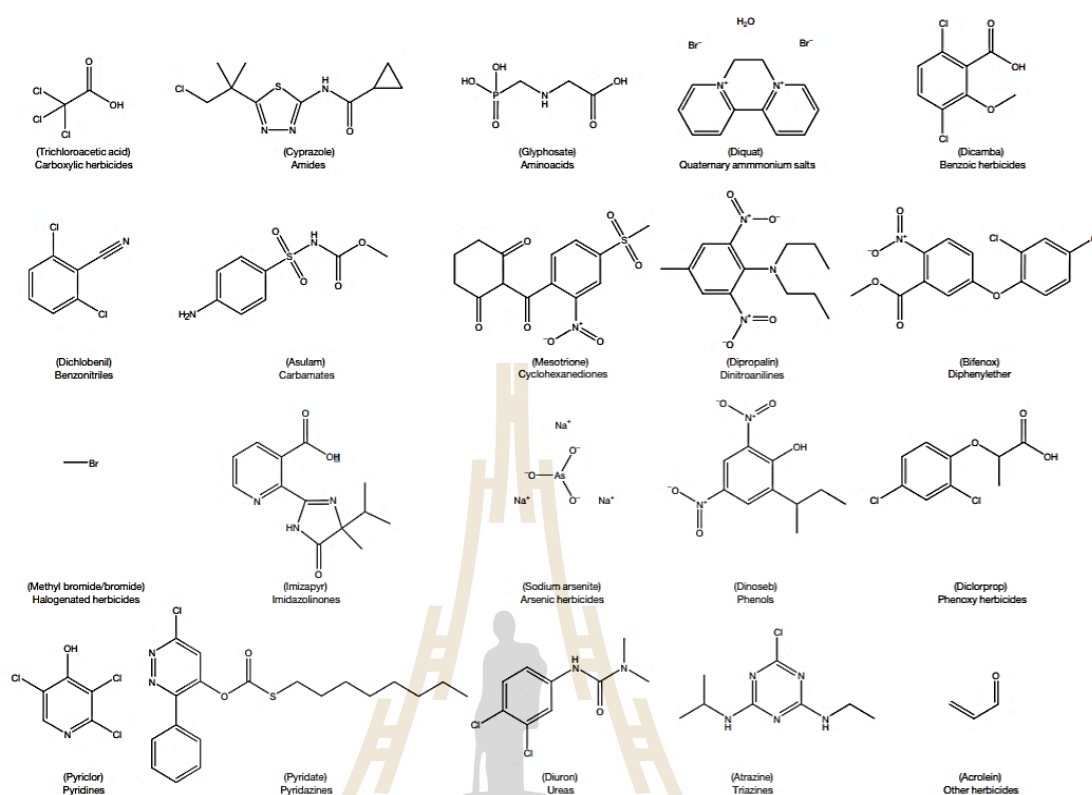


Figure 2.6 Examples of herbicides belonging to different chemical families (Herrera-Herrera et al., 2016).

Herbicides in the group of lipid biosynthesis inhibitors, also known as grass killers, can block the activity of acetyl CoA carboxylase enzyme (ACCase), the essential enzyme in de novo fatty acid synthesis. The inhibition of this enzyme causes the interruption of the phospholipid synthesis of the cell membrane during cell division (Yang et al., 2010). Examples of these herbicides are aryloxyphenoxypropionate, cyclohexanedione, and phenylpyrazolin.

Herbicides in the group of amino acid biosynthesis inhibitors are known to interrupt the synthesis of branched-chain amino acids (such as leucine, isoleucine, and valine), which the mechanism involves the blocking of acetolactate synthase (ALS)

enzyme activity (LaRossa and Schloss, 1984). So, it prevents the activity of the intermediate enzyme, 5-enolpyruvylshikimate-3-phosphate (EPSP) synthase enzyme, in the shikimic acid pathway (Duke and Powles, 2008). As the result, the aromatic amino acids (tryptophan, tyrosine, and phenylalanine) that are the essential amino acids for plant growth are insufficient, leading to plant death (Maeda and Dudareva, 2012). Thus, these herbicides are also called the aromatic amino acid inhibitors. Examples are glyphosate, imidazolinones, pyrimidinylthiobenzoates, sulfonylaminocarbonyl-triazolinones, and sulfonylureas. Glyphosate is the most commonly used herbicides in this group that can exhibit specific activity to control weeds.

The plant growth regulators, or auxin herbicides, are the herbicides that can activate the adenosine triphosphate (ATP)ase proton pump, resulting in increasing enzyme activities in cell wall and inhibiting a nucleic acid metabolism. These herbicides also activate RNA polymerase, leading to the increase of protein expression and causing the uncontrolled cell division and growth. As the results, cells burst and ultimately die. Herbicides in this group include benzoic acid, phenoxy-carboxylic acid, pyridine carboxylic acid, and quinoline carboxylic acid (Grossmann, 2010). The photosynthesis inhibitor group of herbicides can inhibit photosystem II (PSII) and photosystem I (PSI). Inhibition at PSII causes the interruption of ATP and NADPH₂ syntheses via the blocking of electron transport and CO₂ fixation. As the electron transport chain is blocked, the triplet state chlorophyll is generated and induces the releasing of hydrogen of lipid, leading to lipid peroxidation. Lipid peroxidation can induce reactive oxygen species (ROS) and affect other biosynthetic pathways in the cells, leading to oxidative stress and cell death (Roach and Krieger-Liszkay, 2014). Herbicides in this group include phenylcarbamates, pyridazinones, triazines, and

triazinones. The nitrogen-metabolism inhibitor herbicides are the herbicides functioning through nitrogen metabolisms, especially glufosinate. Glufosinate and bialophos, or phosphinic acids, can inhibit the activity of glutamine synthetase (GS) that can convert glutamate and ammonia to glutamine. These herbicides degraded GS, leading to accumulation of ammonia in plants. The high level of ammonia directly shuts down the PSI and PSII reactions and reduces the pH gradient across the membrane that are important for uncoupling of the photophosphorylation (Obojska et al., 2004). Since GS is located in important organelles (such as the chloroplast) and cytoplasm, these herbicides are highly effective in controlling weeds and other undesired plants.

For the pigment inhibitors, these herbicides can disrupt the activity of enzymes in the carotenoid biosynthetic pathway (Qin et al., 2007). For example, the pigment inhibitor isoxazole can inhibit the essential enzyme for pigment synthesis, 4-hydroxyphenyl pyruvate dioxygenase (HPPD). In response to these herbicides, level of carotenoid in plants are decreased and free radicals are greatly produced, causing the cell toxicity and cell death. Examples of these herbicides are amides, anilidex, furanones, phenoxybutan-amides, pyridiazinones, and pyridines.

Cell-membrane disruptor herbicides control weeds by blocking the protoporphyrinogen oxidase (PPO) enzyme, the enzyme for converting protoporphyrinogen IX (PPGIX) to protoporphyrin IX (PPIX) in the chlorophyll and heme biosynthesis. As this enzyme is inhibited, the high level of PPIX can induce the lipid peroxidation to generate free radicals. As a result, the chlorophylls and carotenoids are degraded and pores are generated on cell membranes, causing leakage of chlorophyll and other pigments, and cell death (Duke et al., 1991). Examples of these

herbicides are diphenylether, oxadiazoles, aryl triazolinone, N-phenylphthalimides, phenylpyrazoles, oxazolidinediones, pyrimidindiones, and thiadiazoles.

The seedling-growth inhibitor herbicides can prevent growth of seeds via several mechanisms. They can inhibit root cell division, leading to the inhibition of root growth and extension. They can inhibit the polymerization of microtubules (Wloga and Gaertig, 2010). They can block the essential biomolecule synthesis such as lipids and protein (Trenkamp et al., 2004). These herbicides are greatly effective when used before grasses and broadleaf weeds emerge. Examples of these herbicides are benzamide, benzoic acid, dimethyl-2,3,5,6-tetrachloroterephthalate (DCPA), dinitroaniline, phosphoramidate, and pyridine.

Globally, there are widespread applications of pesticides to improve crop production and efficiency, thus there is a strong risk that such chemicals may be introduced into the environment (soil, water, and air) and polluted in nourishment (especially, vegetables and fruits). Substantial quantities of contaminated pesticide residues in nourishment and environment have been a significant issue in their impacts on human health and ecosystems (Shamsipur et al., 2016). Sapbamrer reported the data of imported pesticides in Thailand in 2012-2016, showing that the most imported pesticides were herbicides (67,445.87 tons with the value of 296.99 million USD) for agriculture. These data also suggested the high possibility of these herbicides released into the environment. Among these herbicides, paraquat is the one of top 3 of the imported herbicides during 2012-2016 (Sapbamrer, 2018). Paraquat could cause skin wounds and even fatalities owing to its widespread usage, easy acquisition, and lack of an antidote (Lin et al., 2010). For these reasons, the system used to detect paraquat residues, as well as other pesticide residues, in food and the environment is important

for human safety and awareness. In general, the official regulations of the maximum residue limits (MRLs) for paraquat in agricultural products were in a range of 0.01 to 1 mg kg⁻¹ in United States (Luo et al., 2018). Also, the maximum permissible levels for paraquat residues in water are from 40 to 400 nM in USA and EU countries. (Li et al., 2020).

2.2 Pesticide detection methods

The analytical methods for pesticide detection are divided into two major groups: conventional and advanced detection methods (Figure 2.7). The conventional methods for detecting pesticides involves chromatography, immunoassay, and capillary electrophoresis. In general, the conventional methods, also known as classical methods, offer high sensitivity and selectivity with low detection limits. However, these methods are complicated, need advanced laboratory instruments and professional staff, and high costs. For these reasons, advanced methods including molecular imprinted polymers and biosensor have been developed. These methods are easy, simple, and cost-effective approaches with high sensitivity and selectivity for pesticide detection (Songa and Okonkwo, 2016).

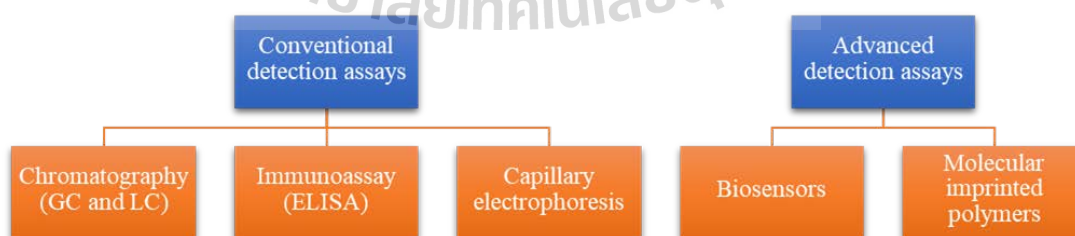


Figure 2.7 Detection system for pesticide determination modified from (Samsidar et al., 2018).

2.2.1 Chromatography

Chromatography is used for the separation of target molecules from samples based on their volatilities, in which the target molecules are diffused between two phases. One is a stationary phase and the other is a mobile phase. The chromatographic methods to determine pesticides commonly used are the gas and liquid chromatography. Gas chromatography (GC) is this method that uses the gas phase such as He or N₂ as the mobile phase and the stationary phase are solids that can absorb the gas of the separated molecules. Moreover, the GC coupled with mass spectrometric detectors (MS and tandem MS) has been developed and widely used for enhancing the sensitivity of pesticide analysis (Shamsipur et al., 2016) because of greater efficacy in getting rid the interference (Jiang et al., 2014). For liquid chromatography (LC), liquid is used as a mobile phase. This method is the well-known detection method for various pesticide residues (Vidal et al., 2009). To improve sensitivity, high performance liquid chromatography (HPLC) have been developed. This technique is used to separate the target molecule under the liquid pressure based on the compatibility of the substance with the stationary phase or mobile phase. The compound that is favorable with the mobile phase will be separated first. The substance compatible with the stationary phase will be separated later. Recently, HPLC assay becomes the conventional method to analyze various pesticide residues in the environment (Huang et al., 2019). Although chromatography-based detection methods are the common methods to detect pesticides due to their efficiency, sensitivity, and reliability, these methods also relatively complicated, require expensive instruments and trained personnel to handle it, and are not suitable for real-time detection.

2.2.2 Enzyme-linked immunosorbent assay

The immunoassay usually uses the antigen or antibody as the probe for pesticide detection. This assay relies on the specific binding between the target molecule and its antibody coupled with the enzyme to change substance to detectable product for quantitation. Thus, this technique is called the enzyme-linked immunosorbent assay (ELISA). As compared with chromatography assay, ELISA offers the advantages in rapid detection, low cost, and easy process (Watanabe, 2011). Moreover, this technique provides high sensitivity and specificity to specific pesticides based on antigen-antibody interaction. However, this assay has a short window of color detection and difficulty of antibody production.

2.2.3 Capillary electrophoresis

Capillary electrophoresis (CE) is a method of separating the substance based on the charged molecules to move under the electric field in the capillary tube containing the buffer or electrolyte solution. This assay needs low amount of samples and reagents, and demonstrates the outstanding isolation efficiency with less operating time. However, this assay has low sensitivity due to low sample injection volume into the capillary system (Watanabe, 2011).

2.2.4 Molecular imprinted polymers

Molecularly-imprinted polymers (MIPs) are the synthetic materials that have a recognition site for a target molecule (Cieplak and Kutner, 2016). These polymers have been widely used in various fields of detection applications due to their high specificity and selectivity. MIPs are produced by polymerizing the functional monomers with high affinity to target molecule, leading to a highly cross-linked three-

dimensional network polymer. MIPs offer the consistency and enhancement of detection sensitivity, which are more effective than the uses of the conventional antibodies, peptides, and enzymes (Sun et al., 2018). Nevertheless, this method still has several challenges such as the defective dislocation of the synthesized MIPs from the template caused by the irregular shape of polymers, thus reducing the selectivity of detection (de Dieu Habimana et al., 2018).

2.2.5 Biosensors

Biosensors are the analytical devices for detecting a chemical molecule, which require the uses of biological component (such as enzymes, antibodies, and nucleic acids) and physiochemical detecting system. When a target molecule interacts with a specific biological component, it causes unique physical or chemical changes of electrical intermediates, ions, electrons, moisture, oxygen, heat, or color. These changes can be converted by transducers into electrical, piezoelectric, and optical signals (Figure 2.8). Because of high sensitivity, great specificity, and low cost, this technique is attractive to many researches in pesticide detection (Vigneshvar et al., 2016). In general, there are 3 types of biosensors; electrochemical, piezoelectric, and optical biosensors.

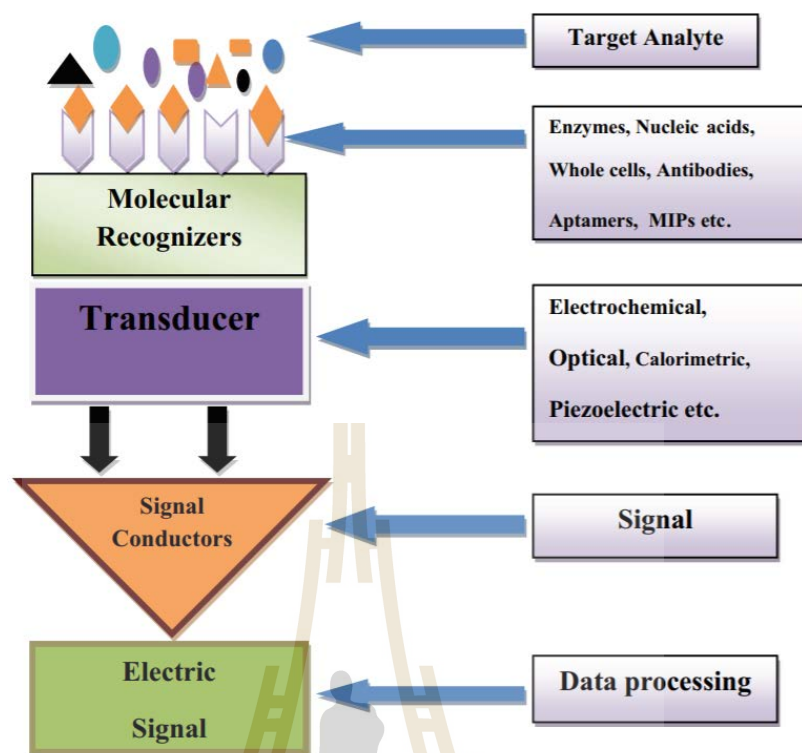


Figure 2.8 Basic layout of elements of biosensor for its construction (Verma and Bhardwaj, 2015).

The electrochemical biosensor is based on the use of current detection system, which often used the amperometric technique (Grieshaber et al., 2008). In general, this method coated enzymes on the surface of the electrode. When the enzyme reacts with the desired substance, it produces an electrical intermediate, thus giving the appropriate electrical potential to the oxidation or reduction reaction of the product. The occurring current flow of electrons is related to the number of intermediates and target substances. Nevertheless, this method has a few limitations such as the high specific energy consumption and the corrosion of equipment from the saline (or acidic) electrolyte.

The piezoelectric biosensor is a technique that uses crystals that can generate a vibration with a specific frequency when receiving electric potentials. This vibration occurs freely on the crystal surface, thus using as sensing signals. In this technique, the crystal surface is coated by a specific probe for target analysis. The interaction of biological recognition element and the target analyte changes the frequency of vibration, which the changed signals are measured for quantification purpose (Pohanka, 2018). In this technique, the detection accuracy is sensitive to temperature, which the optimized temperature is required.

The optical biosensor is an analytical device using an optical transducer. This transducer works by the optical properties such as absorption, reflection, transmission, and scattering. Although the optical signal is often used for sensing system, the detected signals can be changed into an electrical signal for electrical sensing. The optical biosensor offers the low limit of detection, less external signal interference, and suitable for applications in various fields. A lot of studies have been conducted for the detection of pesticides based on optical biosensors (Yan et al., 2018). Although this assay is still costly as compared with other biosensors, they have high sensitivity, small and lightweight, easy result-analysis, and suitable for on-site detection. As the colorimetric detection is one of the conveniences and simple sensors, which provides notable advantages of direct visualization output, it is the promising candidate for a simple on-site detection system. Recent novel colorimetric methods have been developed, which nanomaterials are often used as colorimetric sensing for pesticide residues. Among these nanoparticles, gold nanoparticles have extensively used to develop sensitive colorimetric sensors for contaminated pesticide in the environment.

2.3 Gold nanoparticles

Gold nanoparticles (AuNPs) are the particles of gold with the average diameter in a range of 1–100 nm (Schmid, 2008). With their unique properties such as catalytic, electronic, chemical, and especially optical properties, AuNPs have become interested as a sensing probe for biochemical, biomedicine, immunological, and electrochemical analyses. AuNPs has the unique surface plasmon resonance (SPR) absorption that occurs from the local electrons on the surface of AuNPs. The changes of particle size, shape, and state of free or aggregated form can induce the changes of maximal SPR peak and color of AuNPs (Liu, Lu, et al., 2018). Recently, the AuNPs-based colorimetric detection assays have been developed in several strategies such as aggregation-, etching-, growth-, and nanozyme-based sensors (Chang et al., 2019). The aggregation-based sensors have gained attractive from many researchers owing to their easy, simple, rapid, colorimetric, and economical advantages. Thus, these assays have been established for the wide-ranging detections of proteins (Wang et al., 2017), small molecules (Liu, Zhang, et al., 2018), inorganic ions (Wang et al., 2018), enzyme activities (Wu et al., 2017), and oligonucleotides (Zou et al., 2018). The key mechanism of the aggregation-based sensors mainly relies on a distance between AuNPs (Chen et al., 2018). Dispersive AuNPs appears in red color, which the characteristic SPR peak is in a range of 510–570 nm. At the aggregation state, they appears in blue color, which their characteristic SPR peak is shifted to a longer wavelength (red shift) (Njoki et al., 2007). Generally, AuNPs have the tendency to aggregate due to the van der Waals attractive forces. Thus, in a synthesis process, a stabilizing agent is added to prevent aggregation of the formed AuNPs. Even though, the stability of AuNPs can be disturbed

upon the presence of analyte, in which the interaction between analyte and stabilizing agent may induce the aggregation of AuNPs. Thus, this principle can be applied for developing the colorimetric sensor. However, these methods have some drawbacks such as low sensitivity and selectivity. To improve the sensitivity and specificity of the detection, the ligands with specific binding to analyte such as DNA, aptamers, peptides, or antibodies have been used with AuNPs as the more efficient sensor.

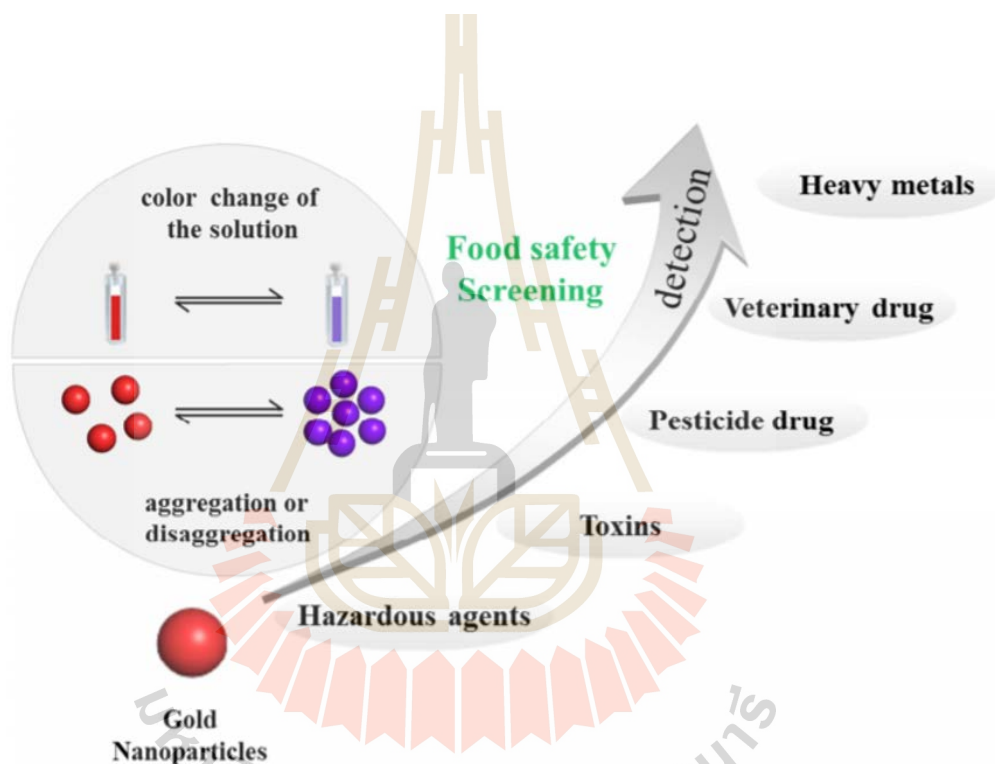


Figure 2.9 Colorimetric AuNPs-based sensor for the detection of food nuisances, including heavy metals, veterinary drug residues, pesticide drug residues, toxin, and hazardous substances (Chen et al., 2018).

2.4 Aptamers

Aptamers are the short, single-stranded DNA or RNA oligonucleotides that can selectively bind to the specific molecules or live cells. Their target molecules can be proteins, peptides, carbohydrates, small molecules, and toxins. The aptamer can be

obtained via the *in vitro* selection for a certain target molecule, known as SELEX (Systematic Evolution of Ligands by Exponential enrichment) (Bayat et al., 2018). Aptamers can fold into the three-dimensional structures to stabilize and contribute to the spatial structure of the binding. The structures of aptamers can be characterized as stems, loops, hairpins, bulges, triplexes, and quadruplexes. These regions play vital roles to interact with various target molecules from small molecules to the whole organism. The selectively binding of aptamers and target molecules based on electrostatic interactions, van der Waals forces, hydrogen bonding, stacking of aromatic rings, or combination of these (Groher and Sues, 2016). Due to the unique properties of aptamers, they have the ability to bind a wide range of targets such as ions, drugs, toxins, viruses, and pesticides with significant specificity and affinity (Zhang et al., 2018). In addition, aptamers give more advantages as compared to the traditional antibody including easy and low cost for synthesis, prolonged shelf life, and sustainable (Lan et al., 2017). According to these advantages, aptamers have been attractive for researchers to develop the rapid, sensitive, and selective methods for the detection of pesticide residues substitute to antibodies.

The novel colorimetric detections of pesticides based on aptamer were reported. For example, Shi and co-workers developed the AuNPs aggregation-based methods for detection of acetamiprid, the commonly used insecticide in agriculture (Figure 2.10). With the presence of aptamer, the surface of AuNPs was more stable against salt-induced aggregation as they were covered by aptamers. However, when acetamiprid was added, the aptamers specifically bound to acetamiprid, forming the aptamer-target complexes. Thus, AuNPs were unprotected and easily aggregated by salt induction. The changes of AuNPs state caused the color change from red to blue (Shi et al., 2013). In

addition, this strategy has been applied to detect various pesticides such as organophosphorus pesticides (Bai et al., 2015), malathion (Bala et al., 2016), omethoate (Wang et al., 2016), and atrazine (Abraham et al., 2018).

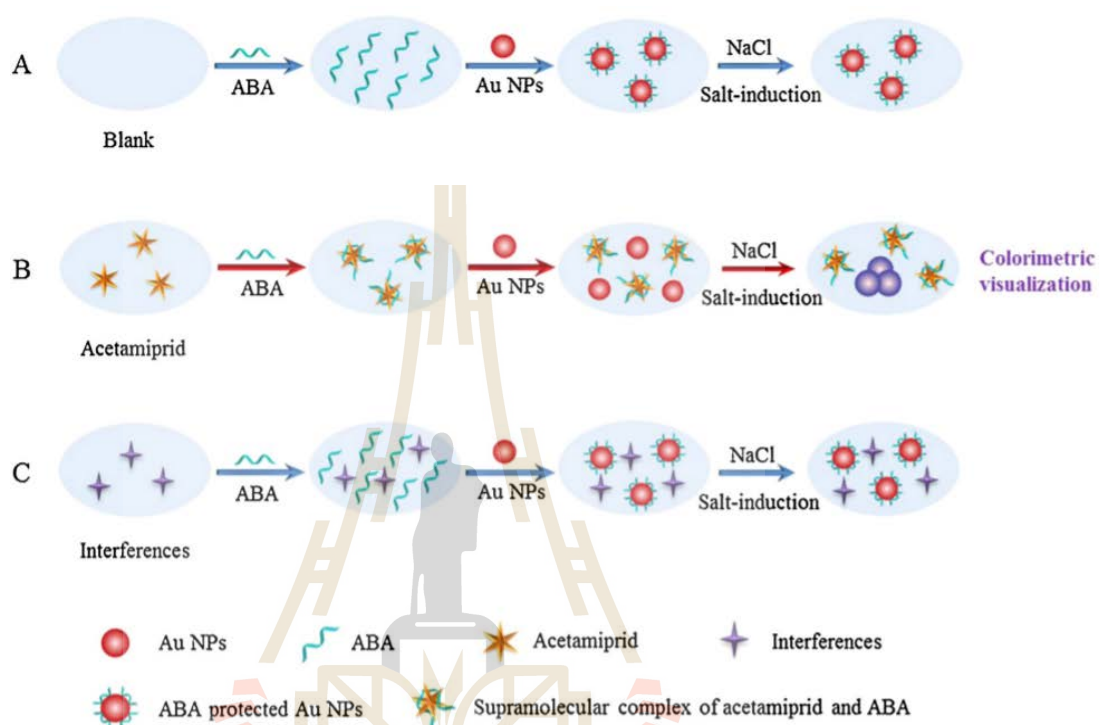


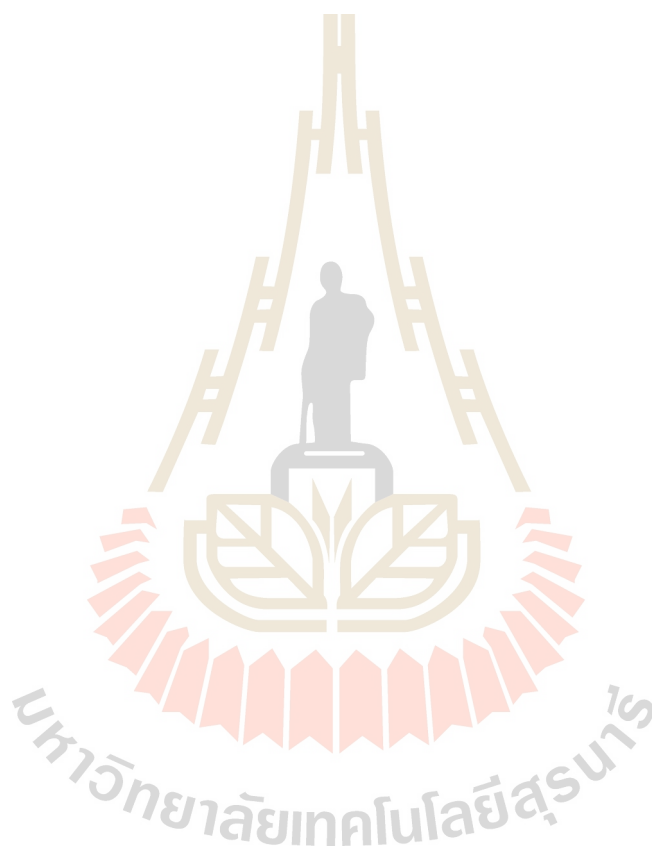
Figure 2.10 The mechanism of the colorimetric detection of acetamiprid utilizing the acetamiprid binding aptamer (ABA) and unmodified AuNPs as well as its selective performance (Shi et al., 2013).

2.5 Review of related studies

This work is interested in the development of the paraquat detection based on AuNPs and DNA aptamer. Published articles relating to paraquat detection are reviewed as follows. The common strategy of AuNPs-based colorimetric detection for pesticide is based on the pesticide-induced aggregation of AuNPs, resulting in the color change. For this approach, AuNPs containing the charged surface and attach to

functional groups or synthetic polymers are used to interact with paraquat, resulting in colorimetric changes. The paraquat detection system based on the negatively charged AuNPs was first developed by Li and co-workers. They synthesized carboxylatopillar [5]arene or CP[5]A as the probe for paraquat detection. Based on the carboxylate anions on the CP[5]A structure, the CP[5]A-capped AuNPs exhibited the negatively charged surface. Thus, the strong positive charge of paraquat can interact with the CP[5]A-capped AuNPs via the electrostatic interaction, resulting in the induced aggregation of the AuNPs and the change of color from red to blue (Li et al., 2013). However, this assay showed the low sensitivity as the limit of detection was at 2 μM . Later in 2018, there was the report of the paraquat detection system with the improvement of its sensitivity by Dong and co-colleagues. The para-sulfonatocalix[4]arene (pSC₄) was synthesized as the detection probe. The pSC₄ is the calixarene derivative, which can specifically bind to pyridylum ions. Therefore, the pSC₄-capped AuNPs was used to detect paraquat and this system demonstrated the limit of detection at 2.2 pM (Dong et al., 2018). Although the detection systems based on negatively charged AuNPs were produced, the detection system based on the highly specific binding between AuNPs and paraquat has been a research challenge in order to enhance the sensitivity of the detection. Aptamers have been reported as the highly bio-recognized elements for enhancing the sensitivity and specificity of detection of the designed molecules (Jalalian et al., 2018). Ran and Wu isolated the specifically binding aptamer to paraquat and developed as the colorimetric detection using poly(diallyldimethylammonium chloride) (PDDA) to induce the aggregation of AuNPs. With the presence of paraquat, the aptamers selectively bounded to paraquat and forming to complexes. Hence, the adding of positively charged PDDA led to electric neutralization on the surface of

AuNPs, resulting in the aggregation of AuNPs (Ran and Wu, 2019). However, the color changes of AuNPs from dark purple to blue made them difficult to observe by naked eyes and low sensitivity. Therefore, this work is interesting to design the DNA aptamer specific to paraquat and to use it for developing the highly sensitive detection system for paraquat.



CHAPTER III

MATERIAL AND METHODS

3.1 Preparation and characterization of citrate-capped AuNPs

AuNPs were synthesized using the classical citrate reduction method (McFarland et al., 2004). Sodium citrate solution (58 mM, 2 ml) was rapidly injected into the boiling solution of H₂AuCl₄ (1 mM, 20 ml) with vigorous stirring. After the reactions were boiled for various times (3, 5, 10, and 15 min), they were cooled down at room temperature. The reactions were measured the absorbance in a range of 300–900 nm using a UV-Vis spectrophotometer (Analytik Jena Specord® 250 Plus, Jena, Germany). The formation of AuNPs was determined by the wine-red color of the reaction and the characteristic surface plasmon resonance peak of AuNPs. The optimal reaction time was determined by the lowest time that yield the highest amount of AuNPs. The synthesized AuNPs were stored at 4 °C until use.

The morphology and size of the synthesized AuNPs were analyzed by transmission electron microscope (TEM; Tecnai G2 S-Twin, FEI, Hillsboro, OR, USA). The colloidal AuNPs were dropped on a carbon-coated copper holder and dried at room temperature. Then, the samples were observed under TEM operating at 200 kV and TEM images were taken by a Gatan Orius 200 CCD Camera equipped with the TEM. The particle size and its distribution were determined from 500 particles in TEM images, which were analyzed by ImageJ software (National Institutes of Health, Bethesda, MD, USA) and OriginPro 2015 software (OriginLab Corporation,

Northampton, MA, USA), respectively. Furthermore, the crystalline nature of AuNPs was further identified by selected area electron diffraction (SAED) analysis, which were equipped with TEM.

3.2 Production of DNA-aptamer selective for paraquat

The DNA-aptamers were designed based on the aptamer reported by Ran and Wu (Ran and Wu, 2019), which it contained 68 oligonucleotides. Based on the secondary structure of this aptamer (Figure 3.1), it contained three small structural loops.

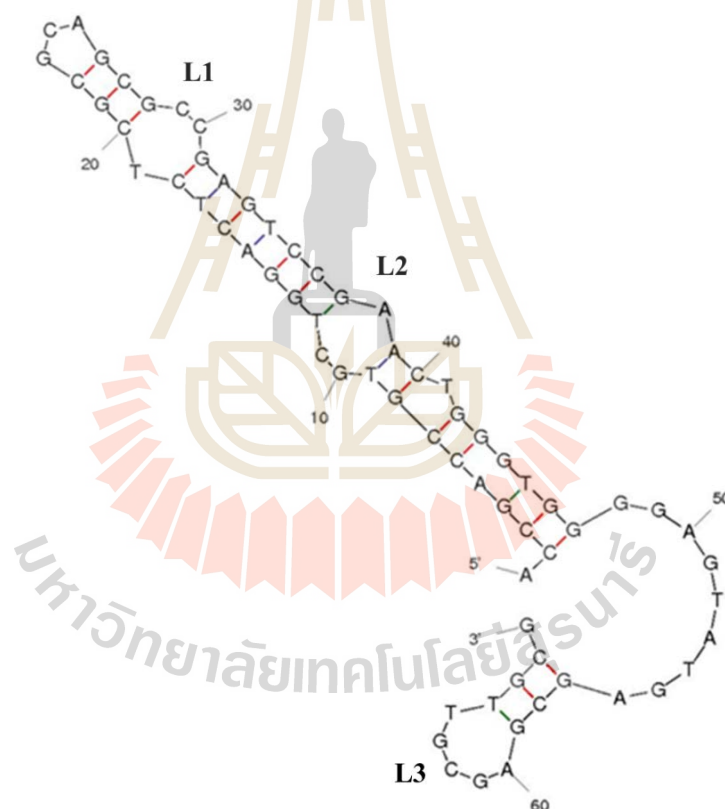


Figure 3.1 The secondary structure of paraquat aptamer containing 3 small structural loops (L1, L2, and L3).

The DNA-aptamers for paraquat were designed, which were based on these small structural loops; L2 and L3 aptamers. Also, the aptamers contained multiple structural loops in the linear (L) and branched (B) shapes were designed as seen in Figure 3.2. The aptamers with 2-5 structural loops in a linear shape referred to as P3-L2, P3-L3, P3-L4, and P3-L5, which consisted of 22, 31, 40, and 49 nucleotides, respectively. Those in a branched shape referred to P3-B2, P3-B3, P3-B4, and P3-B5, which consisted of 31, 45, 59, and 73 nucleotides, respectively.

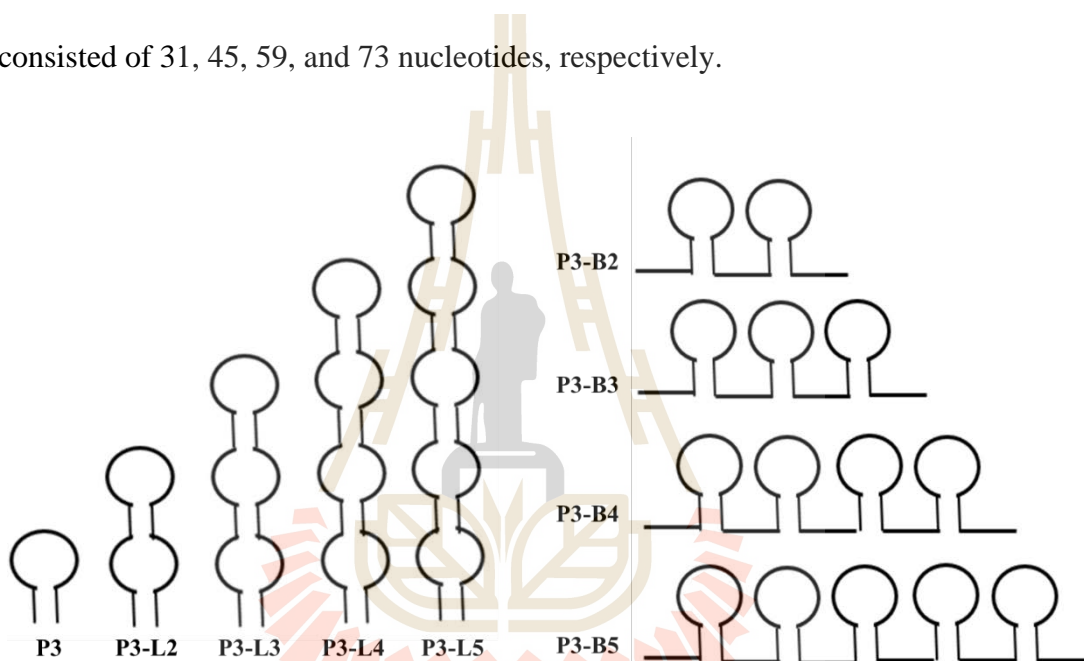


Figure 3.2 The designed aptamers in this work.

The efficiency of the designed DNA aptamers were evaluated by SYBR Green I competitive assay (McKeague et al., 2014), which was based on the competitive binding between paraquat and SYBR Green I to the active stem-loop structure of DNA-aptamer. In this assay, each DNA-aptamer was denatured at 95 °C for 5 min and cooled down slowly at room temperature. Then, the DNA-aptamer was incubated with or without paraquat for 5 min, followed by SYBR Green I (SG, 4×) for 30 min. The

fluorescence spectra were measured using the excitation at 497 nm and the emission in a range of 510– 700 nm. The efficiency of DNA-aptamer was determined using the equation (1), where F_0 was the fluorescence intensity in the absence of paraquat and F was the fluorescence intensity with the presence of paraquat.

$$\text{DNA aptamer efficiency} = (F_0 - F) / F_0 \quad \dots\dots\dots (1)$$

3.3 Production of paraquat detection systems

In this work, two paraquat detection systems were developed; citrate-capped AuNP and aptamer-AuNP systems.

3.3.1 Citrate-capped AuNP system

The optimized condition for the paraquat detection based on citrate-capped AuNP system was determined, in which the optimal NaCl concentration was determined. In a total volume of 100 μl , the citrate-capped AuNPs (9 nM) were mixed with different concentrations of NaCl ranging from 0-50 mM, before incubating at room temperature for 10 min. The absorbance at 525 nm (A_{525}) was measured by the Bio Tek® microplate reader (Winooski, VT, USA). The optimized concentration of NaCl was determined by the lowest concentration of NaCl that induced a complete aggregation of AuNPs.

3.3.2 Aptamer-AuNP system

The optimized condition for the paraquat detection based on aptamer-AuNPs was determined, in which NaCl and DNA-aptamer concentrations were determined. To determine the optimal concentration of NaCl, the synthesized AuNPs (9 nM) were mixed with various concentrations of NaCl (0–50 mM) in a total volume of 100 μl before incubating at room temperature for 10 min. The A_{525} values were measured by

the microplate reader. The optimized concentration of NaCl was determined by the lowest concentration of NaCl that induced a complete aggregation of AuNPs. To determine the optimal concentration of aptamer, the synthesized AuNPs (9 nM) were mixed with various concentrations of DNA-aptamer (5–35 nM) before incubating for 30 min at room temperature. The optimal concentration of NaCl was then added to the solution and further incubated for 10 min before measuring the A_{525} values. The optimized concentration of aptamer was determined by the lowest concentration of aptamer that prevent the NaCl-induced aggregation of AuNPs.

3.4 Sensitivity of detection

3.4.1 Sensitivity of detection of citrate-capped AuNP system

To evaluate the sensitivity of detection of the citrate-capped AuNP system, in a total volume of 200 μ l, citrated-capped AuNPs (9 nM) were mixed with/without NaCl (optimized concentration, 9 μ l) before various concentrations (4-320 μ M) of paraquat (100 μ l) were added. After incubating for 10 min, the absorbance spectra at 300-900 nm were measured by a UV-Vis spectrophotometer. The absorption ratio of A_{690}/A_{525} was determined, in which A_{690} and A_{525} were used to determine the aggregated and free forms of AuNPs, respectively. The sensitivity of detection of the citrate-capped AuNP system was determined by the limit of detection concentration (C_{LOD}). The C_{LOD} was calculated by the equation (2), where “a” represented the y-intercept and “b” represented the slope of the paraquat calibration curve. The calibration curve was plotted between the A_{650}/A_{525} values and the paraquat concentrations with the linear regression fit ($y = a + bx$), which A_{525} and A_{690} referred to the maximum absorptions of free and aggregated states of AuNPs, respectively. The minimum

detectable signal of replicated blank readings (Y_{LOD}) is calculated by the equation (3), where Y_{blank} and SD_{blank} were the average A_{690}/A_{525} value and the standard deviation as determined by a measurement of blank samples in the condition without paraquat, respectively.

$$C_{LOD} = (Y_{LOD} - a)/b \quad \dots\dots\dots(2)$$

$$Y_{LOD} = Y_{Blank} + 3SD_{Blank} \quad \dots\dots\dots(3)$$

3.4.2 Sensitivity of detection of aptamer-AuNP system

The sensitivity of the aptamer-AuNP system was determined by incubating the optimal aptamer concentration with 9 nM AuNPs at room temperature for 30 min before adding different concentrations of paraquat (0.5-10 nM). After incubating for 30 min, 10 μ l NaCl (optimized concentration) was added into the mixture and incubated at room temperature for 10 min. The absorption spectra at 300-900 nm were measured and the A_{650}/A_{525} values were determined by a microplate reader. The sensitivity of detection of the aptamer-AuNP system was determined by the C_{LOD} as mentioned above.

3.5 Selectivity of detection

3.5.1 Selectivity of detection of citrate-capped AuNP system

The selectivity of the citrate-capped AuNP system was determined by testing with the commonly used herbicides, including difenzoquat, glufosinate, 2,4-D dimethyl ammonium, atrazine, and ametryn (Figure 3.3). The citrate-capped AuNPs (9 nM) and NaCl (optimized concentration) were mixed well before adding the equal volume (100 μ l) of the tested herbicides (40 μ M). After incubating at ambient temperature for 5 min,

the A_{690}/A_{525} values were determined. The A_{690}/A_{525} values of the tested herbicides were compared with that of paraquat.

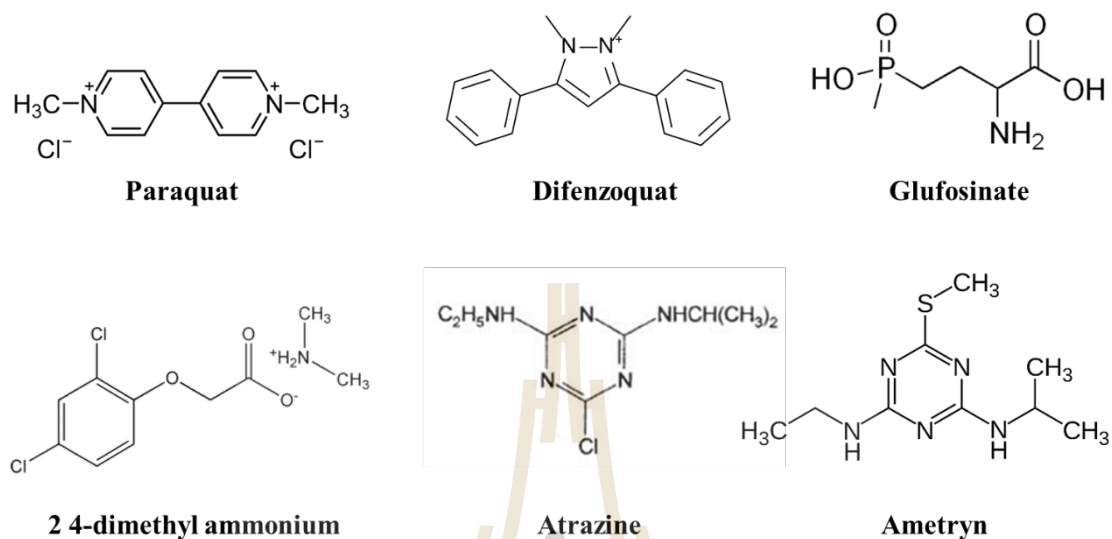


Figure 3.3 The structures of the tested herbicides.

3.5.2 Selectivity of detection of aptamer-AuNP system

The selectivity of detection of the aptamer-AuNP system was also determined. The mixture (120 μl) of aptamer and AuNPs (optimized concentrations) were prepared and incubated at room temperature for 30 min. Then, 15 μl of 25 nM tested herbicides were added and incubated for 30 min. The optimal concentration NaCl was added (15 μl) into the solution and further incubated for 10 min. The A_{650}/A_{525} values were measured by a microplate reader. The selectivity of detection was compared among these herbicides.

3.6 Interference of natural water on the detection

3.6.1 Evaluation of spiked paraquat in tap and pond water by the citrate-capped AuNP system

To determine whether water from different sources could interfere the detection of the developed system, the recovered concentration of the standard paraquat spiked in tap-water and pond-water was determined. These water samples were collected from the Suranaree University of Technology. One hundred microliters of paraquat (2, 4, and 8 μM), that was dissolved in tap-water and pond-water, were mixed with equal volume of citrate-capped AuNPs (9 nM) containing NaCl. After incubating at room temperature for 10 min, the A_{690}/A_{525} values were measured. The paraquat concentration was calculated by the standard curve plotted between the A_{690}/A_{525} values and the standard paraquat concentrations. The percent recovery of paraquat was determined by the division between the measured concentration (C_{measured}) and the known concentration (C_{known}) as shown in equation (4). To confirm the precision of this system, the percent relative standard deviation (%RSD) was calculated by the equation (5).

$$\text{The percent of recover} = (C_{\text{measured}} / C_{\text{known}}) \times 100\% \quad \dots\dots (4)$$

$$\text{The percent relative standard deviation} = (\text{standard deviation}/\text{mean}) \times 100\% \quad \dots\dots (5)$$

3.6.2 Evaluation of spiked paraquat in kale sample by the citrate-capped AuNP system

Paraquat (2.0, 4.0, and 8.0 μM) was added onto the organic kale and kept at room temperature for 6 h. The spiked-paraquat was extracted from kale samples according the method of Zou (Zou et al., 2014). Grinded kale sample (1 g) was mixed

with 10 ml water before incubating in the sonication water bath at 50 °C for 1 h. The sample was centrifuged at 6,000×g for 20 min and the supernatant was collected. To detect the spiked-paraquat, AuNPs (9 nM) was mixed with the extracted supernatant, following by the addition of NaCl. After incubating at ambient temperature for 5 min, the sample was measured at A_{690} and A_{525} . The recovery rate and the %RSD were calculated according to the equations 4 and 5, respectively.

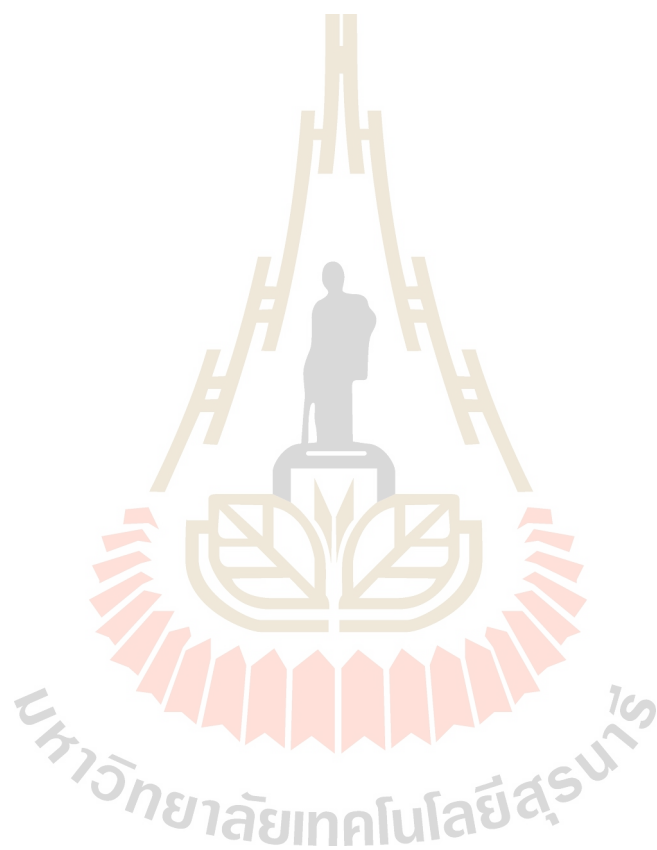
3.6.3 Evaluation of spiked paraquat in tap and pond water by the aptamer-AuNP system

The effect of water from different sources to interfere the detection of the aptamer-AuNP system was determined by measuring the concentration of the standard paraquat spiked in tap-water and pond-water, which were collected from the Suranaree University of Technology. AuNPs (9 nM, 100 μ l) were incubated with aptamer (optimal concentration, 20 μ l) for 30 min at room temperature. Fifteen μ l of paraquat (0.5, 2.0, and 8.0 nM in tap-water and pond-water) were added and further incubated for 30 min. NaCl was then added and incubated at room temperature for 10 min before measuring the A_{650}/A_{525} values. The paraquat concentration was calculated by the standard curve plotted between the A_{650}/A_{525} values and the standard paraquat concentrations. The percent recovery of paraquat was determined by equation (4). The percent of RSD was calculated by equation (5) to evaluate the precision of the system.

3.7 Statistical analysis

All experiments were performed at least three replicates and represented as means and standard deviations (SD). The statistical analysis was performed using SPSS version 11.5 statistical software program (SPSS, Chicago, IL, USA). For more than 2

groups of samples, one-way ANOVA was used to analyze their variances and the differences of each data pair were determined by Tukey's multiple comparison test. The statistical difference was significant at $p < 0.05$.



CHAPTER IV

RESULTS AND DISCUSSIONS PART I

Development of paraquat detection system based on citrate-capped AuNPs

4.1 Synthesis and characterization of citrate-capped AuNPs

Citrate-capped AuNPs were produced by the reduction synthesis (Doyen et al., 2013). The formation of AuNPs in a time course of 15 min was determined, which the results were shown in Figure 4.1. The formation of AuNPs was determined by the red-wine color of the reaction and the characteristic surface plasmon resonance (SPR) peak of AuNPs at 525 nm (Paul et al., 2015). The optimal time for the synthesis was 5 min, which indicated by the highest intensity of the SPR peak. The synthesized AuNPs were well dispersed, suggesting that AuNPs were well coated with citrate. The citrate-capped AuNPs were negatively charges due to the charge of citrate, resulting in electrostatic repulsion between the particles (Huang et al., 2018).

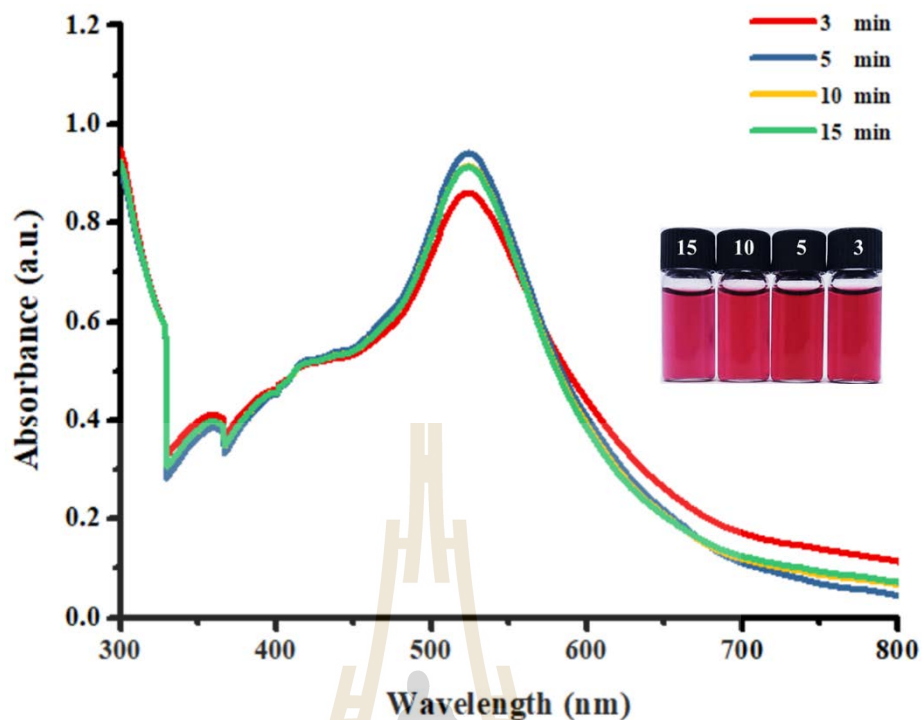


Figure 4.1 UV-Vis spectra of the formation of AuNPs in a time course of 15 min.

The morphology and size of the synthesized AuNPs were analyzed by TEM analysis. The TEM image (Figure 4.2A) revealed the spherical AuNPs and their average size was 12.88 ± 3.02 nm as determined by measuring 500 particles. To confirm the identity of the synthesized AuNPs, the SAED-TEM was analyzed. The SAED pattern (Figure 4.2B) demonstrated four diffraction rings of the synthesized AuNPs, which were (111), (200), (220), and (311) planes of Au^0 (Umamaheswari et al., 2018).

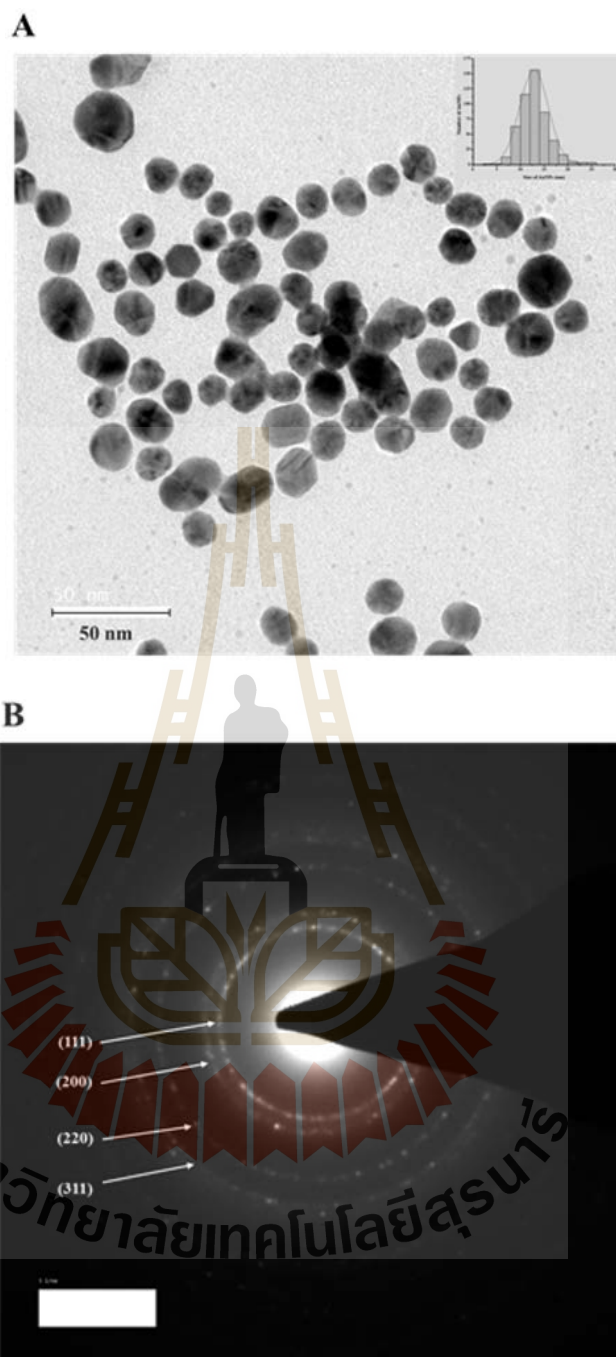


Figure 4.2 TEM image (A) and SAED pattern (B) of the citrate-capped AuNPs.

4.2 Optimal condition for paraquat detection by citrate-capped

AuNPs

The paraquat detection system based on citrate-capped AuNPs under the presence and absence of NaCl was studied in this chapter. The optimal concentration of NaCl was determined, which the results are shown in Figure 4.3. The UV-Vis spectra indicated that the increased concentrations of NaCl resulted in the reduction of the A_{525} values, suggesting that the aggregation of AuNPs depended on NaCl concentration. The optimal concentration of NaCl was 35 mM since it was the lowest concentration of NaCl causing an entire aggregation of AuNPs. NaCl can stimulate the aggregation of AuNPs due to the interaction between sodium ion and the carboxyl group of citrates on the surface of AuNPs. This process decreased the surface charges of AuNPs, therefore disrupted the stability of AuNPs and allowed the formation of larger AuNPs, resulting in the aggregation of AuNPs (Dominguez-Medina et al., 2013).

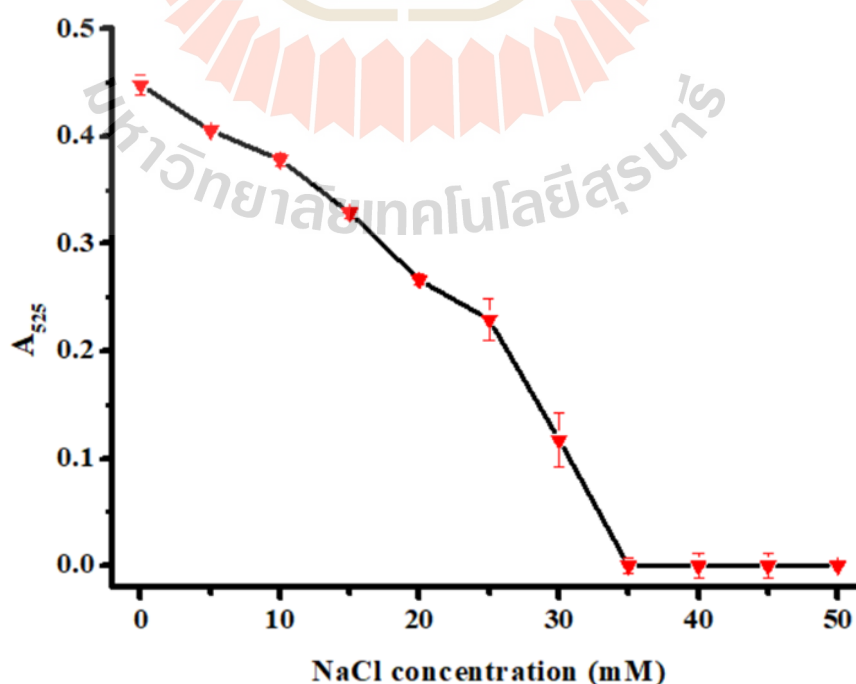


Figure 4.3 Optimal concentration of NaCl for the paraquat detection system.

4.3 Sensitivity of the citrate-capped AuNP system

In this system, the negatively charged citrate-capped AuNPs could interact with the positively charged paraquat via the electrostatic force under the NaCl condition, resulting in the aggregation of AuNPs. Thus, the color of AuNPs was changed from red to blue, which the intensity of blue color reflected the concentration of paraquat (Siangproh et al., 2017). It is noted that paraquat comprises quaternary amines at both ends of the molecule, which tend to be positively charged and readily interact with the negatively charged molecules of the citrate.

4.3.1 The citrate-capped AuNP system without NaCl

The detection sensitivity of this system was determined by varying the concentration of paraquat (4-320 μM), which the results were shown in Figure 4.4. With the increasing paraquat concentrations, the SPR peak intensity of the dispersed AuNPs at 525 nm decreased (Figure 4.4A). In contrast, the SPR peak intensity of the aggregated AuNPs at 690 nm of increased, which well corresponded to the appearance of blue color. As the A_{690}/A_{525} values were plotted against the concentration of paraquat (Figure 4.4B), both values were in a fitted linear relationship in a range of 4-160 μM paraquat. The limit of detection concentration (C_{LOD}) of the citrate-capped AuNP system for paraquat detection was at 15.32 μM . It is noted that a maximum concentration allowance (MAC) of paraquat in water for a freshwater animal defined by the Pollution Control Department of Thailand is 2.0 μM (0.5 mg/L) (Chuntib and Jakmune, 2015). At this permission level, this detection sensitivity of the developed system is inadequate, therefore, the enhancement of detection sensitivity was further studied.

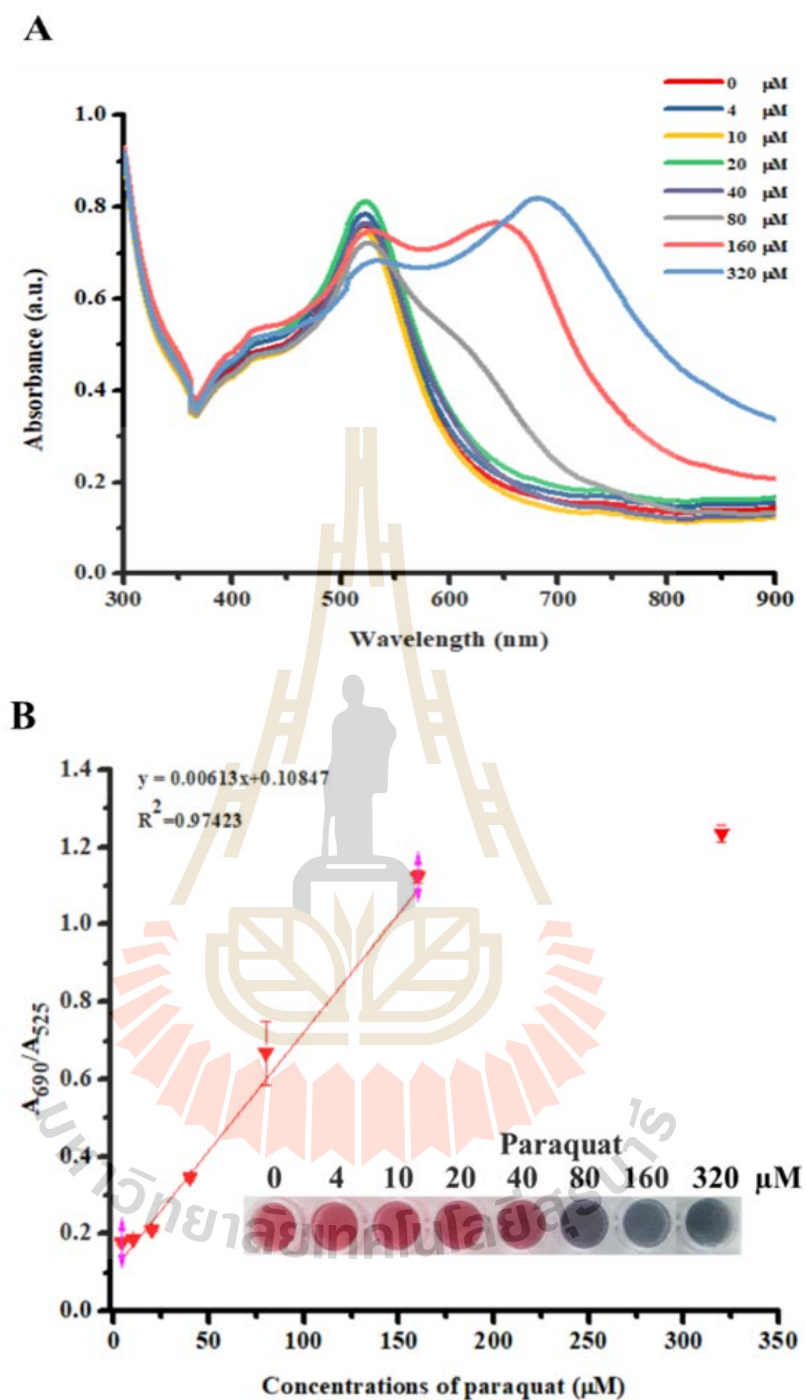


Figure 4.4 UV-Vis spectra of the citrate-capped AuNPs without NaCl in the presence of different concentrations of paraquat (A) and the linear relationship between the A_{690}/A_{525} values and paraquat concentrations (B).

4.3.2 The citrate-capped AuNP system with NaCl

To enhance the detection sensitivity, the citrate-capped AuNP system with NaCl was studied. The citrate-capped AuNPs were mixed with an optimum concentration of NaCl before adding paraquat. Figure 4.5A shows the UV-Vis spectra of AuNPs in the presence of various concentrations of paraquat (4-320 μM). The results clearly demonstrated that the SPR peak intensity at 525 nm of the dispersed AuNPs was gradually decreased with increasing concentrations of paraquat, while the SPR peak intensity at 690 nm was significantly increased. The blue color of AuNPs was observed by naked eyes as low as 4 μM paraquat. The calculated C_{LOD} was at 1.59 μM , which was lower than that of the citrate-capped AuNP system without NaCl. The A_{690}/A_{525} values were plotted against the concentration of paraquat (Figure 4.5B). The linear relationship between the A_{690}/A_{525} values and paraquat concentrations was in a range of 2-32 μM with the correlation coefficient of 0.99425. Compared to the previous system (without NaCl), the sensitivity of paraquat detection was greatly improved for 5 folds from the naked eyes and 10 folds from the C_{LOD} . It was proposed that NaCl could reduce the negative charges on the surface of AuNPs, resulting in the increased aggregation of colloid AuNPs with lower concentration of paraquat, often referred to as the "salting-out" effect. As this detection limit of the developed assay, it was feasible for the evaluation of paraquat residue in the aquatic environment of Thailand, in which the permission level of paraquat in water for was 2.0 μM (0.5 mg/L) (Chuntib et al., 2017).

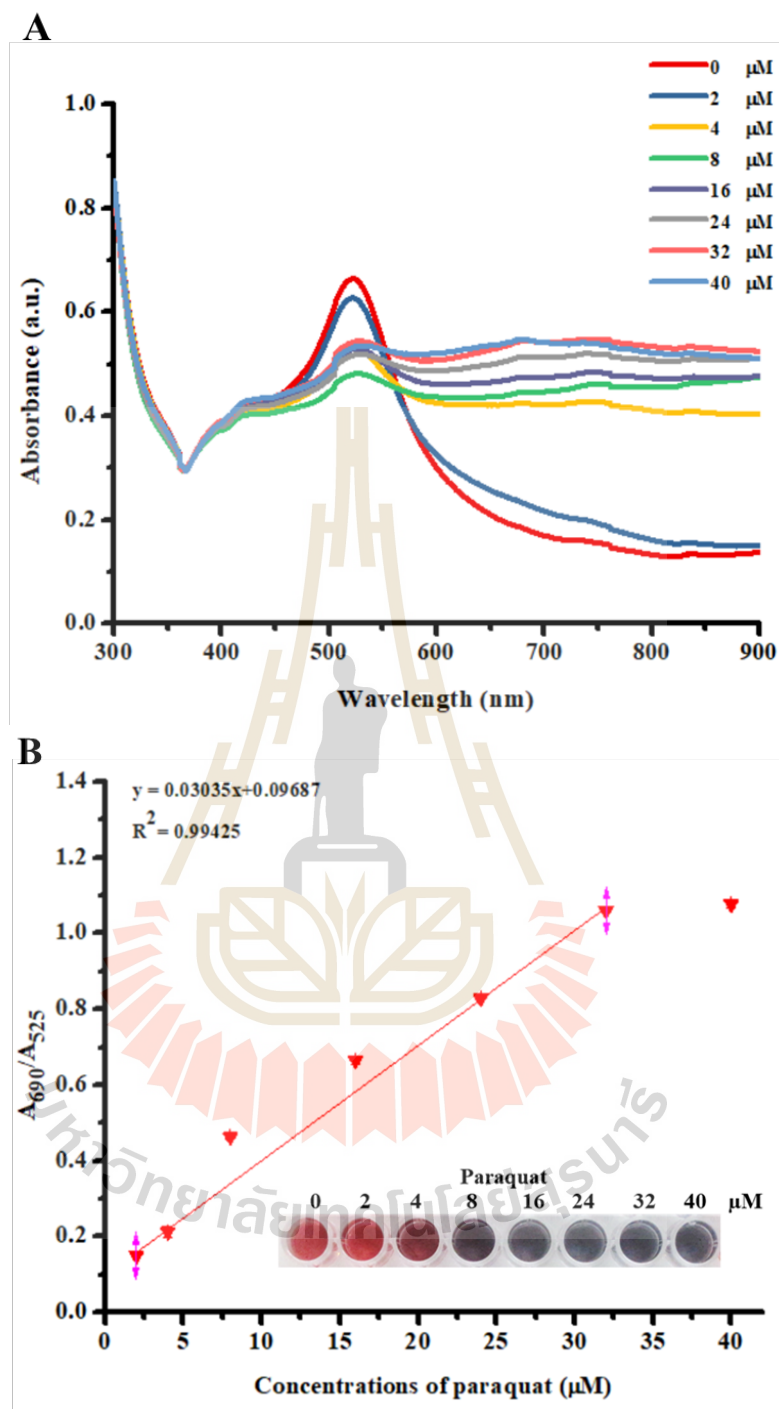


Figure 4.5 UV-Vis spectra of the citrate-capped AuNPs with NaCl in the presence of different concentrations of paraquat (A) and the linear relationship between the A_{690}/A_{525} values and paraquat concentrations (B).

4.4 Selectivity of the citrate-capped AuNP system

The commonly used herbicides in Thailand, including the positively charged herbicides (difenzoquat, atrazine, and ametryn) and negatively charged herbicides (glufosinate and 2,4-D dimethyl ammonium), were tested to evaluate the selectivity of the citrate-capped AuNPs system. As seen in Figure 4.6, the absorption ratio of A_{690} and A_{525} indicates low and negligible values for these tested herbicides as compared to paraquat under the same condition. The citrate-capped AuNP system demonstrated a selective binding to paraquat, even when compared to difenzoquat, which has a similar structure and charge. It is likely that difenzoquat has a lower water-soluble capacity and contains only a single positively-charged site (Siangproh et al., 2017). Therefore, it has a significantly low selectivity to the developed system. Based on their structure, atrazine and ametryn contain a three-nitrogen hybrid ring similar to melamine, which can effectively disturb the stabilization of AuNPs (Wei et al., 2010). However, they have a steric hindrance of the structure as compared with paraquat. Therefore, they are difficult to interact with the citrate-capped AuNPs, resulting in no induction of AuNP-aggregation. In the case of the negatively charged herbicides, the effect of the electrostatic interaction introduces the repulsion of citrate and the negatively charged herbicides. As a result, the dispersed AuNPs were still held by the surrounded citrate.

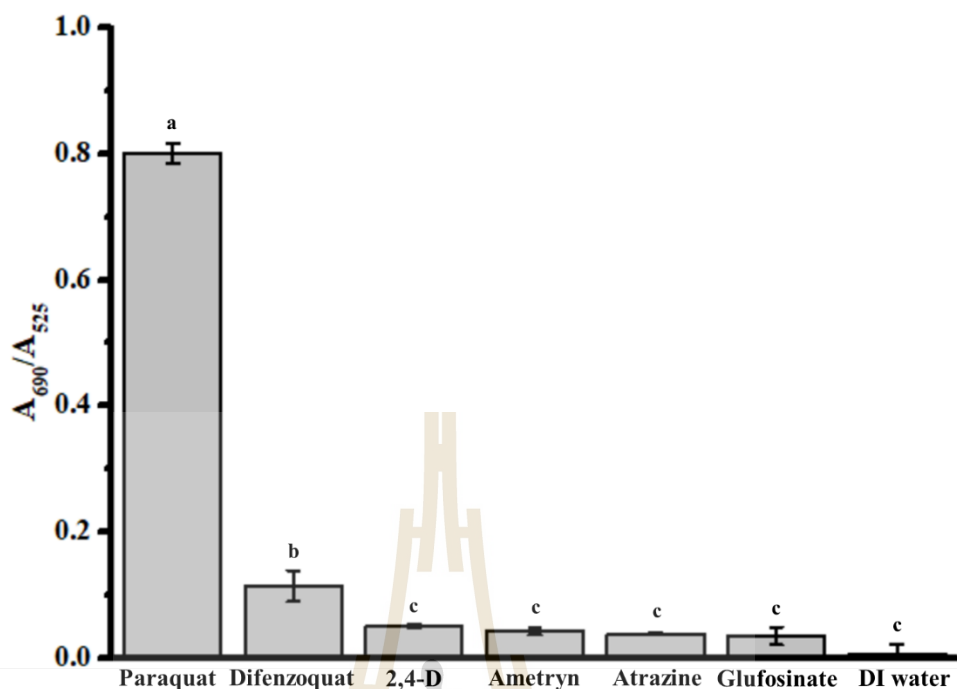


Figure 4.6 The selectivity of the citrate-capped AuNP system for paraquat detection

4.5 Interference of natural water on the detection by the citrate-capped AuNP system

To evaluate the practical application of the citrate-capped AuNP system, paraquat-spiked water, derived from the tap- and pond-water, was determined by the developed system. As illustrated in Table 4.1, the recovery rates of paraquat in the tap- and pond-water were in a range of 98.3–109.5 %. The corresponding standard deviations were less than 5.0 %. The results indicated the adequate precision and reliability of paraquat detection in actual samples (Qi et al., 2019).

Table 4.1 Detection of paraquat-spike water using the citrate-capped AuNP system.

Sample	Added (μM)	Found (μM)	Recovery (%)	RSD (%) ⁿ
Tap water	2.0	2.10	105.0	3.88
	4.0	4.38	109.5	3.66
	8.0	8.20	102.5	2.92
Pond water	2.0	1.99	99.5	3.95
	4.0	3.93	98.3	3.17
	8.0	8.35	104.4	4.27

Note: n = 3.

4.6 Interference of vegetable samples on the detection by the citrate-capped AuNP system

To further verify the practical capability and reliability of the developed system, the paraquat-spiked organic kale was chosen for spiking experiments. The result was showed in Table 4.2, in which the recovery rate of paraquat in the kale samples was in a range of 90.5–107.8 % and RSD were less than 3.0 %. These results suggested that the developed system was reliable and practical for paraquat detection in vegetable samples because of the low interference from the vegetable components.

Table 4.2 Detection of paraquat-spike vegetable using the citrate-capped AuNP system.

Sample	Added (μM)	Found (μM)	Recovery (%)	RSD (%) ⁿ
Kale	2.0	1.81	90.5	2.74
	4.0	3.76	94.0	0.44
	8.0	8.62	107.8	0.56

Note: n = 3.



CHAPTER V

RESULTS AND DISCUSSIONS PART II

Development of paraquat detection system based on aptamer AuNPs

5.1 Production of DNA-aptamer selective for paraquat

In this chapter, the research focused on developing the improved paraquat detection system using a DNA-aptamer. In 2019, Ran and Wu reported the sequence of the paraquat-aptamer containing 68 nucleotides (Ran and Wu, 2019), which its structure consisted of two inner loops and one hairpin structure, designated as the L1 inner loop, L2 inner loop, and L3 hairpin (Figure 5.1A). Based on the report of Eisold and Labudde, they suggested that a specific sequence of a small loop and hairpin structure of an aptamer were potentially vital for the binding affinity and selectivity to its target molecule (Eisold and Labudde, 2018). Thus, this work aimed to investigate the crucial paraquat-binding sequence of the aptamer reported by Ran and Wu. Based on the L1 region of the aptamer, its nucleotide sequence likely unfitted with the paraquat structure. The small L2 loop and L3 hairpin structure of the aptamer consisted of the potential nucleotide sequence to capture a paraquat structure. So they were analyzed for the possible bindings to a paraquat molecule using the molecular dynamic simulation (Gromacs software). So, two aptamers (P2 and P3) were designed and

synthesized as short hairpin aptamers (Figure 5.1B-C). Their sequences were modified from the L2 inner loop and L3 hairpin, respectively.

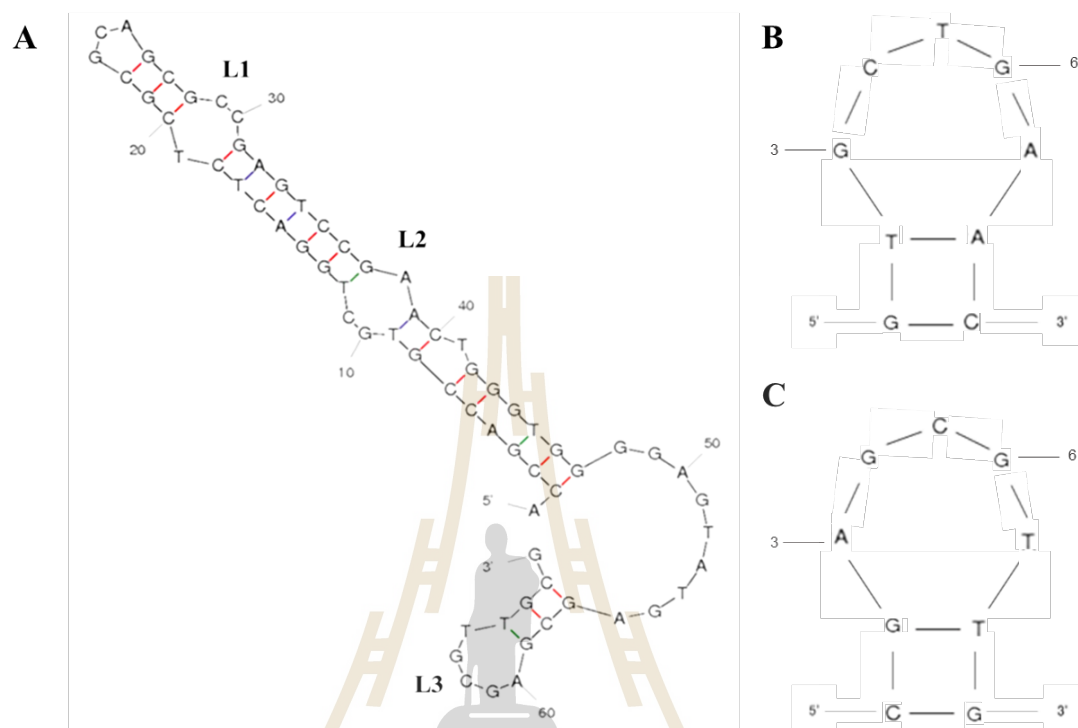


Figure 5.1 The predicted secondary structures of the paraquat-aptamer (A), the modified P2 aptamer (B), and the modified P3 aptamer (C).

The molecular dynamic simulations of the bindings of P2 and P3 aptamers to paraquat were analyzed by GROMACS software. In principle, the binding of target molecules and DNA aptamers is mainly non-covalent bonds, including van der Waals forces, hydrogen bonds, and electrostatic interactions (Phanchai et al., 2018). The distance values of van der Waals forces are typically observed at 0.6 nm for large biomolecules (Rhinehardt et al., 2015). The hydrogen bonding between target and aptamer was generally found with a distance lower than 0.35 nm with a corresponding angle of 30° or less (Rudling et al., 2018). In general, the cutoff distance (d_c) of 0.45 nm was used for noncovalent target-aptamer binding. Also, the proximate or lower d_c

value for at least 20 ns was suggested for the target-aptamer binding (Toomjeen et al., 2019). Therefore, this work was considered the molecular dynamic simulation having d_c of 0.45 nm for at least 20 ns to indicate the binding between paraquat and aptamer.

Figure 5.2 showed the molecular dynamic simulation of P2 aptamer binding to paraquat indicating the distance between the base index and paraquat, and the predicted number of hydrogen bonds in a time course of 0–100 ns. The distances between base index and paraquat were shown with different colors. As seen in Figure 5.2A, the results showed three possible states of paraquat-aptamer interaction; states I, II, and III. State I (7th base) and II (6th base) were transient states as these interactions were less than 20 ns (Figure 5.2C). State III (1st and 9th bases) with the d_c value of 0.25 nm was the bound paraquat-aptamer state since it was stable for more than 30 ns. With hydrogen bond analysis (Figure 5.3B), the result revealed no hydrogen bonding between paraquat and aptamer. Yoshida and colleagues reported the electrostatic interaction between antigen and heavy- and light-chain variable domains had the distance in a range of 0.28-0.43 nm. Therefore, it was possible that the state III of paraquat-aptamer interaction was due to strong electrostatic interaction between paraquat and P2 aptamer (Yoshida et al., 2019).

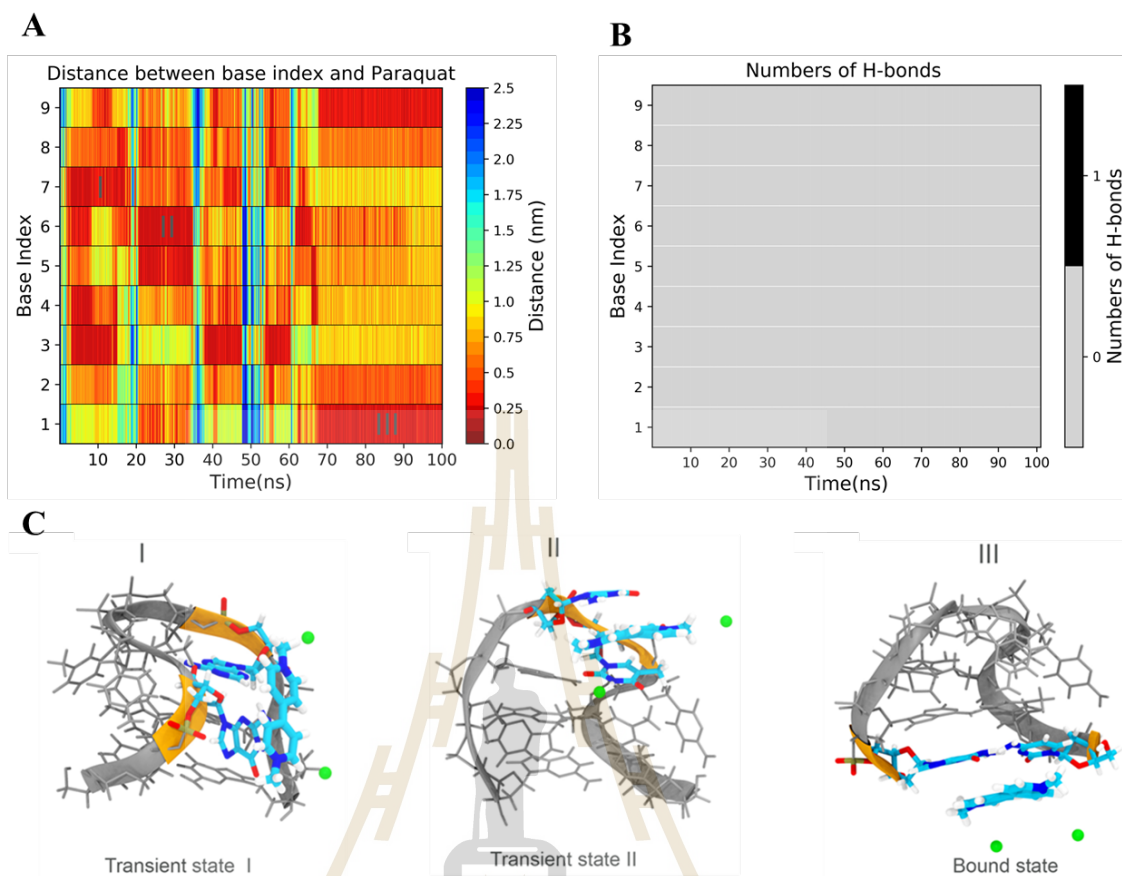


Figure 5.2 The molecular dynamic simulation of P2 aptamer binding to paraquat presenting the average distance (A), the number of hydrogen bond (B), and the interaction states between paraquat and P2 aptamer (C).

In the case of P3 aptamer (Figure 5.3), there were two detected states of paraquat-aptamer interaction; State I and II. State I was transient interaction at the 7th base, which had a distance of 0.25 nm and the interaction time of approximately 10 ns. State II was the bound state at the 2nd and 8th bases, which a distance of 0.25 nm and the interaction time more than 50 ns. Similar to P2 aptamer, the interaction of paraquat and P3 aptamer was not hydrogen bonding but was likely a strong electrostatic interaction between paraquat and P3 aptamer. As compared with P2 aptamer, P3 aptamer exhibited the

greater binding to paraquat considering the longer interaction time of more than 50 ns.

Thus, the P3 aptamer was selected for further experiments.

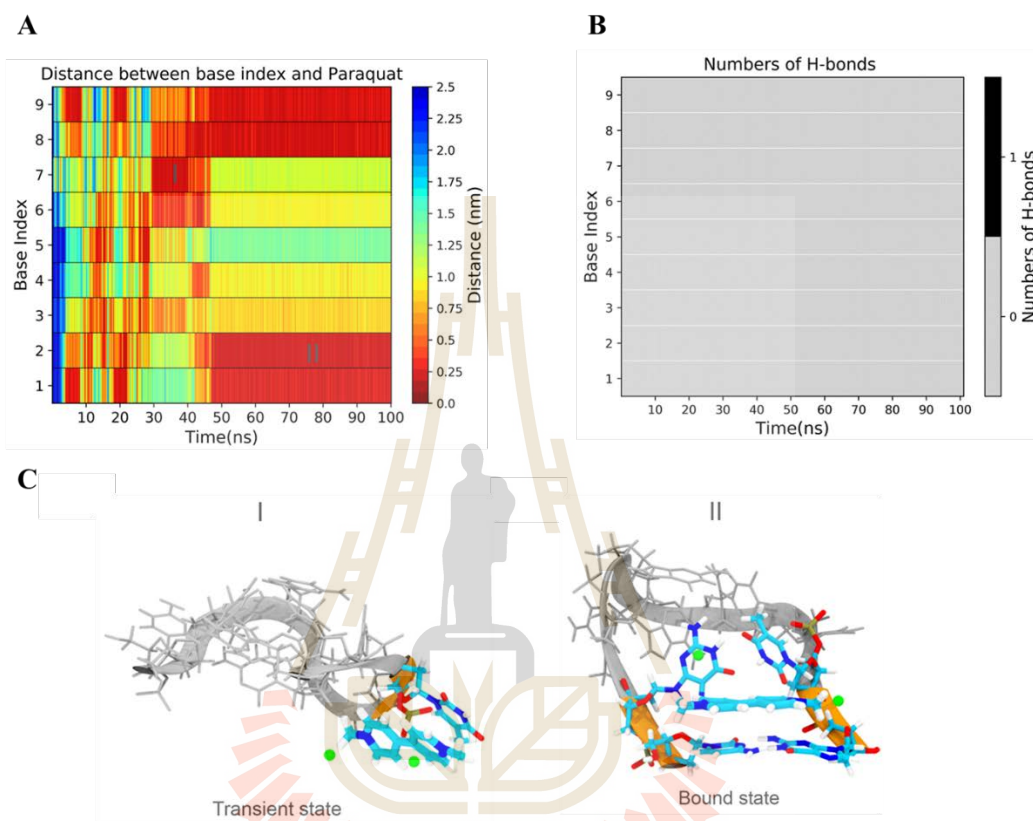


Figure 5.3 The molecular dynamic simulation of P3 aptamer binding to paraquat presenting the average distance (A), the number of hydrogen bond (B), and the interaction states between paraquat and P3 aptamer (C).

To enhance the sensitivity of aptasensors, new aptamers were re-designed using the repetitive sequence of P3 (1-5 repeats) with two different structures (linear and branch). Figure 5.4 shows the new DNA-aptamers in this study, which are the aptamers with linear structure with 2-5 repeated sequences (P3-L2, P3-L3, P3-L4, and P3-L5) and the aptamers with branched structure with 2-5 repeated sequences (P3-B3, P3-B3,

P3-B4, and P3-B5). It was noted that the sequences of all aptamers were not shown as they were in the patenting processes.

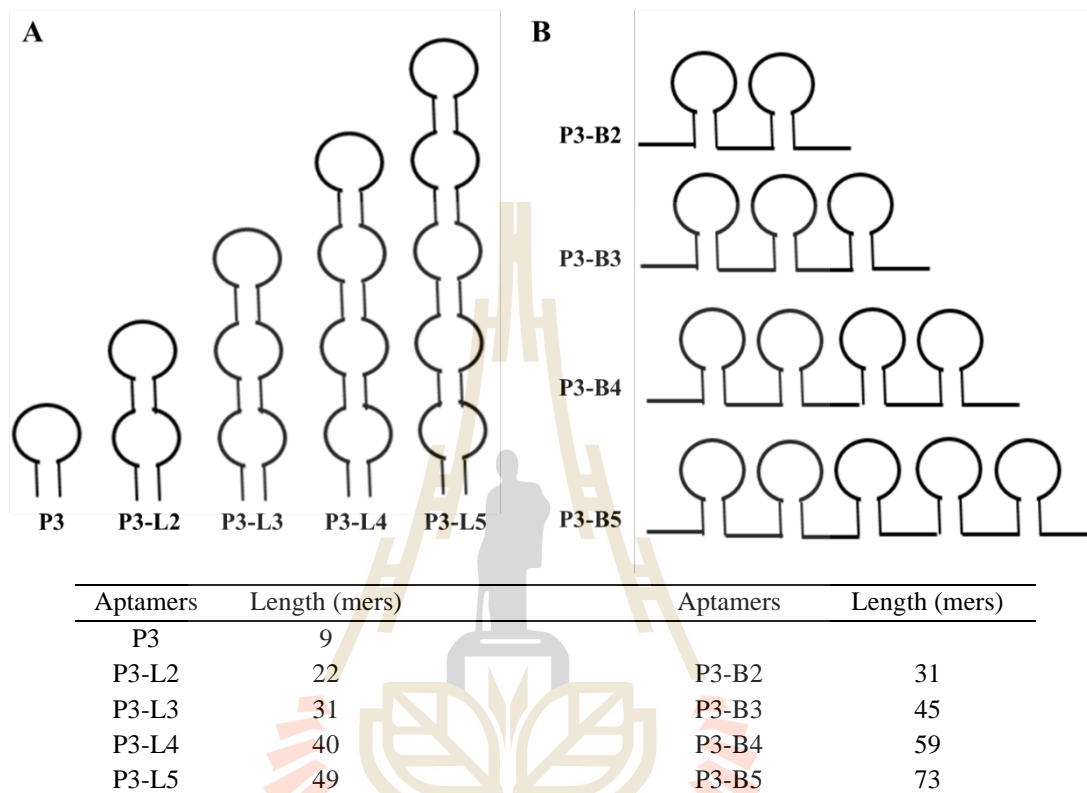


Figure 5.4 The designed DNA-aptamers with the linear structure with 2-5 repeated sequence (P3-L2, P3-L3, P3-L4, and P3-L5) (A) and the branched structure with 205 repeated sequence (P3-B2, P3-B3, P3-B4, and P3-B5) (B) according to the predicted secondary structures by the Mfold software.

The interaction between the designed aptamers and paraquat was evaluated by the SYBR green I competitive assay (McKeague et al., 2014). In principle, when the SYBR green I fluorescent dye intercalates into the secondary structured DNA (aptamer), it has the emission wavelength at 520 nm. With the presence of the target molecule (paraquat), paraquat competitively binds to the aptamer, resulting in the release of free

SYBR green I dye in the solution. Therefore, the intensity of light emission at 520 nm is reduced in response to the strength of aptamer to interact with paraquat. The more reduction of light emission at 520 nm was detected, the greater interaction between aptamer and paraquat was suggested. As seen in Figure 5.5A, all designed aptamers with linear structure (P3-L3, P3-L4, and P3-L5) showed better interaction with paraquat as determined by the greater competitive binding of paraquat to the aptamer. Since P3-L3, P3-L4, and P3-L5 exhibited the highest binding to paraquat, they were selected for the next experiment to develop aptasensors. For the designed aptamers with branched structure, P3-B3, P3-B4, and P3-B5 exhibited a significant increase in binding to paraquat as compared with P3 aptamer.

In this work, the increases of 1-3 loops of the aptamers resulted in the increasing binding capacity of the aptamers to paraquat. It was likely that more loops of aptamers bound more molecules of paraquat, causing the increased sensitivity to detect paraquat. However, the aptamers with 3-5 loops showed no different binding capability to paraquat. It was hypothesized that the given molecules of paraquat were insufficient to show the different capabilities of these aptamers. Comparing between linear and branched structures, linear aptamers exhibited higher binding capability to paraquat as determined by the fluorescence intensity value. For example, the P3-L3 aptamer had a fluorescent value of 0.515, which was higher than that of P3-B3 (0.467). Nevertheless, both structural aptamers of 3-5 loops were used to establish the aptasensor system for paraquat in the next experiment to find the best detection system.

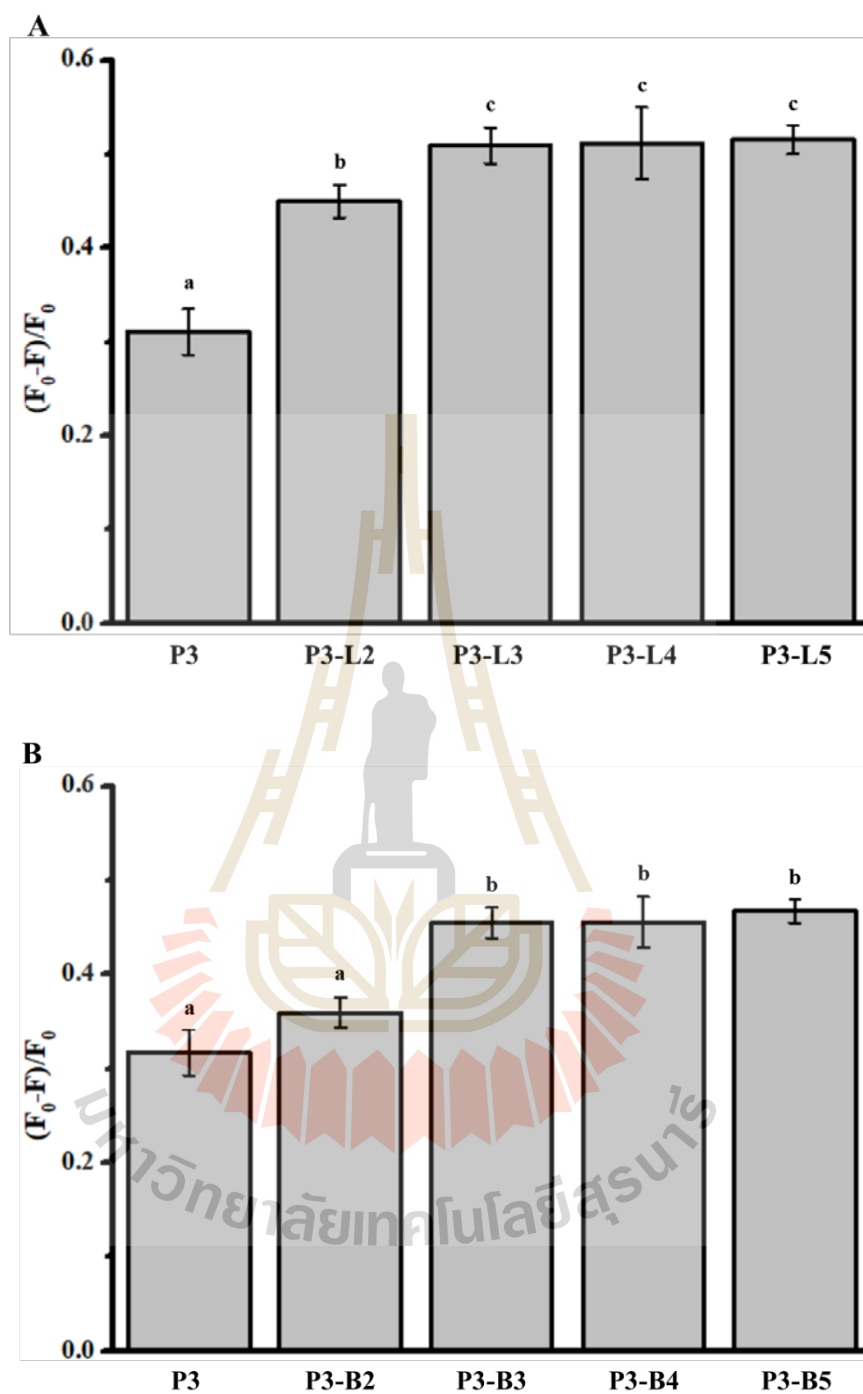


Figure 5.5 The efficiency of the linear form (A) and branched form (B) DNA aptamers evaluated by SYBR Green I competitive assay

5.2 Optimized conditions for the aptamer-AuNP system

In the aptamer-AuNP system, two parameters were needed to optimize before the system was used for paraquat detection; NaCl and aptamer concentrations.

To optimize the concentration of NaCl, AuNPs were mixed with different concentrations of NaCl (0–50 mM) and the SPR peak intensities at 525 nm were monitored. The result showed that the SPR peak intensity was reduced according to the increasing concentrations of NaCl (Figure 5.6), suggesting the effect of NaCl to induce the aggregation of AuNPs. The optimal NaCl concentration was determined by the lowest concentration of NaCl that caused the complete aggregation of AuNPs (the lowest intensity of SPR peak at 525 nm). Therefore, the optimal concentration of NaCl was 35 mM.

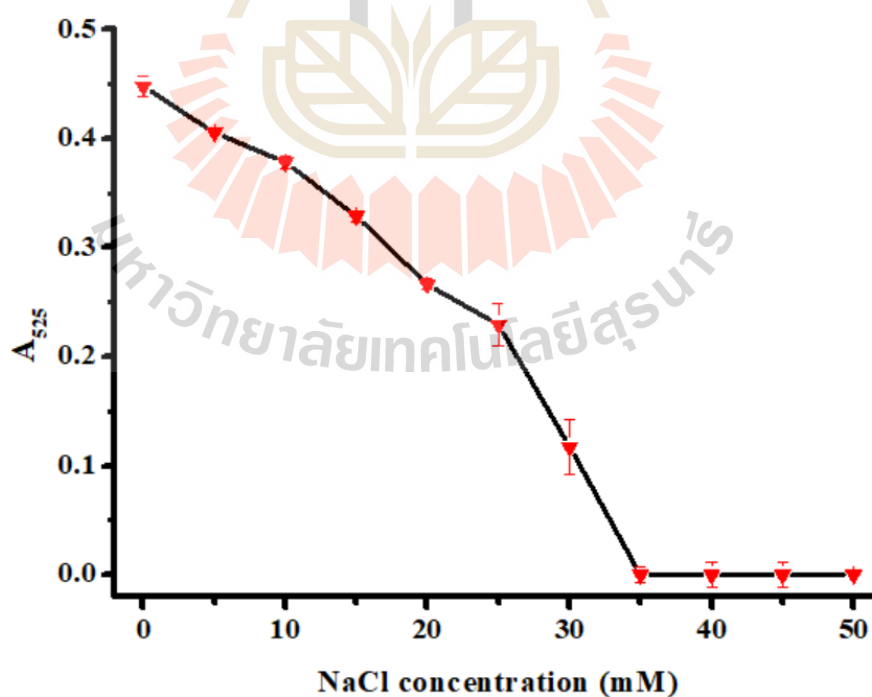


Figure 5.6 Effect of NaCl to induce the aggregation of AuNPs.

In this work, six aptamers were studied; P3-L3, P3-L4, P3-L5, P3-B3, P3-B4, and P3-B5. The optimized concentration of each aptamer was determined by mixing AuNPs with different concentrations of the aptamer before the optimal concentration of NaCl was added. The optimal concentration of aptamer was determined by the lowest concentration of the aptamer that prevented the NaCl-induced aggregation of AuNPs. As seen in Figure 5.7, the increasing concentrations of the aptamer resulted in the greater prevention of the NaCl-induced aggregation of AuNPs as determined by the increasing SPR peak intensities at 525 nm. From the graph, the optimal concentrations of P3-L3, P3-L4, and P3-L5 aptamers were 30, 25, and 25 nM, respectively. Similarly, the optimal concentrations of P3-B3, P3-B4, and P3-B5 aptamers were 30, 25, and 25 nM, respectively. The prevention of the NaCl-induced aggregation of AuNPs occurred from the action of the aptamer to shield the surface of AuNPs from salt ions. Thus, AuNPs were still dispersed even with the presence of salt ions (Alsager et al., 2018).

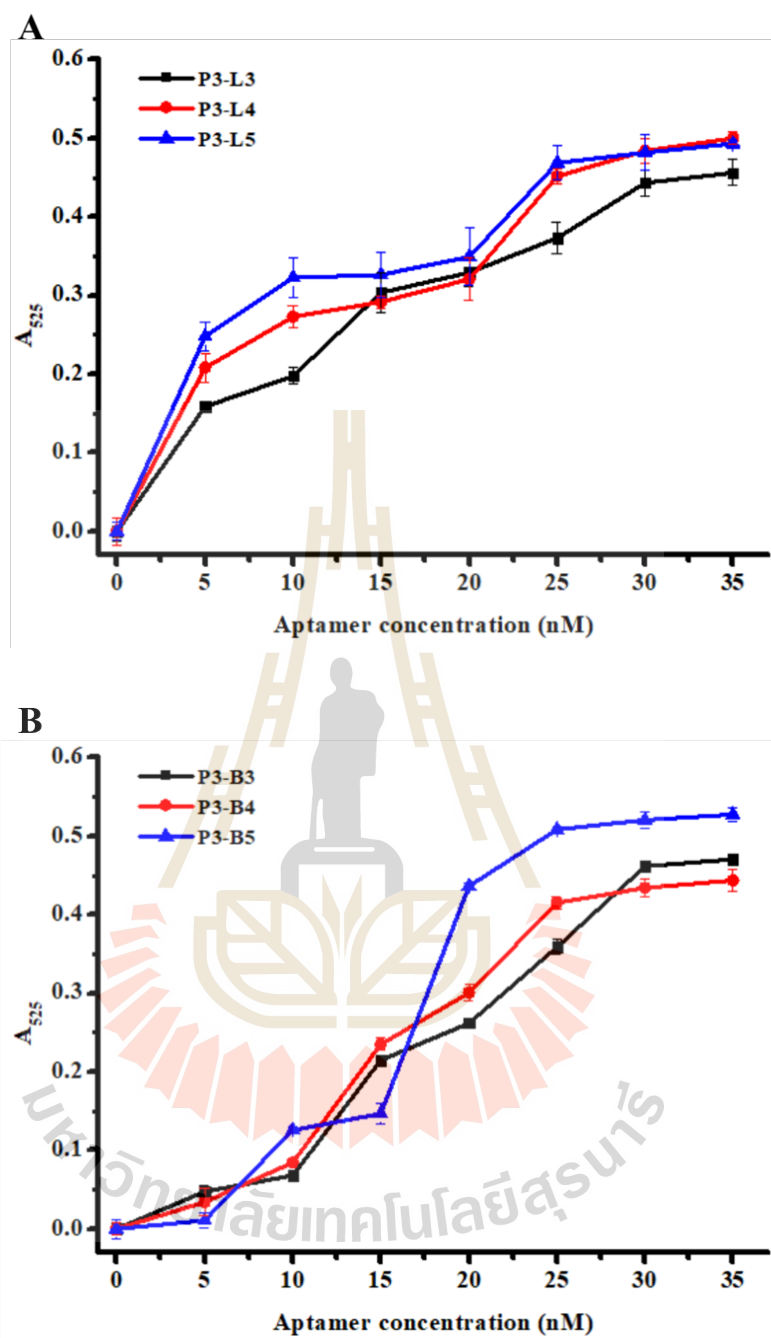


Figure 5.7 Effect of different concentrations of aptamers with linear structure (P3-L3, P3-L4, and P3-L5) (A) and branched structure (P3-B3, P3-B4, and P3-B5) (B) to prevent the NaCl-induced aggregation of AuNPs.

5.3 Sensitivity of the aptamer-AuNP system

Six aptamer-AuNP systems were developed for paraquat detection based on each designed aptamer (P3-L3, P3-L4, P3-L5, P3-B3, P3-B4, and P3-B5). In this system, AuNPs were incubated with each aptamer at the optimized concentration for 30 min before incubating with paraquat. After the additional incubation of 30 min, 35 mM NaCl was then added with further incubation of 10 min. With paraquat, the color of the system changed from red to blue, which could be determined by the absorbance ratio of 650 nm/525 nm (Figure 5.8).

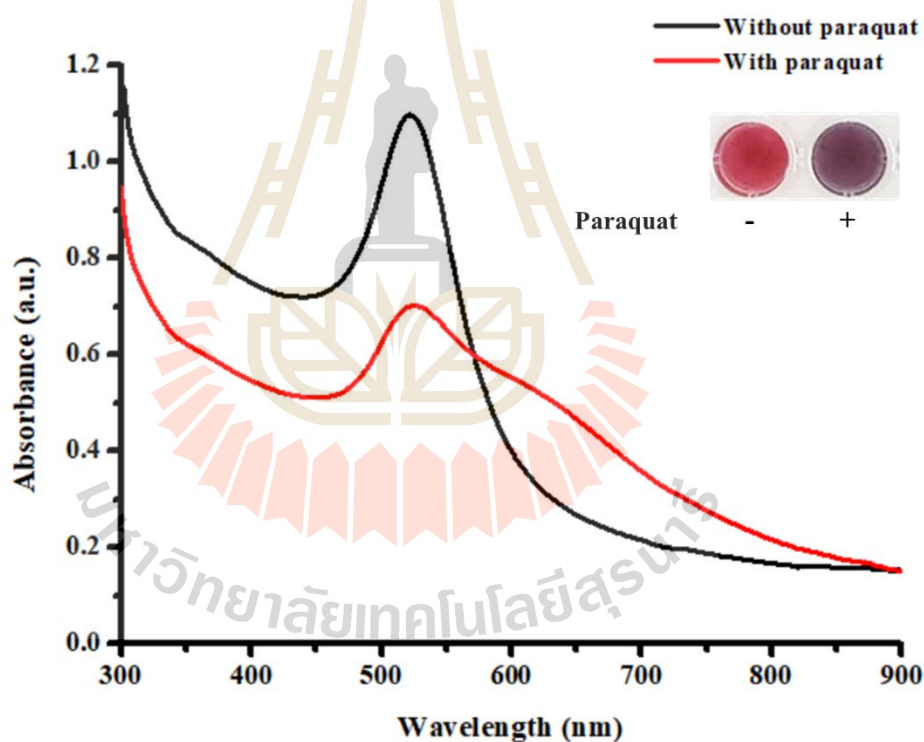


Figure 5.8 UV-Vis-spectra of the developed aptasensor in the conditions with and without paraquat.

5.3.1 Sensitivity of the aptasensors based on linear aptamers

The sensitivity of each aptamer-AuNP system for paraquat detection was

evaluated by using various concentrations of paraquat (0.5–10 nM). In this work, the aptamers with linear structure of 3-5 repeated sequences (P3-L3, P3-L4, and P3-L5) were compared with the aptamers with branched structure of 3-5 repeated sequences (P3-B3, P3-B4, and P3-B5).

The sensitivities of the aptasensors based on linear aptamers (P3-L3, P3-L4, and P3-L5) are shown in Figure 5.9. For the P3-L3 aptasensor (Figure 5.9A), the increasing concentrations of paraquat resulted in the gradually reduced SPR peak intensity at 525 nm, suggesting the reduction of free AuNPs. Also, the peak intensity at 650 nm was appeared, suggesting the induction of aggregated AuNPs. The aggregated AuNPs were caused by the interaction between paraquat and aptamer, resulting in desorption of aptamer from AuNPs' surface. As a result, sodium ions could induce the aggregation of bare AuNPs (Qi et al., 2020). Figure 5.9B demonstrated the fitted linear relationship between the A_{650}/A_{525} values and the paraquat concentrations in a range of 0.5–10 nM with R^2 of 0.95209. The calculated C_{LOD} of the P3-L3 aptasensor system was 0.11 nM. Although the P3-L4 and P3-L5 aptasensor systems contained more repeated structural loops, they did not detect paraquat as well as the P3-L3 aptasensor system. The P3-L4 aptasensor system showed the changes of A_{650} and A_{525} values in the conditions with paraquat (Figure 5.9C). But its calculated C_{LOD} was increased to 0.14 nM (Figure 5.9D). In contrast, with the presence of paraquat, the P3-L5 aptasensor system did not show the clear changes of A_{650} and A_{525} values (Figure 5.9E). As a result, its C_{LOD} value was incalculable (Figure 5.9F).

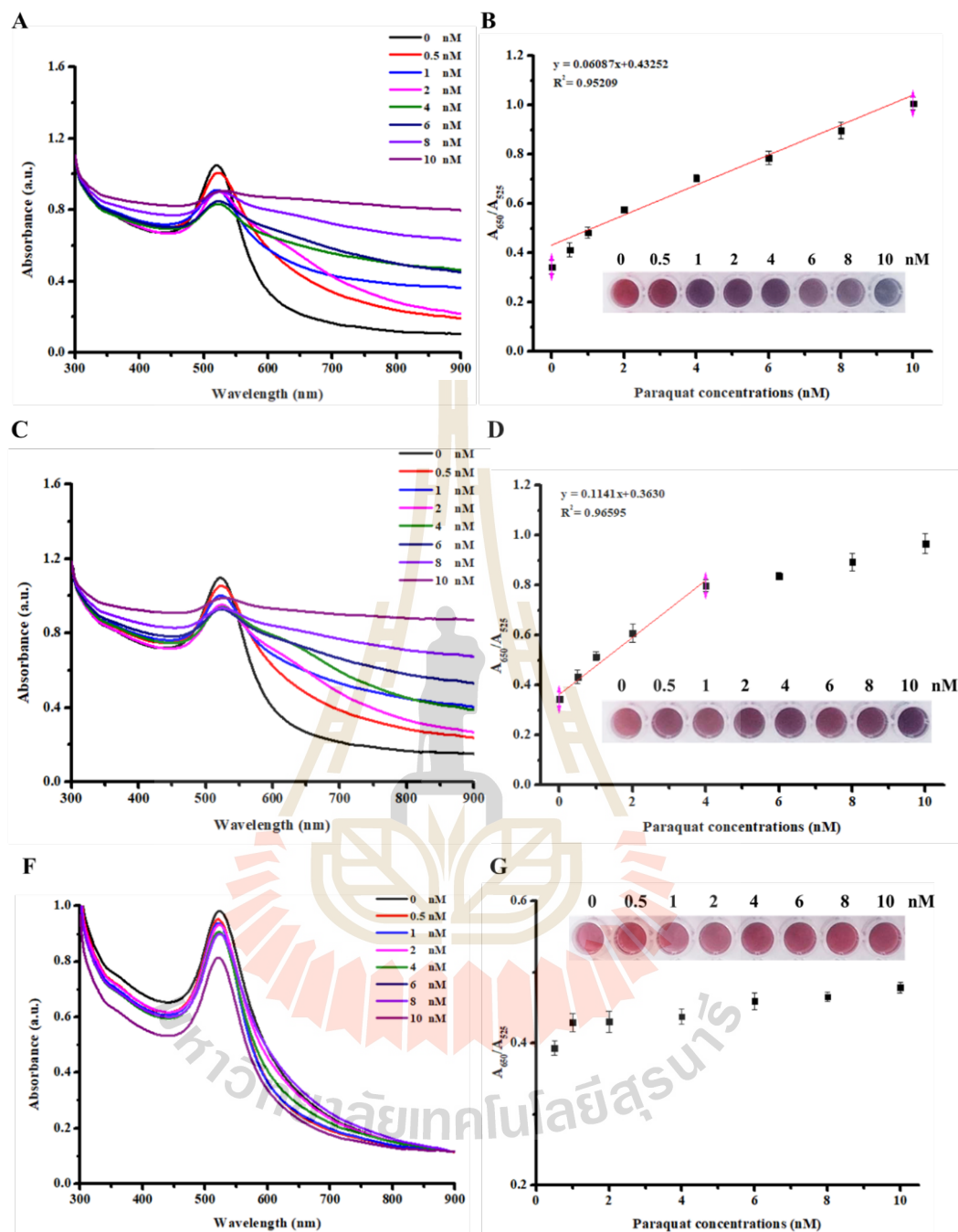


Figure 5.9 UV-Vis spectra of aptasensors based on linear aptamers (P3-L3 (A), P3-L4 (C), and P3-L5 (E)) and their linear relationship plots between A_{650}/A_{525} and paraquat concentration (P3-L3 (B), P3-L4 (D), and P3-L5 (F)).

Based on the principle, the paraquat detection by an aptasensor system is based on the highly selective interaction between DNA-aptamer and paraquat. The DNA-aptamers provided strong noncovalent adsorption to the surface of AuNPs, which maintained the dispersion of AuNPs under the high salt conditions (Lee et al., 2019). With the presence of paraquat, the displacement of aptamer from the surface of AuNPs occurred, which decreased the stability of AuNPs and contributed to aggregate after salt addition. DNA-aptamer would interact with paraquat, leaving the surface of AuNPs unprotected. As the result, NaCl ions interacted with the surface of AuNPs and induced them to aggregate.

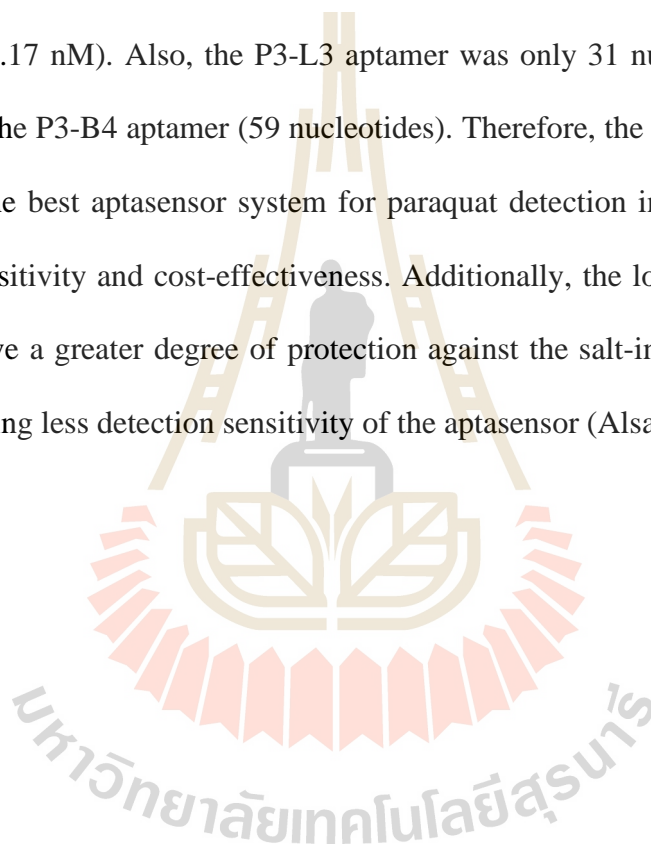
5.3.2 Sensitivity of the aptasensors based on linear aptamers

The aptasensors based on branched aptamers with 3-5 loops were developed and tested for their sensitivities of detection for paraquat. The P3-B3 aptasensor system could detect paraquat as seen from the changes of A_{650} and A_{525} values and their color changes from red to blue (Figure 5.10A). Its C_{LOD} value was 0.22 nM with an R^2 of 0.96241 (Figure 5.10B). Similar results were detected by using the P3-B4 aptasensor system to detect paraquat, but these changes were slightly higher than those by the P3-B3 aptasensor system. Its C_{LOD} value was also decreased to 0.17 nM, suggesting a slightly improved sensitivity of the detection for paraquat (Figure 5.10D). Unlike both systems, the P3-B5 aptasensor system could not detect paraquat in a range of 0.5-10 nM as observed from the reaction colors and absorbance values (Figure 5.10E). Therefore, its C_{LOD} could not be calculated (Figure 5.10F).

It was noted that the C_{LOD} value of each aptasensor system was based on the measured light absorbance at 650 and 525 nm. With naked-eyes, paraquat could be detected at 1 nM, which was higher than the C_{LOD} value. Nevertheless, since the

maximum permissible level of paraquat in the drinking water is at 40 nM in many countries (Nasir et al., 2018), these aptasensor systems are possible to use for paraquat detection with naked eyes, which is useful for developing into the detection system for household applications.

Comparing between the best aptasensors containing linear and branched aptamers, the C_{LOD} of the P3-L3 aptasensor (0.11 nM) was slightly lower than that of the P3-B4 aptasensor (0.17 nM). Also, the P3-L3 aptamer was only 31 nucleotides, which was shorter than the P3-B4 aptamer (59 nucleotides). Therefore, the P3-L3 aptasensor was considered the best aptasensor system for paraquat detection in this work due to its detection sensitivity and cost-effectiveness. Additionally, the longer DNA sequences tended to have a greater degree of protection against the salt-induced aggregation of AuNPs, causing less detection sensitivity of the aptasensor (Alsager et al., 2018).



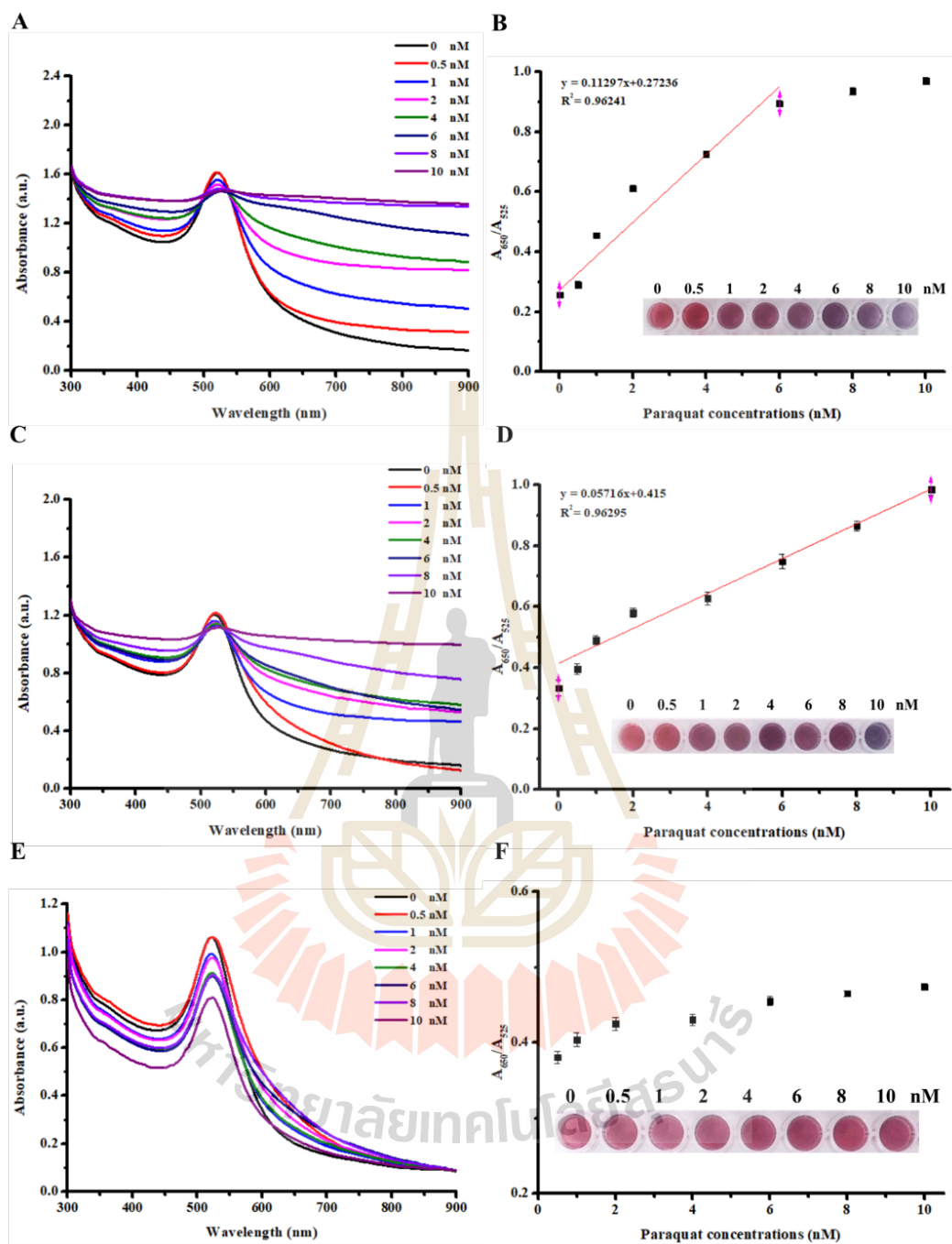


Figure 5.10 UV-Vis spectra in the presence of different paraquat concentrations of the P3-B3 (A), P3-B4 (C), and P3-B5 (E) aptamer-AuNP systems and their linear relationships between the A_{650}/A_{525} values and paraquat concentrations of these systems (B, D, and F, respectively).

5.4 Selectivity of the aptamer-AuNP system

The selectivity of the aptasensor for paraquat is quite important, particularly for environmental applications. As the aptasensor based on P3-L3 linear aptamer and P3-B4 branched aptamer were the most sensitive detection systems for paraquat, they were chosen to study their selectivity for paraquat as compared with other herbicides. In this work, six commonly used herbicides in Thailand were tested; difenzoquat, atrazine, ametryn, 2,4-D dimethyl ammonium, glufosinate, and paraquat. All herbicides were used at the same molar concentration at 40 nM as this concentration was the maximum acceptable concentration (MAC) for paraquat in drinking water (Dong et al., 2018).

The selectivity data of the P3-L3 aptasensor were illustrated in Figure 5.11A. This aptasensor showed strong recognition for paraquat as determined by the highest A_{650}/A_{525} value of 0.46. This aptasensor was slightly cross-interact with difenzoquat, atrazine, ametryn, and 2,4-D dimethyl ammonium, which were A_{650}/A_{525} value 6.36, 6.44, 8.63, and 14.80 folds lower than that for paraquat. Therefore, this aptasensor was still possible to use for paraquat detection with less interference from these commonly used herbicides.

The selectivity data of the P3-B4 aptasensor were illustrated in Figure 5.11B. Similarly, the P3-B4 aptasensor selectively detected paraquat with the highest A_{650}/A_{525} value (0.32). It had low cross-interaction with the other herbicides, which A_{650}/A_{525} values for the difenzoquat, atrazine, ametryn, 2,4-D dimethyl ammonium, and glufosinate were detected, but only 3.19, 3.87, 3.90, 4.88, and 5.67 folds lower than paraquat detection, respectively.

The slight cross-interaction of both aptasensors to other tested herbicides was likely due to their structure and charge. Paraquat is a quaternary ammonium compound with

divalent cations (Pateiro-Moure et al., 2010). Difenzoquat is the monocationic bipyridylium herbicide, which is a close analog to paraquat with a positively charged structure (Zhao et al., 2018). Therefore, this cross-interaction was likely due to the structure and charge of difenzoquat similar to paraquat. Nevertheless, this work demonstrated that both P3-L3 and P3-B4 aptasensors were more selective to paraquat than difenzoquat. Atrazine and ametryn are the triazine herbicides and have positive charges from the presence of amino groups and carbon-nitrogen double bonds in their structures (Qu et al., 2020). Therefore, they exhibited a slight cross-detection by both developed aptasensor systems. Unlike other tested compounds, 2,4-D and glufosinate illustrated the negative charges and different structures from paraquat, resulting in no significant detection by the developed aptasensor systems. Nevertheless, these results suggest the possible applications of the developed aptasensors as they were paraquat-selective and low cross-interaction with other herbicides.

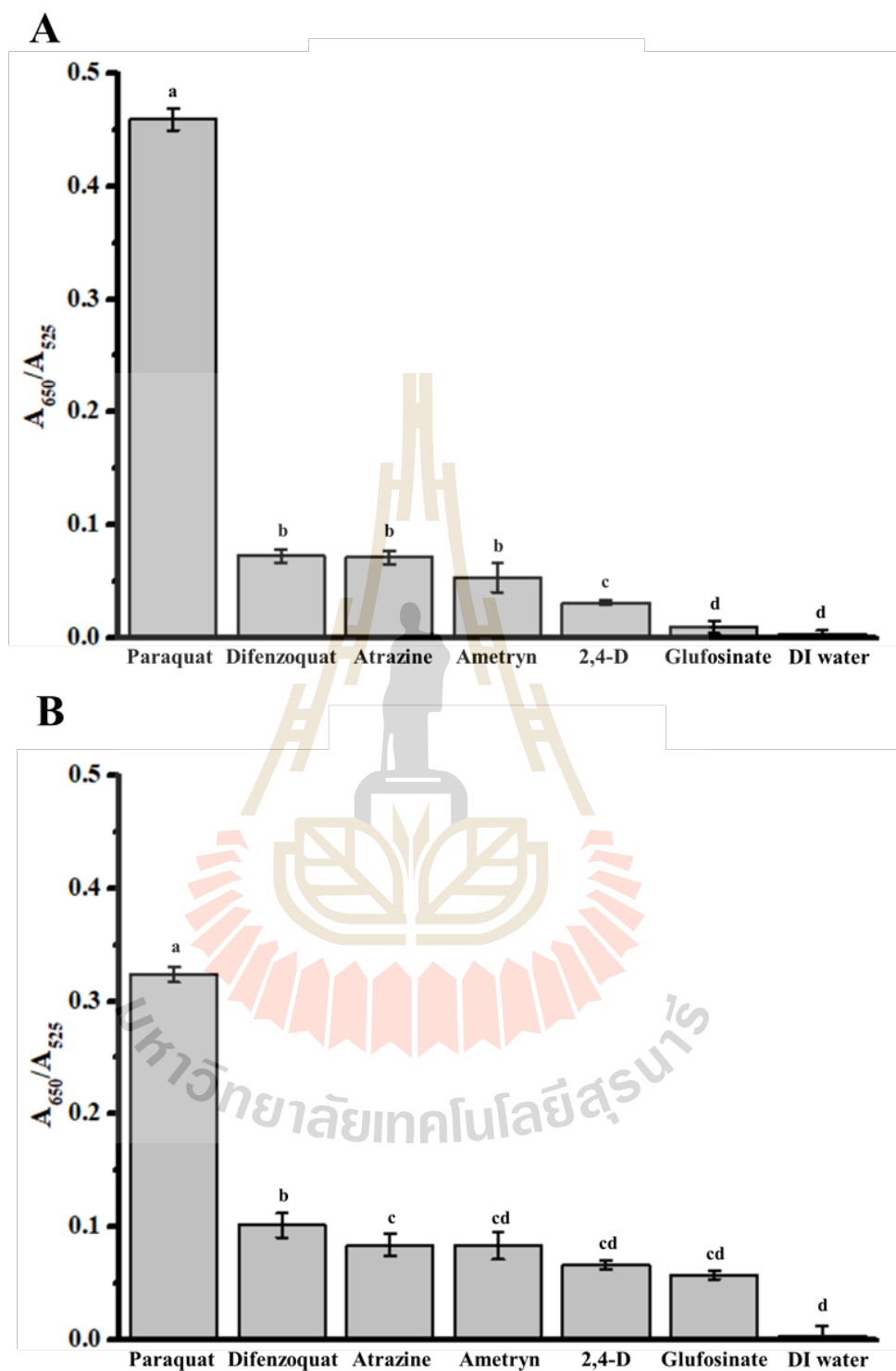


Figure 5.11 Paraquat-selectivity of P3-L3 (A) and P3-B4 aptasensors as compared with other herbicides.

5.5 Detection of paraquat dissolved in pond and tap water by the developed aptasensors

In this work, the detections of paraquat s (5, 10, and 20 nM) dissolved in pond and tap water were evaluated by the developed aptasensors.

The results of paraquat detection by the P3-L3 aptasensor are shown in Table 5.1. The efficiency of the aptasensor for paraquat detection was obtained by comparing the detected paraquat with the accurate value, which was reported as the percent recovery rate. Also, the percent relative standard deviation (%RSD) was calculated to confirm the precision of the assay. The recovery rates of paraquat dissolved in tap water were in a range of 105.4–108.0% and the RSD values were 3.64–4.58%. Similarly, the recovery rates of paraquat dissolved in pond water were 97.0–102.1% and the RSD values were 3.03–4.20%. Generally, the accepted recovery rate and RSD value according to the AOAC official methods of analysis guidelines were 80.0–110.0% and <8%, respectively (AOAC, 2016). Therefore, this aptasensor could be used to detect paraquat in pond and tap water with very low interference from these sources of water.

Another detection system (the P3-B4 aptasensor) showed the recovery of paraquat in the tap water of 101.6–108.5% with the RSD values in the range of 3.64–4.58%. Similarly, the recovery rates of the pond water were 97.9–108.0% with the RSD ranging from 1.45–4.08%, as shown in Table 5.2. Therefore, this aptasensor could also be used to detect paraquat in pond and tap water with very low interference from these sources of water. The results of this work indicated that both aptasensors had relatively stable precision and satisfactory reproducibility, which were practical for paraquat detection in different water resources in the environment.

Table 5.1 Determination of paraquat in spiked water by P3-L3 aptasensor.

Sample	Added (nM)	Found (nM)	Recovery (%)	RSD (%) ⁿ
Tap water	0.5	0.54	108.0	3.68
	2.0	2.16	108.0	4.58
	8.0	8.43	105.4	3.64
Pond water	0.5	0.51	102.0	3.03
	2.0	1.94	97.0	3.10
	8.0	8.17	102.1	4.20

Remark: n=3.

Table 5.2 Determination of paraquat in spiked water by P3-B4 aptasensor.

Sample	Added (nM)	Found (nM)	Recovery (%)	RSD (%) ⁿ
Tap water	0.5	0.53	106.0	3.00
	2.0	2.17	108.5	4.11
	8.0	8.13	101.6	4.55
Pond water	0.5	0.54	108.0	4.08
	2.0	2.08	104.0	3.61
	8.0	7.83	97.9	1.45

Remark: n=3.

CHAPTER VI

CONCLUSIONS

This work reported two optical systems for paraquat detection, based on DNA aptamers and AuNPs. The first system is based on the use of citrate-capped AuNPs as the colorimetric detecting probe for paraquat. In principle, this coloristic system appears in red in a condition without paraquat and changes to a blue color with paraquat. Paraquat can interact with the negatively charged surface of citrated-capped AuNPs, leading to an induced aggregation of AuNPs, thus the system color turns into blue color. This developed system can detect paraquat in a range of 4-160 μM and has a calculated detection sensitivity of 15.32 μM . This detection sensitivity of this system is further improved by an addition of NaCl, in which NaCl causes a neutralization on the surface of AuNPs, thus enhancing the aggregation of AuNPs in the condition with paraquat. The improved system has a lower sensitivity of paraquat detection (1.59 μM), which can increase 10-fold sensitivity. Moreover, the developed system selectively interacts with paraquat, but not with other tested herbicides, commonly used in Asian agriculture. The developed system is applied to detect paraquat in tap water and vegetables, which shows high detection accuracy and reliability.

The second system is developed to improve sensitivity and specificity for paraquat detection, which is based on newly designed DNA aptamers and AuNPs referred to as aptasensors. Aptamers with specific binding to paraquat are designed, among which the P3 aptamer exhibits the highest capability to interact with paraquat. New structural

aptamers are designed, based on multiple repeats of P3 sequences in linear and branched structures. Among the developed aptasensors, the ones with P3-L3 and P3-B4 aptamers exhibit the highest sensitivity of paraquat detection as compared within the same groups of linear and branched structural aptamers, respectively. Under the optimal condition, the P3-L3 aptasensor can detect paraquat in a range of 0.5-10 nM with a limit of detection as low as 0.11 nM. The P3-B4 aptasensor can detect paraquat in a linear range of 0.5-10 nM with a detection limit of 0.17 nM. Furthermore, both aptasensors are selective to paraquat detection. Both aptasensors show high recovery rates of paraquat detection in the paraquat-spiked tap water and pond water in a range of 97.0-108.5% and the RSD values of less than 5%. These recovery rates and RSD values are accepted according to the AOAC official methods of analysis guidelines. Results of these show the success to produce the paraquat detection systems, which have high precision and reliability of detection. They are potentially applied as simple, rapid, and sensitive systems for on-site paraquat detection.



REFERENCES

มหาวิทยาลัยเทคโนโลยีสุรนารี

REFERENCES

- Abraham, K. M., Roueinfar, M., Ponce, A. T., Lussier, M. E., Benson, D. B., and Hong, K. L. (2018). In vitro selection and characterization of a single-stranded DNA aptamer against the herbicide atrazine. **ACS Omega**. 3(10): 13576-13583.
- Aktar, W., Sengupta, D., and Chowdhury, A. (2009). Impact of pesticides use in agriculture: Their benefits and hazards. **Interdiscip Toxicol**. 2(1): 1-12.
- Alsager, O. A., Alotaibi, K. M., Alswieleh, A. M., and Alyamani, B. J. (2018). Colorimetric aptasensor of vitamin D3: A novel approach to eliminate residual adhesion between aptamers and gold nanoparticles. **Sci Rep**. 8(1): 12947.
- AOAC. (2016). Appendix F: Guidelines for standard method performance requirements. **AOAC Official Methods of Analysis**: 1-18.
- Awadalla, E. A. (2012). Efficacy of vitamin C against liver and kidney damage induced by paraquat toxicity. **Exp Toxicol Pathol**. 64(5): 431-434.
- Bai, W., Zhu, C., Liu, J., Yan, M., Yang, S., and Chen, A. (2015). Gold nanoparticle-based colorimetric aptasensor for rapid detection of six organophosphorous pesticides. **Environ Toxicol Chem**. 34(10): 2244-2249.
- Bajgar, J. (2004). Organophosphates/nerve agent poisoning: Mechanism of action, diagnosis, prophylaxis, and treatment. **Adv Clin Chem**. 38(1): 151-216.
- Bala, R., Kumar, M., Bansal, K., Sharma, R. K., and Wangoo, N. (2016). Ultrasensitive aptamer biosensor for malathion detection based on cationic polymer and gold nanoparticles. **Biosens Bioelectron**. 85: 445-449.

- Baltazar, M. T., Dinis-Oliveira, R. J., de Lourdes Bastos, M., Tsatsakis, A. M., Duarte, J. A., and Carvalho, F. (2014). Pesticides exposure as etiological factors of Parkinson's disease and other neurodegenerative diseases—A mechanistic approach. **Toxicol Lett.** 230(2): 85-103.
- Bauer, A., Luetjohann, J., Rohn, S., Kuballa, J., and Jantzen, E. (2018). Development of an LC-MS/MS method for simultaneous determination of the quaternary ammonium herbicides paraquat, diquat, chlormequat, and mepiquat in plant-derived commodities. **Food Anal Method.** 11(8): 2237-2243.
- Bayat, P., Nosrati, R., Alibolandi, M., Rafatpanah, H., Abnous, K., Khedri, M., and Ramezani, M. (2018). SELEX methods on the road to protein targeting with nucleic acid aptamers. **Biochimie.** 154: 132-155.
- Becker, J. O. (2014). Plant health management: Crop protection with nematicides. In: Van Alfen, N. K. (ed.). *Encyclopedia of agriculture and food systems*. Oxford, Academic Press, pp. 400-407
- Bell, C., Price, N., and Chakrabarti, B. (1996). *The methyl bromide issue*. New York, USA, John Wiley and Sons, 1-412.
- Brannen, K. C., Devaud, L. L., Liu, J., and Lauder, J. M. (1998). Prenatal exposure to neurotoxicants dieldrin or lindane alters tert-butylbicyclophosphorothionate binding to GABA_A receptors in fetal rat brainstem. **Dev Neurosci.** 20(1): 34-41.
- Chang, C.-C., Chen, C.-P., Wu, T.-H., Yang, C.-H., Lin, C.-W., and Chen, C.-Y. (2019). Gold nanoparticle-based colorimetric strategies for chemical and biological sensing applications. **Nanomaterials.** 9(6): 861.

- Chen, H., Zhou, K., and Zhao, G. (2018). Gold nanoparticles: From synthesis, properties to their potential application as colorimetric sensors in food safety screening. **Trends Food Sci Technol.** 78: 83-94.
- Chuntib, P., and Jakmune, J. (2015). Simple flow injection colorimetric system for determination of paraquat in natural water. **Talanta.** 144: 432-438.
- Chuntib, P., Themsirimongkon, S., Saipanya, S., and Jakmune, J. (2017). Sequential injection differential pulse voltammetric method based on screen printed carbon electrode modified with carbon nanotube/Nafion for sensitive determination of paraquat. **Talanta.** 170: 1-8.
- Cieplak, M., and Kutner, W. (2016). Artificial biosensors: How can molecular imprinting mimic biorecognition? **Trends Biotechnol.** 34(11): 922-941.
- de Dieu Habimana, J., Ji, J., and Sun, X. (2018). Minireview: Trends in optical-based biosensors for point-of-care bacterial pathogen detection for food safety and clinical diagnostics. **Anal Lett.** 51(18): 2933-2966.
- Ding, Y., Ling, J., Wang, H., Zou, J., Wang, K., Xiao, X., and Yang, M. (2015). Fluorescent detection of Mucin 1 protein based on aptamer functionalized biocompatible carbon dots and graphene oxide. **Anal Methods.** 7(18): 7792-7798.
- Doble, M., and Kumar, A. (2005). CHAPTER 8 - Biodegradation of pesticides. In: Doble, M. and A. Kumar (ed.). Biotreatment of industrial effluents. Burlington, Butterworth-Heinemann, pp. 89-100
- Dominguez-Medina, S., Blankenburg, J., Olson, J., Landes, C. F., and Link, S. (2013). Adsorption of a protein monolayer via hydrophobic interactions prevents

- nanoparticle aggregation under harsh environmental conditions. **ACS Sustain Chem Eng.** 1(7): 833-842.
- Dong, H., Zou, F., Hu, X., Zhu, H., Koh, K., and Chen, H. (2018). Analyte induced AuNPs aggregation enhanced surface plasmon resonance for sensitive detection of paraquat. **Biosens Bioelectron.** 117: 605-612.
- Doyen, M., Bartik, K., and Bruylants, G. (2013). UV-Vis and NMR study of the formation of gold nanoparticles by citrate reduction: Observation of gold-citrate aggregates. **J Colloid Interface Sci.** 399: 1-5.
- Duke, S. O., Lydon, J., Becerril, J. M., Sherman, T. D., Lehnen, L. P., and Matsumoto, H. (1991). Protoporphyrinogen oxidase-inhibiting herbicides. **Weed Sci.** 39(3): 465-473.
- Duke, S. O., and Powles, S. B. (2008). Glyphosate: A once-in-a-century herbicide. **Pest Manag Sci.** 64(4): 319-325.
- Eivazzadeh-Keihan, R., Pashazadeh, P., Hejazi, M., de la Guardia, M., and Mokhtarzadeh, A. (2017). Recent advances in nanomaterial-mediated bio and immune sensors for detection of aflatoxin in food products. **Trends Analyt Chem.** 87: 112-128.
- Ensley, S. M. (2018). Chapter 38 - Organochlorines. Academic Press,
- Fishel, F. M. (2005). Pesticide toxicity profile: Triazole pesticides. **University of florida, ifas extension. PI68.**
- Golichenari, B., Nosrati, R., Farokhi-Fard, A., Abnous, K., Vaziri, F., and Behravan, J. (2018). Nano-biosensing approaches on tuberculosis: Defy of aptamers. **Biosens Bioelectron.** 117: 319-331.

- Grieshaber, D., MacKenzie, R., Vörös, J., and Reimhult, E. (2008). Electrochemical biosensors - sensor principles and architectures. **Sensors (Basel)**. 8(3): 1400-1458.
- Groher, F., and Suess, B. (2016). In vitro selection of antibiotic-binding aptamers. **Methods**. 106: 42-50.
- Grossmann, K. (2010). Auxin herbicides: Current status of mechanism and mode of action. **Pest Manag Sci**. 66(2): 113-120.
- Guo, L., and Zhao, Q. (2016). Thrombin-linked aptamer assay for detection of platelet derived growth factor BB on magnetic beads in a sandwich format. **Talanta**. 158: 159-164.
- Gupta, R. C. (2018). Non-anticoagulant rodenticides. In: **Veterinary Toxicology**. Elsevier, pp. 613-626
- Gupta, R. C., Sachana, M., Mukherjee, I. M., Doss, R. B., Malik, J. K., and Milatovic, D. (2018). Chapter 37 - Organophosphates and carbamates. In: Gupta, R. C. (ed.). **Veterinary toxicology (third edition)**. Academic Press, pp. 495-508
- Hasanzadeh, M., Razmi, N., Mokhtarzadeh, A., Shadjou, N., and Mahboob, S. (2018). Aptamer based assay of plated-derived grow factor in unprocessed human plasma sample and MCF-7 breast cancer cell lysates using gold nanoparticle supported α -cyclodextrin. **Int J Biol Macromol**. 108: 69-80.
- Heggem-Perry, B., McMichael, M., O'Brien, M., and Moran, C. (2016). Intravenous lipid emulsion therapy for bromethalin toxicity in a dog. **J Am Anim Hosp Assoc**. 52(4): 265-268.

- Herrera-Herrera, A., Asensio-Ramos, M., Hernandez-Borges, J., and Rodríguez-Delgado, M. (2016). Pesticides and herbicides: Types, uses, and determination of herbicides. In: *Encyclopedia of food and health*. pp. 326–332
- Hirooka, T., and Ishii, H. (2013). Chemical control of plant diseases. **J Gen Plant Pathol.** 79(6): 390-401.
- Huang, H., Toit, H. d., Besenhard, M. O., Ben-Jaber, S., Dobson, P., Parkin, I., and Gavriilidis, A. (2018). Continuous flow synthesis of ultrasmall gold nanoparticles in a microreactor using trisodium citrate and their SERS performance. **Chem Eng Sci.** 189: 422-430.
- Huang, Y., Shi, T., Luo, X., Xiong, H., Min, F., Chen, Y., Nie, S., and Xie, M. (2019). Determination of multi-pesticide residues in green tea with a modified QuEChERS protocol coupled to HPLC-MS/MS. **Food Chem.** 275: 255-264.
- Huntington, S., Fenik, Y., Vohra, R., and Geller, R. J. (2016). Human bromethalin exposures reported to a US Statewide Poison Control System. **Clin Toxicol.** 54(3): 277-281.
- Isman, M. B., and Akhtar, Y. (2007). Plant natural products as a source for developing environmentally acceptable insecticides. In: *Insecticides design using advanced technologies*. Springer, pp. 235-248
- Jalalian, S. H., Karimabadi, N., Ramezani, M., Abnous, K., and Taghdisi, S. M. (2018). Electrochemical and optical aptamer-based sensors for detection of tetracyclines. **Trends Food Sci Technol.** 73: 45-57.
- Jiang, Y.-B., Zhong, M., and Ma, Y.-Y. (2014). The rapid selecting of precursor ions and product ions of thirty-four kinds of pesticide for content determination by GC–EI/MS/MS. **Food Control.** 43: 110-114.

- Konthonbut, P., Kongtip, P., Nankongnab, N., Tipayamongkholgul, M., Yoosook, W., and Woskie, S. (2018). Paraquat exposure of pregnant women and neonates in agricultural areas in Thailand. **Int J Environ Res Public Health**. 15(6): 1163.
- Laghrib, F., Bakasse, M., Lahrich, S., and El Mhammedi, M. A. (2020). Electrochemical sensors for improved detection of paraquat in food samples: A review. **Mater Sci Eng C**. 107: 110349.
- Lan, L., Yao, Y., Ping, J., and Ying, Y. (2017). Recent progress in nanomaterial-based optical aptamer assay for the detection of food chemical contaminants. **ACS Appl Mater Interfaces**. 9(28): 23287-23301.
- LaRossa, R. A., and Schloss, J. V. (1984). The sulfonylurea herbicide sulfometuron methyl is an extremely potent and selective inhibitor of acetolactate synthase in *Salmonella typhimurium*. **J Biol Chem**. 259(14): 8753-8757.
- Lee, E.-H., Lee, S. K., Kim, M. J., and Lee, S.-W. (2019). Simple and rapid detection of bisphenol A using a gold nanoparticle-based colorimetric aptasensor. **Food Chem**. 287: 205-213.
- Li, H., Chen, D.-X., Sun, Y.-L., Zheng, Y. B., Tan, L.-L., Weiss, P. S., and Yang, Y.-W. (2013). Viologen-mediated assembly of and sensing with carboxylatopillar [5] arene-modified gold nanoparticles. **J Am Chem Soc**. 135(4): 1570-1576.
- Li, Y., Liu, L., Kuang, H., and Xu, C. (2020). Preparing monoclonal antibodies and developing immunochromatographic strips for paraquat determination in water. **Food Chem**. 311: 125897.
- Lin, H.-M., Liu, H.-L., Yang, M.-C., Tsai, T.-H., Chou, C.-C., Chang, C.-F., Chen, H.-M., and Lin, Y.-R. (2010). Clinical features and outcome analysis of patients

- suffer from paraquat intoxication in central Taiwan. **J Emerg Med.** 12(4): 99-106.
- Liu, G., Lu, M., Huang, X., Li, T., and Xu, D. (2018). Application of gold-nanoparticle colorimetric sensing to rapid food safety screening. **Sensors.** 18(12): 4166.
- Liu, G., Zhang, R., Li, L., Huang, X., Li, T., Lu, M., Xu, D., and Wang, J. (2018). Anti-agglomeration behavior and sensing assay of chlorsulfuron based on acetamiprid-gold nanoparticles. **Nanomaterials.** 8(7): 499.
- Liu, M., Khan, A., Wang, Z., Liu, Y., Yang, G., Deng, Y., and He, N. (2019). Aptasensors for pesticide detection. **Biosens Bioelectron.** 130: 174-184.
- Luo, H., Wang, X., Huang, Y., Lai, K., Rasco, B. A., and Fan, Y. (2018). Rapid and sensitive surface-enhanced Raman spectroscopy (SERS) method combined with gold nanoparticles for determination of paraquat in apple juice. **J Sci Food Agric.** 98(10): 3892-3898.
- Maeda, H., and Dudareva, N. (2012). The Shikimate pathway and aromatic amino acid biosynthesis in plants. **Annu Rev Plant Biol.** 63(1): 73-105.
- Malik, J. K., Aggarwal, M., Kalpana, S., and Gupta, R. C. (2017). Chapter 36 - Chlorinated hydrocarbons and pyrethrins/pyrethroids. In: Gupta, R. C. (ed.). Reproductive and developmental toxicology (second edition). Academic Press, pp. 633-655
- Manahan, S. (2017). Environmental chemistry. 10 ed., CRC press, 1-784.
- McFarland, A. D., Haynes, C. L., Mirkin, C. A., Van Duyne, R. P., and Godwin, H. A. (2004). Color my nanoworld. **J Chem Educ.** 81(4): 544.

- McKeague, M., Velu, R., Hill, K., Bardóczy, V., Mészáros, T., and DeRosa, M. (2014). Selection and characterization of a novel DNA aptamer for label-free fluorescence biosensing of ochratoxin A. **Toxins**. 6(8): 2435-2452.
- Medicine, U. N. L. o. (1995). Hazardous substances data bank: US national library of medicine bethesda, MD.
- Mehrotra, P. (2016). Biosensors and their applications—A review. **J Oral Biol Craniofac Res**. 6(2): 153-159.
- Nasir, T., Herzog, G., Hébrant, M., Despas, C., Liu, L., and Walcarius, A. (2018). Mesoporous silica thin films for improved electrochemical detection of paraquat. **ACS Sen**. 3(2): 484-493.
- Nath, N. S., Bhattacharya, I., Tuck, A. G., Schlipalius, D. I., and Ebert, P. R. (2011). Mechanisms of phosphine toxicity. **J Toxicol**. 2011.
- Njoki, P. N., Lim, I.-I. S., Mott, D., Park, H.-Y., Khan, B., Mishra, S., Sujakumar, R., Luo, J., and Zhong, C.-J. (2007). Size correlation of optical and spectroscopic properties for gold nanoparticles. **J Phys Chem C**. 111(40): 14664-14669.
- Nosrati, R., Dehghani, S., Karimi, B., Yousefi, M., Taghdisi, S. M., Abnous, K., Alibolandi, M., and Ramezani, M. (2018). Siderophore-based biosensors and nanosensors; new approach on the development of diagnostic systems. **Biosens Bioelectron**. 117: 1-14.
- Obojska, A., Berlicki, L., Kafarski, P., Lejczak, B., Chicca, M., and Forlani, G. (2004). Herbicidal pyridyl derivatives of aminomethylene-bisphosphonic acid inhibit plant glutamine synthetase. **J Agric Food Chem**. 52(11): 3337-3344.

- Pateiro-Moure, M., Arias-Estévez, M., and Simal-Gándara, J. (2010). Competitive and non-competitive adsorption/desorption of paraquat, diquat and difenzoquat in vineyard-devoted soils. **J Hazard Mater.** 178(1-3): 194-201.
- Paul, I. E., Rajeshwari, A., Prathna, T. C., Raichur, A. M., Chandrasekaran, N., and Mukherjee, A. (2015). Colorimetric detection of melamine based on the size effect of AuNPs. **Anal Methods.** 7(4): 1453-1462.
- Phanchai, W., Srikulwong, U., Chompoosor, A., Sakonsinsiri, C., and Puangmali, T. (2018). Insight into the molecular mechanisms of AuNP-based aptasensor for colorimetric detection: A molecular dynamics approach. **Langmuir.** 34(21): 6161-6169.
- Pohanka, M. (2018). Overview of piezoelectric biosensors, immunosensors and DNA sensors and their applications. **Materials (Basel).** 11(3): 448-461.
- Posecion, N. C., Ostrea, E. M., and Bielawski, D. M. (2008). Quantitative determination of paraquat in meconium by sodium borohydride-nickel chloride chemical reduction and gas chromatography/mass spectrometry (GC/MS). **J Chromatogr B.** 862(1): 93-99.
- Proudfoot, A. T., Bradberry, S. M., and Vale, J. A. (2006). Sodium fluoroacetate poisoning. **Toxicol Rev.** 25(4): 213-219.
- Qi, Y., Chen, Y., Xiu, F.-R., and Hou, J. (2020). An aptamer-based colorimetric sensing of acetamiprid in environmental samples: Convenience, sensitivity and practicability. **Sens Actuators B Chem.** 304: 127359.
- Qi, Y., He, J., Xiu, F.-R., Yu, X., Gao, X., Li, Y., Lu, Y., and Song, Z. (2019). A convenient chemiluminescence detection for bisphenol A in E-waste

dismantling site based on surface charge change of cationic gold nanoparticles.

Microchem J. 147: 789-796.

Qin, G., Gu, H., Ma, L., Peng, Y., Deng, X. W., Chen, Z., and Qu, L.-J. (2007).

Disruption of phytoene desaturase gene results in albino and dwarf phenotypes in *Arabidopsis* by impairing chlorophyll, carotenoid, and gibberellin biosynthesis. **Cell Res.** 17(5): 471-482.

Qu, Y., Qian, H., Mi, Y., He, J., Gao, H., Lu, R., Zhang, S., and Zhou, W. (2020). Rapid

determination of the pesticide ametryn based on a colorimetric aptasensor of gold nanoparticles. **Anal Methods.** 12(14): 1919-1925.

Ran, X. D., and Wu, Y. G. (2019). Screening aptamers and development of colorimetric

detection method of paraquat pesticide. **Chin J Anal Chem.** 47: 567-575.

Rattner, B. A., and Mastrotta, F. N. (2018). Anticoagulant rodenticide toxicity to non-

target wildlife under controlled exposure conditions. In: Anticoagulant rodenticides and wildlife. Springer, pp. 45-86

Ray, D. E., and Fry, J. R. (2006). A reassessment of the neurotoxicity of pyrethroid

insecticides. **Pharmacol Therapeut.** 111(1): 174-193.

Rhinehardt, K. L., Srinivas, G., and Mohan, R. V. (2015). Molecular dynamics

simulation analysis of anti-MUC1 aptamer and mucin 1 peptide binding. **J Phys Chem B.** 119(22): 6571-6583.

Roach, T., and Krieger-Liszkay, A. (2014). Regulation of photosynthetic electron

transport and photoinhibition. **Curr Protein Pept Sci.** 15(4): 351-362.

Rudling, A., Orro, A., and Carlsson, J. (2018). Prediction of ordered water molecules

in protein binding sites from molecular dynamics simulations: The impact of ligand binding on hydration networks. **J Chem Inf Model.** 58(2): 350-361.

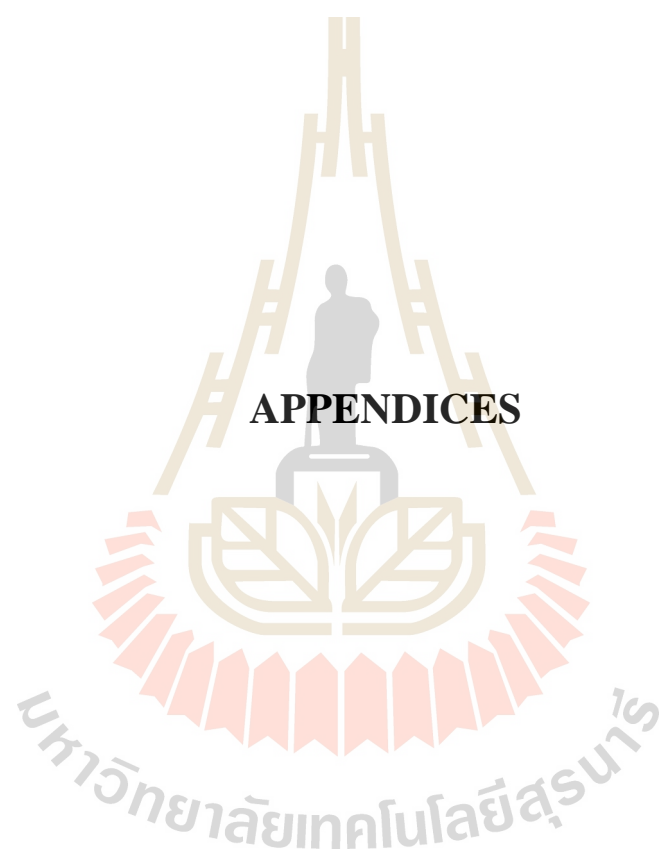
- Samsidar, A., Siddiquee, S., and Shaarani, S. M. (2018). A review of extraction, analytical and advanced methods for determination of pesticides in environment and foodstuffs. **Trends Food Sci Technol.** 71: 188-201.
- Sapbamrer, R. (2018). Pesticide use, poisoning, and knowledge and unsafe occupational practices in Thailand. **New Solut.** 28(2): 283-302.
- Schmid, G. (2008). Clusters and colloids: From theory to applications. John Wiley & Sons, 1-570.
- Shamsipur, M., Yazdanfar, N., and Ghambarian, M. (2016). Combination of solid-phase extraction with dispersive liquid-liquid microextraction followed by GC-MS for determination of pesticide residues from water, milk, honey and fruit juice. **Food Chem.** 204: 289-297.
- Shi, H., Zhao, G., Liu, M., Fan, L., and Cao, T. (2013). Aptamer-based colorimetric sensing of acetamiprid in soil samples: Sensitivity, selectivity and mechanism. **J Hazard Mater.** 260: 754-761.
- Siangproh, W., Somboonsuk, T., Chailapakul, O., and Songsrirote, K. (2017). Novel colorimetric assay for paraquat detection on-silica bead using negatively charged silver nanoparticles. **Talanta.** 174: 448-453.
- Songa, E. A., and Okonkwo, J. O. (2016). Recent approaches to improving selectivity and sensitivity of enzyme-based biosensors for organophosphorus pesticides: A review. **Talanta.** 155: 289-304.
- Spangenberg, B. (2012). Standard addition method for the quantification of paraquat, diquat, difenzoquat, mepiquat, and chloromequat in water by thin-layer chromatography. **JPC-J Planar Chromat.** 25(3): 262-268.

- Sukumar, C. A., Shanbhag, V., and Shastry, A. B. (2019). Paraquat: The poison potion. **Indian J Crit Care Med.** 23(Suppl 4): S263-S266.
- Sun, L., Guan, J., Xu, Q., Yang, X., Wang, J., and Hu, X. (2018). Synthesis and applications of molecularly imprinted polymers modified TiO₂ nanomaterials: A review. **Polymers.** 10(11): 1248.
- Tadeo, J. L. (2008). Analysis of pesticides in food and environmental samples. 1 ed., CRC Press, 1-384.
- Tang, T., Boënne, W., Desmet, N., Seuntjens, P., Bronders, J., and van Griensven, A. (2015). Quantification and characterization of glyphosate use and loss in a residential area. **Sci Total Environ.** 517: 207-214.
- Tcheumi, H. L., Tassontio, V. N., Tonle, I. K., and Ngameni, E. (2019). Surface functionalization of smectite-type clay by facile polymerization of β -cyclodextrin using citric acid cross linker: Application as sensing material for the electrochemical determination of paraquat. **Appl Clay Sci.** 173: 97-106.
- Toomjeen, P., Phanchai, W., Choodet, C., Chompoosor, A., Thanan, R., Sakonsinsiri, C., and Puangmali, T. (2019). Designing an aptasensor based on cysteamine-capped AuNPs for 8-Oxo-dG detection: a molecular dynamics approach and experimental validation. **J Phys Chem B.** 123(5): 1129-1138.
- Trenkamp, S., Martin, W., and Tietjen, K. (2004). Specific and differential inhibition of very-long-chain fatty acid elongases from *Arabidopsis thaliana* by different herbicides. **Proceedings of the National Academy of Sciences of the United States of America.** 101(32): 11903-11908.

- Umamaheswari, C., Lakshmanan, A., and Nagarajan, N. S. (2018). Green synthesis, characterization and catalytic degradation studies of gold nanoparticles against congo red and methyl orange. **J Photoch Photobio B**. 178: 33-39.
- Valchev, I., Binev, R., Yordanova, V., and Nikolov, Y. (2008). Anticoagulant rodenticide intoxication in animals—a review. **Turk J Vet Anim Sci**. 32(4): 237-243.
- Van Gundy, S., and McKenry, M. V. (2012). Action of nematicides. In: *Plant disease: an advanced treatise*. 1 ed., Elsevier, pp. 263-283
- Verma, N., and Bhardwaj, A. (2015). Biosensor technology for pesticides—a review. **Appl Biochem Biotechnol**. 175(6): 3093-3119.
- Vidal, J. M., Plaza-Bolanos, P., Romero-González, R., and Frenich, A. G. (2009). Determination of pesticide transformation products: a review of extraction and detection methods. **J Chromatogr A**. 1216(40): 6767-6788.
- Vigneshvar, S., Sudhakumari, C., Senthilkumaran, B., and Prakash, H. (2016). Recent advances in biosensor technology for potential applications—an overview. **Front Bioeng Biotechnol**. 4: 11-20.
- Wang, F., Lu, Y., Yang, J., Chen, Y., Jing, W., He, L., and Liu, Y. (2017). A smartphone readable colorimetric sensing platform for rapid multiple protein detection. **Analyst**. 142(17): 3177-3182.
- Wang, F., Sun, J., Lu, Y., Zhang, X., Song, P., and Liu, Y. (2018). Dispersion-aggregation-dispersion colorimetric detection for mercury ions based on an assembly of gold nanoparticles and carbon nanodots. **Analyst**. 143(19): 4741-4746.

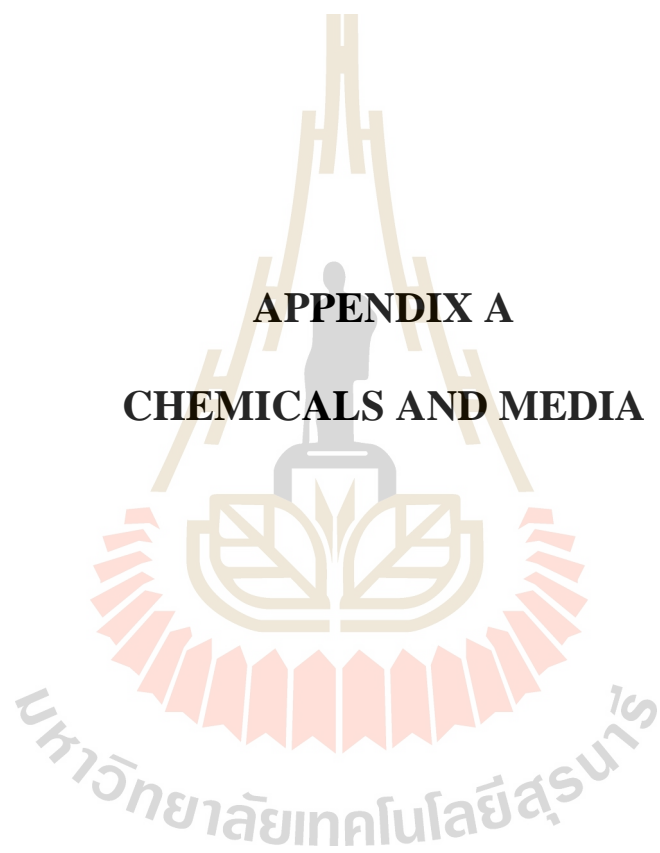
- Wang, P., Wan, Y., Ali, A., Deng, S., Su, Y., Fan, C., and Yang, S. (2016). Aptamer-wrapped gold nanoparticles for the colorimetric detection of omethoate. **Sci China Chem.** 59(2): 237-242.
- Watanabe, E. (2011). The present state and perspective on simple and rapid immunochemical detection for pesticide residues in crops. **JARQ-Jpn Agr Res Q.** 45(4): 359-370.
- Wei, F., Lam, R., Cheng, S., Lu, S., Ho, D., and Li, N. (2010). Rapid detection of melamine in whole milk mediated by unmodified gold nanoparticles. **Appl Phys Lett.** 96(13): 133702.
- Wloga, D., and Gaertig, J. (2010). Post-translational modifications of microtubules. **J Cell Sci.** 123(20): 3447-3455.
- Wright, D. J. (1981). Nematicides: Mode of action and new approaches to chemical control. In: Plant parasitic nematodes. pp. 421-449
- Wu, B., Zou, F., Wang, X., Koh, K., Wang, K., and Chen, H. (2017). The colorimetric assay of diamine oxidase activity with high sensitivity based on calixarene derivative-capped gold nanoparticles. **Anal Methods.** 9(14): 2153-2158.
- Yadav, I., and Devi, N. L. (2017). Pesticides classification and its impact on human and environment. **J Environ Sci Health A Environ Sci Eng.** 6: 140-157.
- Yan, X., Li, H., and Su, X. (2018). Review of optical sensors for pesticides. **Trends Analyt Chem.** 103: 1-20.
- Yang, C., Hamel, C., Vujanovic, V., and Gan, Y. (2011). Fungicide: Modes of action and possible impact on nontarget microorganisms. **ISRN Ecol.** 2011: 1-8.

- Yang, X., Guschina, I. A., Hurst, S., Wood, S., Langford, M., Hawkes, T., and Harwood, J. L. (2010). The action of herbicides on fatty acid biosynthesis and elongation in barley and cucumber. **Pest Manag Sci.** 66(7): 794-800.
- Yoshida, K., Kuroda, D., Kiyoshi, M., Nakakido, M., Nagatoishi, S., Soga, S., Shirai, H., and Tsumoto, K. (2019). Exploring designability of electrostatic complementarity at an antigen-antibody interface directed by mutagenesis, biophysical analysis, and molecular dynamics simulations. **Sci Rep.** 9(1): 4482.
- Zhang, W., Liu, Q., Guo, Z., and Lin, J. (2018). Practical application of aptamer-based biosensors in detection of low molecular weight pollutants in water sources. **Molecules.** 23(2): 1-25.
- Zhao, Z., Zhang, F., and Zhang, Z. (2018). A facile fluorescent “turn-off” method for sensing paraquat based on pyranine-paraquat interaction. **Spectrochim Acta A.** 199: 96-101.
- Zou, L., Shen, R., Ling, L., and Li, G. (2018). Sensitive DNA detection by polymerase chain reaction with gold nanoparticles. **Anal Chim Acta.** 1038: 105-111.
- Zou, T., He, P., Cao, J., and Li, Z. (2014). Determination of paraquat in vegetables using HPLC–MS-MS. **J Chromatogr Sci.** 53(2): 204-209.



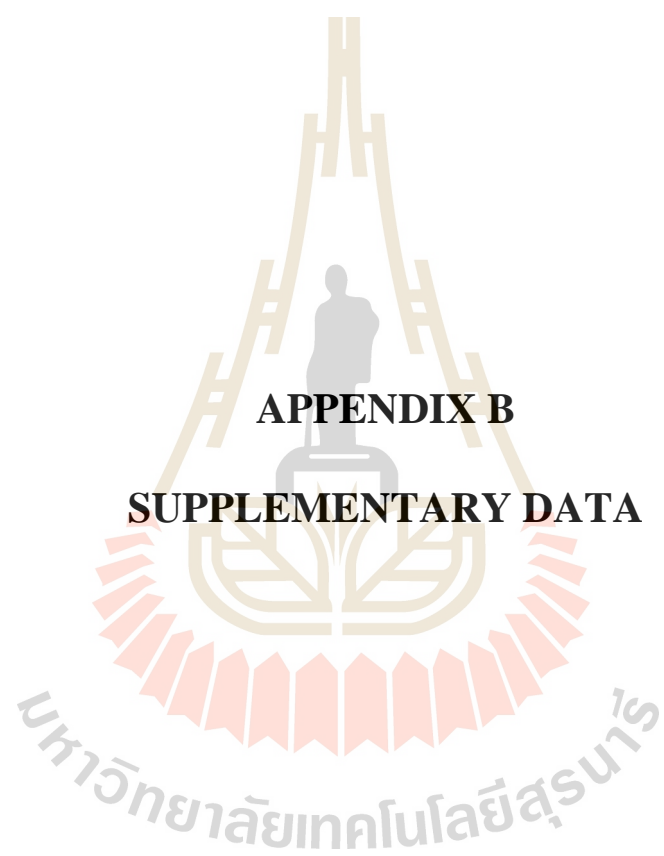
APPENDICES

APPENDIX A
CHEMICALS AND MEDIA



1. General chemicals and materials

Gold (III) chloride trihydrate	Sigma-Aldrich, St. Louis, MO, USA
Trisodium citrate dehydrate	BDH, Poole, England
SYBR Green I	Thermo Fisher Scientific, Waltham, MA, USA
Sodium chloride	BDH, Poole, England
Paraquat dichloride hydrate	Sigma-Aldrich, St. Louis, MO, USA
Difenzoquat	ChemCruz, Dallas, TX, USA
Glufosinate	Bayer Crop Science, Bangkok, Thailand
2,4-D dimethyl ammonium	Thaion Chemical, Bangkok, Thailand
Atrazine	Chiatai, Bangkok, Thailand
Ametryn	Chiatai, Bangkok, Thailand

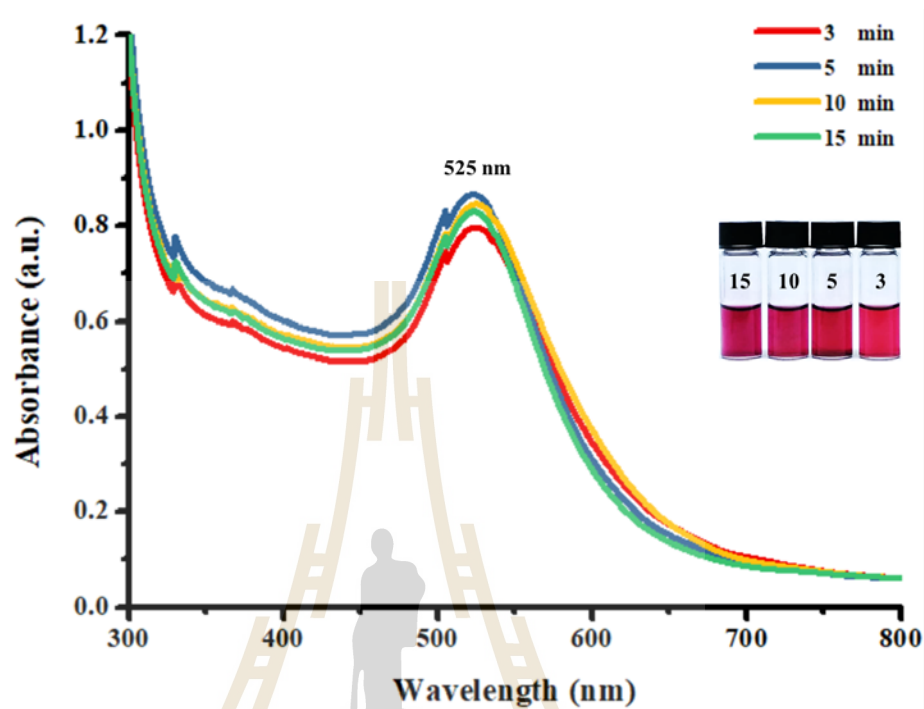


APPENDIX B

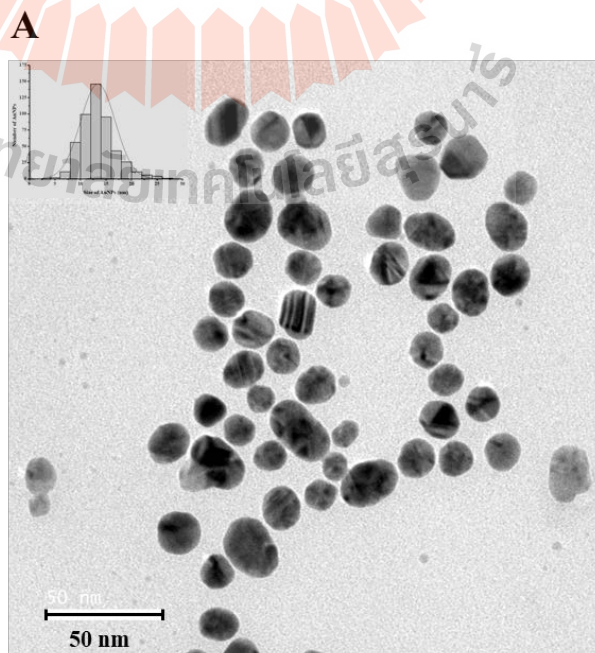
SUPPLEMENTARY DATA

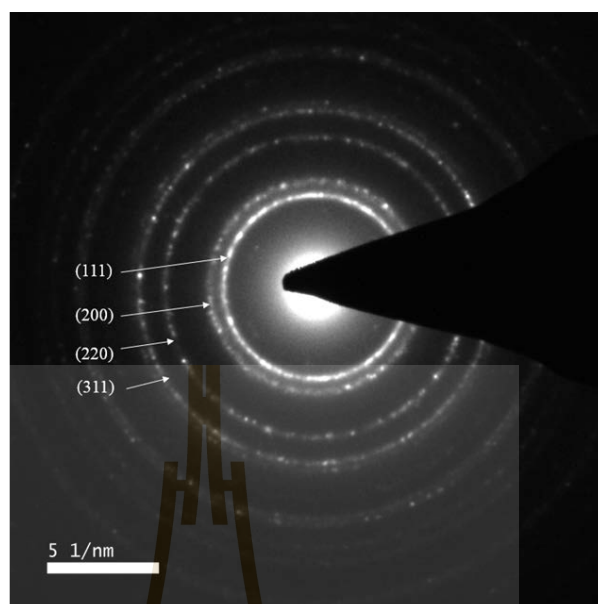
Data of the independently repeated experiments

1. UV-Vis spectra of the formation of AuNPs in a time course of 15 min

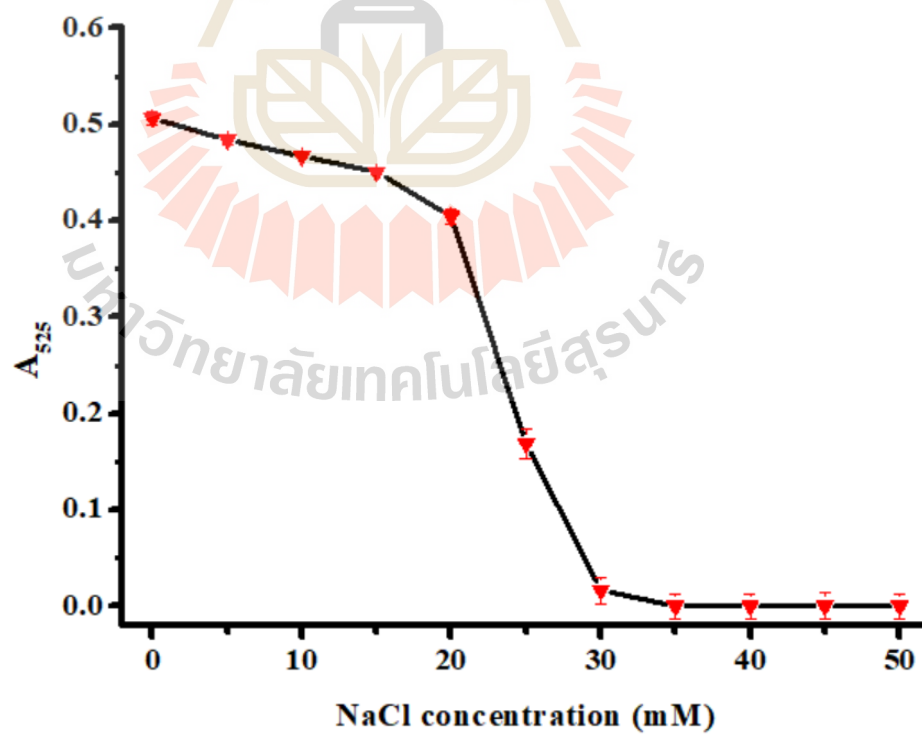


2. TEM image (A) and SAED pattern (B) of the citrate-capped AuNPs.

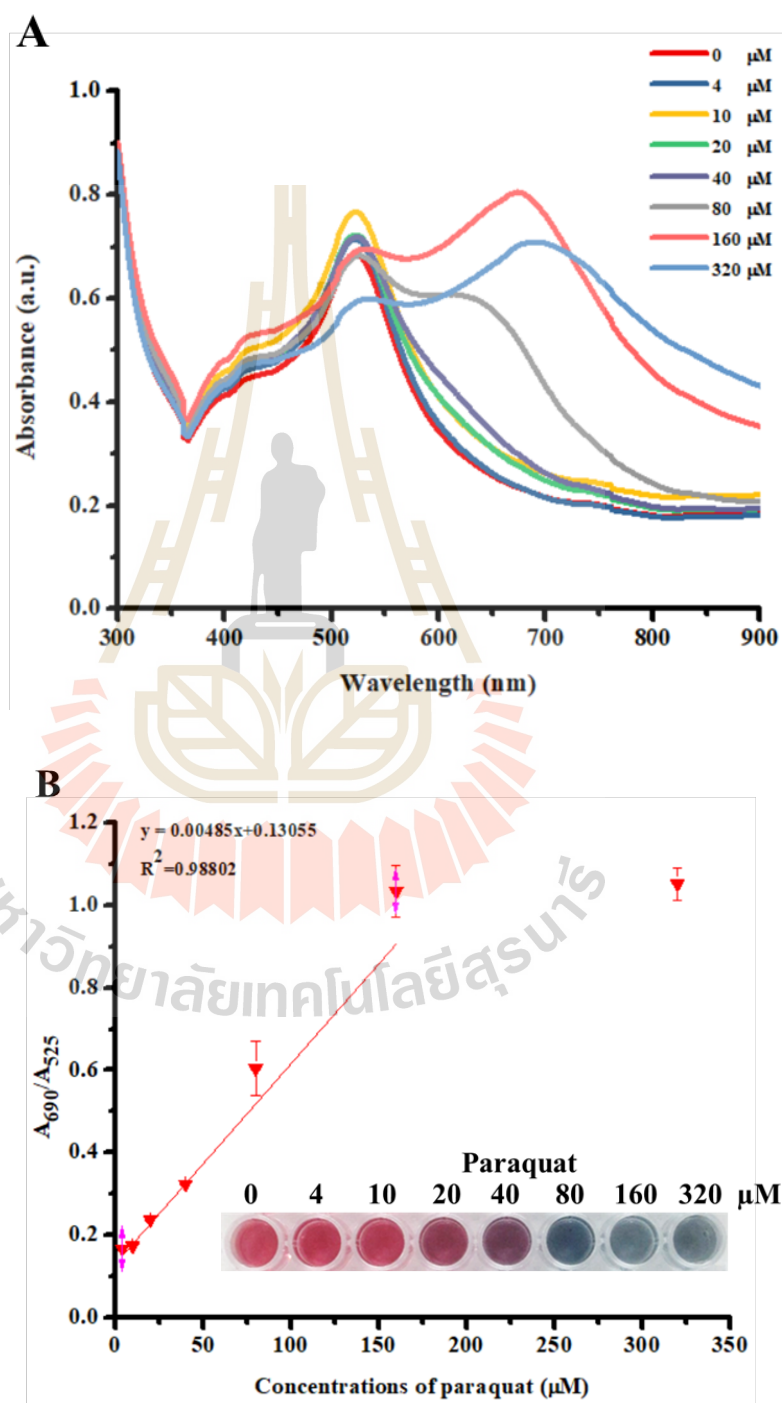


B

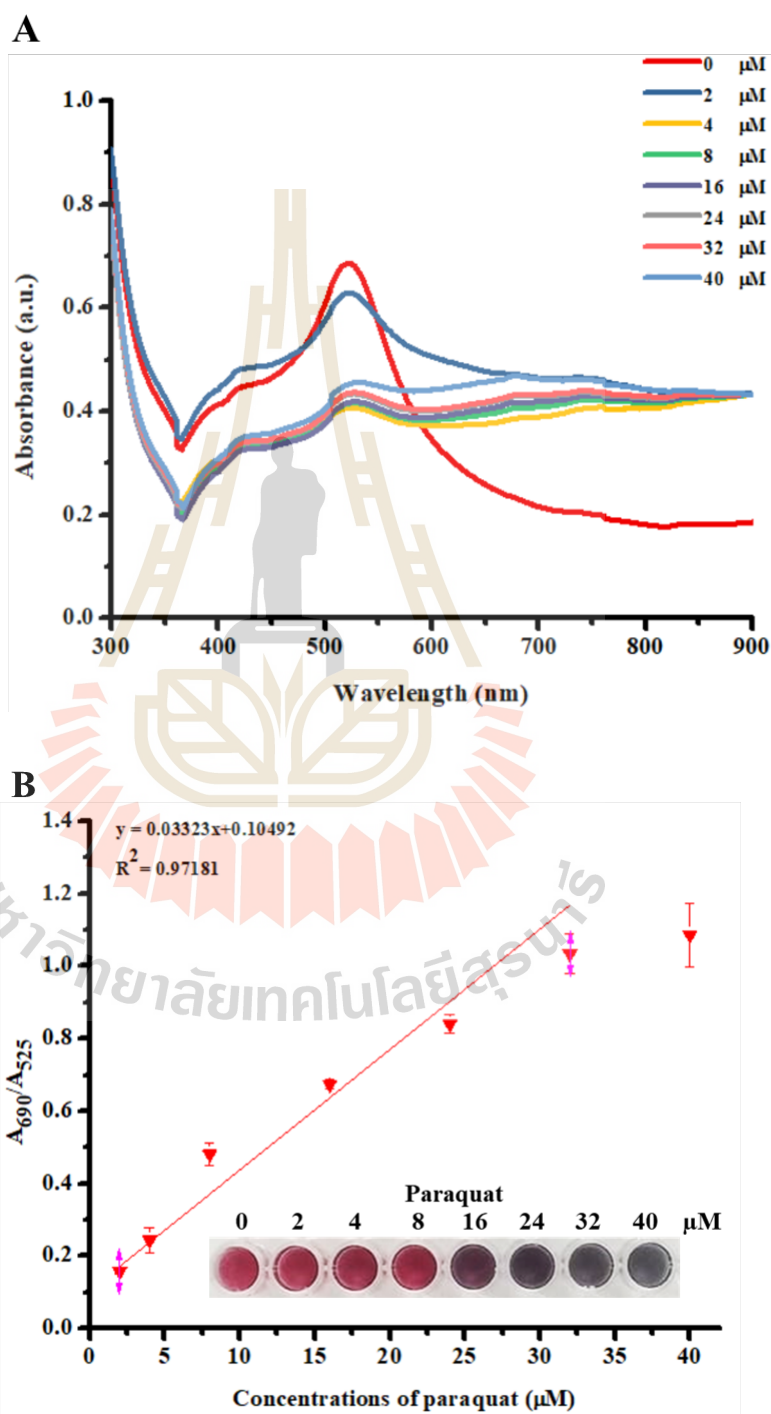
3. Optimal concentration of NaCl for the paraquat detection system



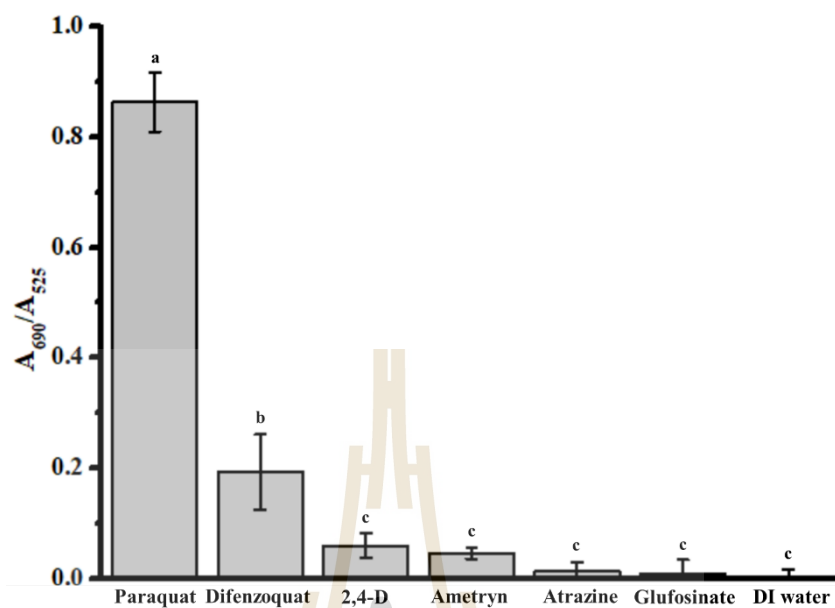
4. UV-Vis spectra of the citrate-capped AuNPs without NaCl in the presence of different concentrations of paraquat (A) and the linear relationship between the A_{690}/A_{525} values and paraquat concentrations (B)



5. UV-Vis spectra of the citrate-capped AuNPs with NaCl in the presence of different concentrations of paraquat (A) and the linear relationship between the A_{690}/A_{525} values and paraquat concentrations (B)



6. The selectivity of the citrate-capped AuNP system for paraquat detection

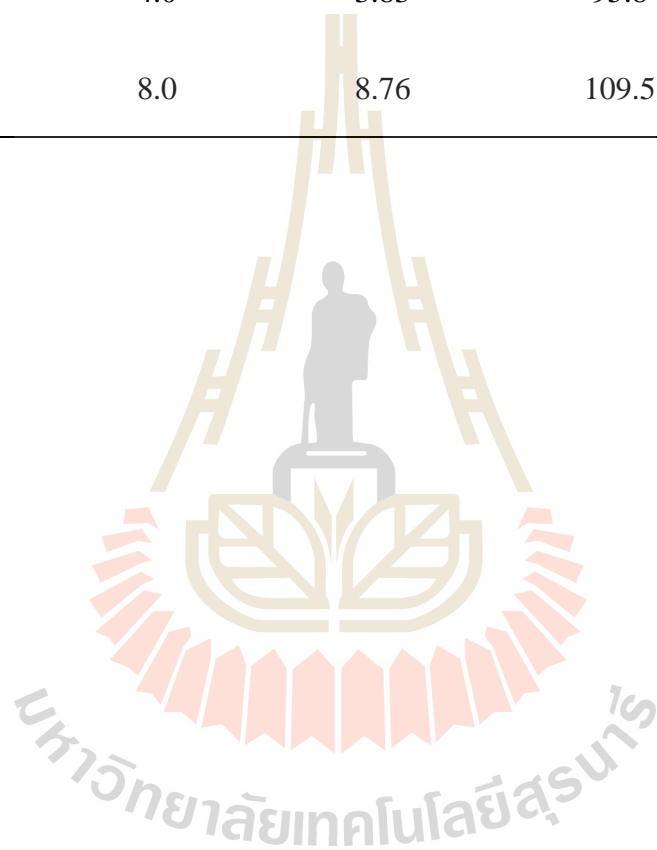


7. Detection of paraquat-spike water using the citrate-capped AuNP system (n=3).

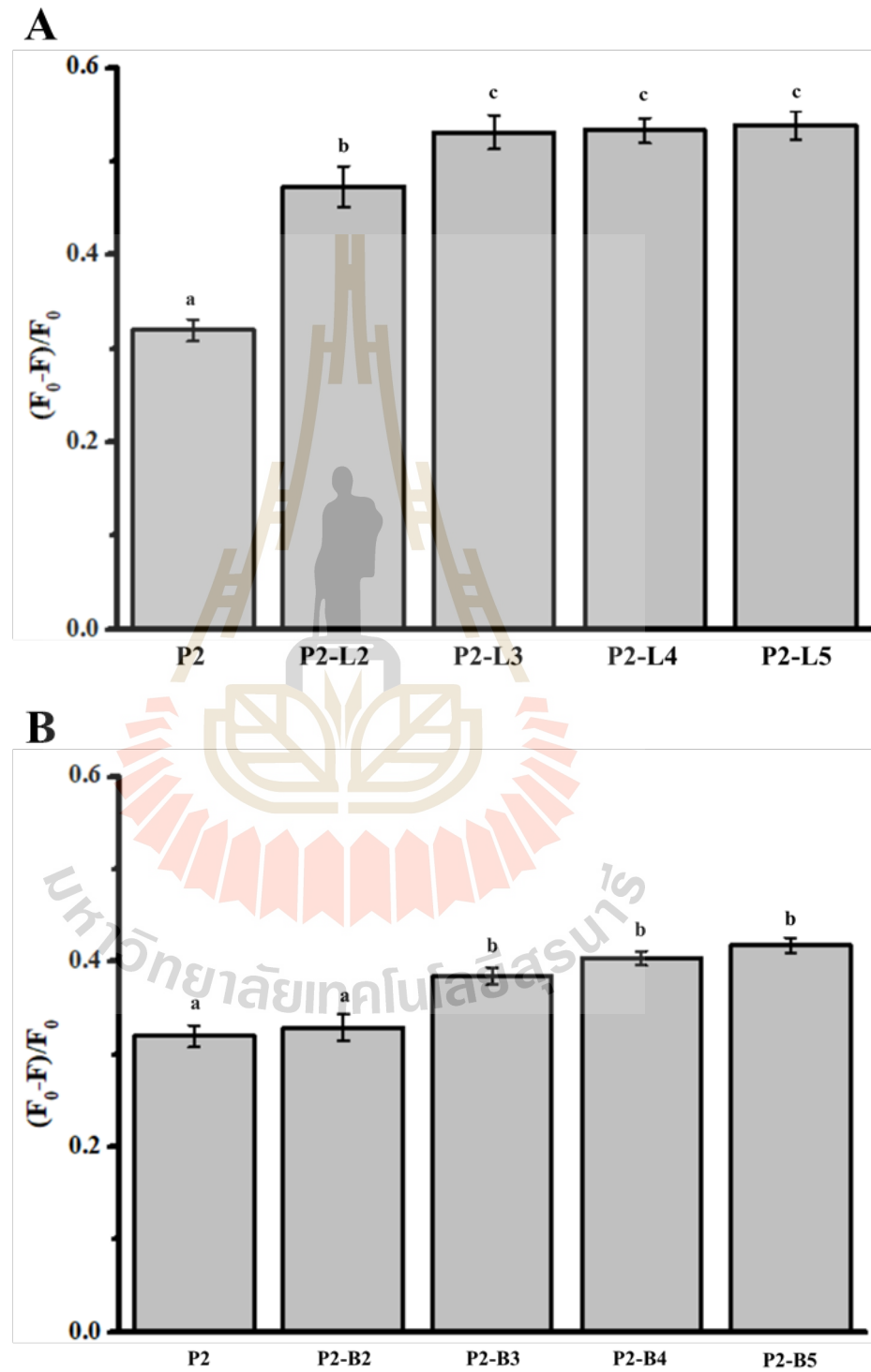
Sample	Added (μM)	Found (μM)	Recovery (%)	RSD (%) ⁿ
Tap water	2.0	2.19	109.5	3.76
	4.0	4.10	102.5	4.01
	8.0	9.16	114.5	4.87
Pond water	2.0	2.16	108	2.88
	4.0	4.09	102.3	3.35
	8.0	7.89	98.6	4.80

8. Detection of paraquat-spike vegetable using the citrate-capped AuNP system (n=3).

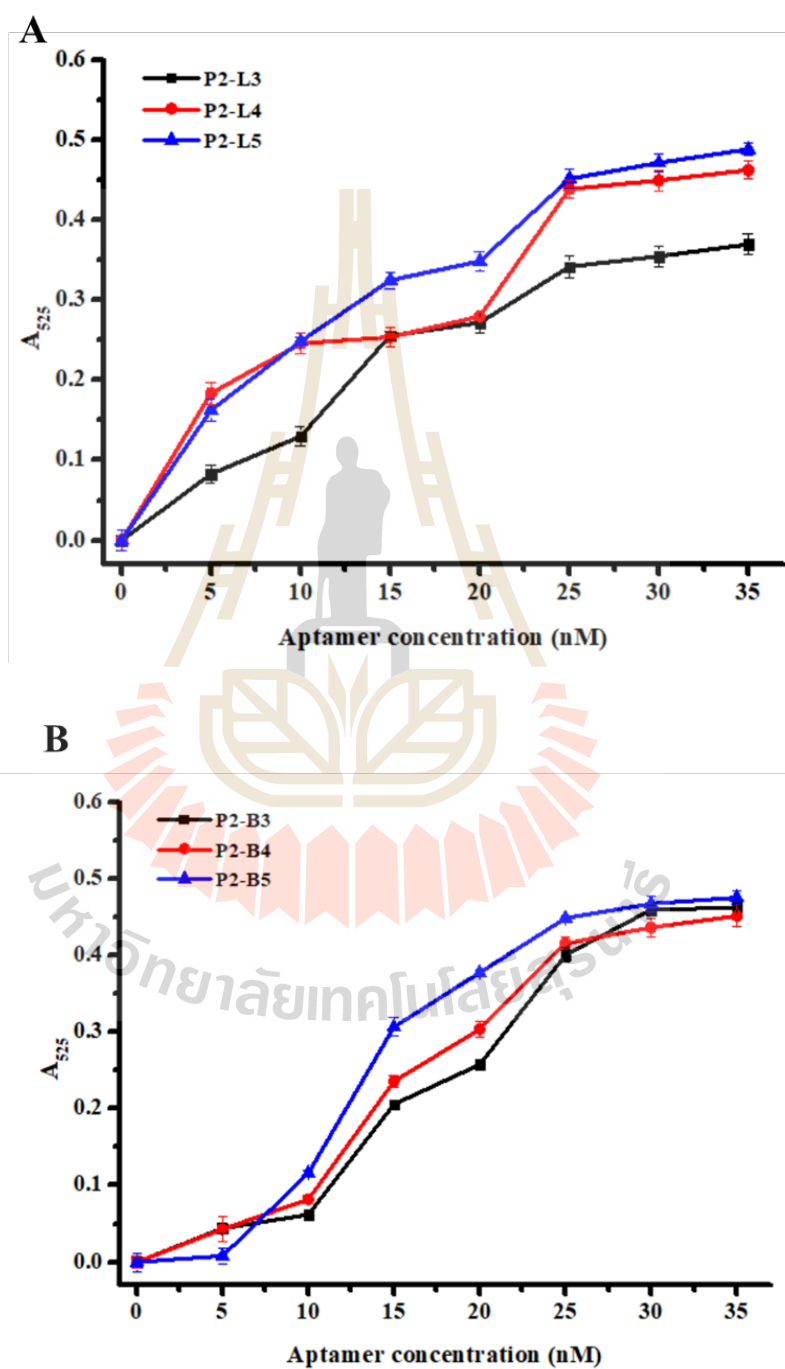
Sample	Added (μM)	Found (μM)	Recovery (%)	RSD (%) ⁿ
Kale	2.0	1.79	89.5	2.79
	4.0	3.83	95.8	1.57
	8.0	8.76	109.5	1.83



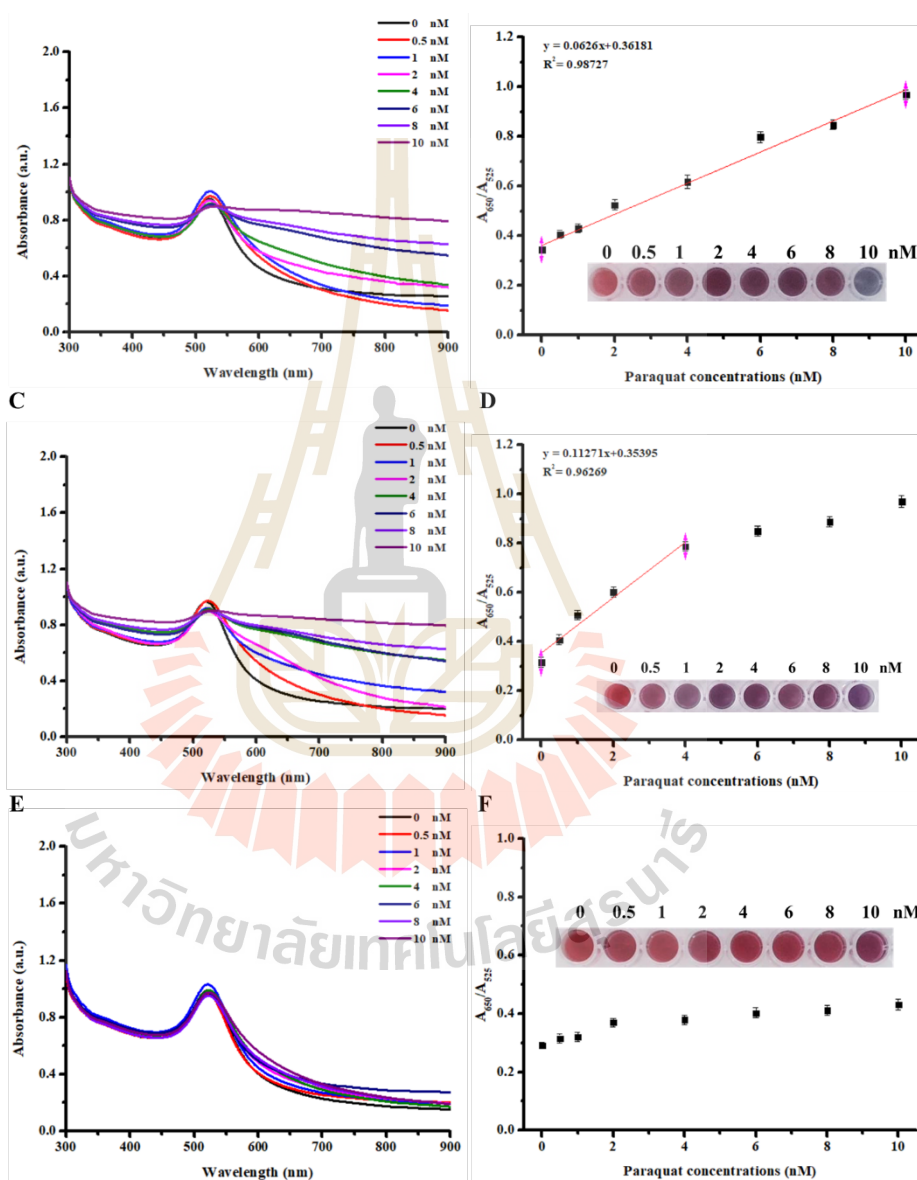
9. The efficiency of the linear form (A) and branched form (B) DNA aptamers evaluated by SYBR Green I competitive assay



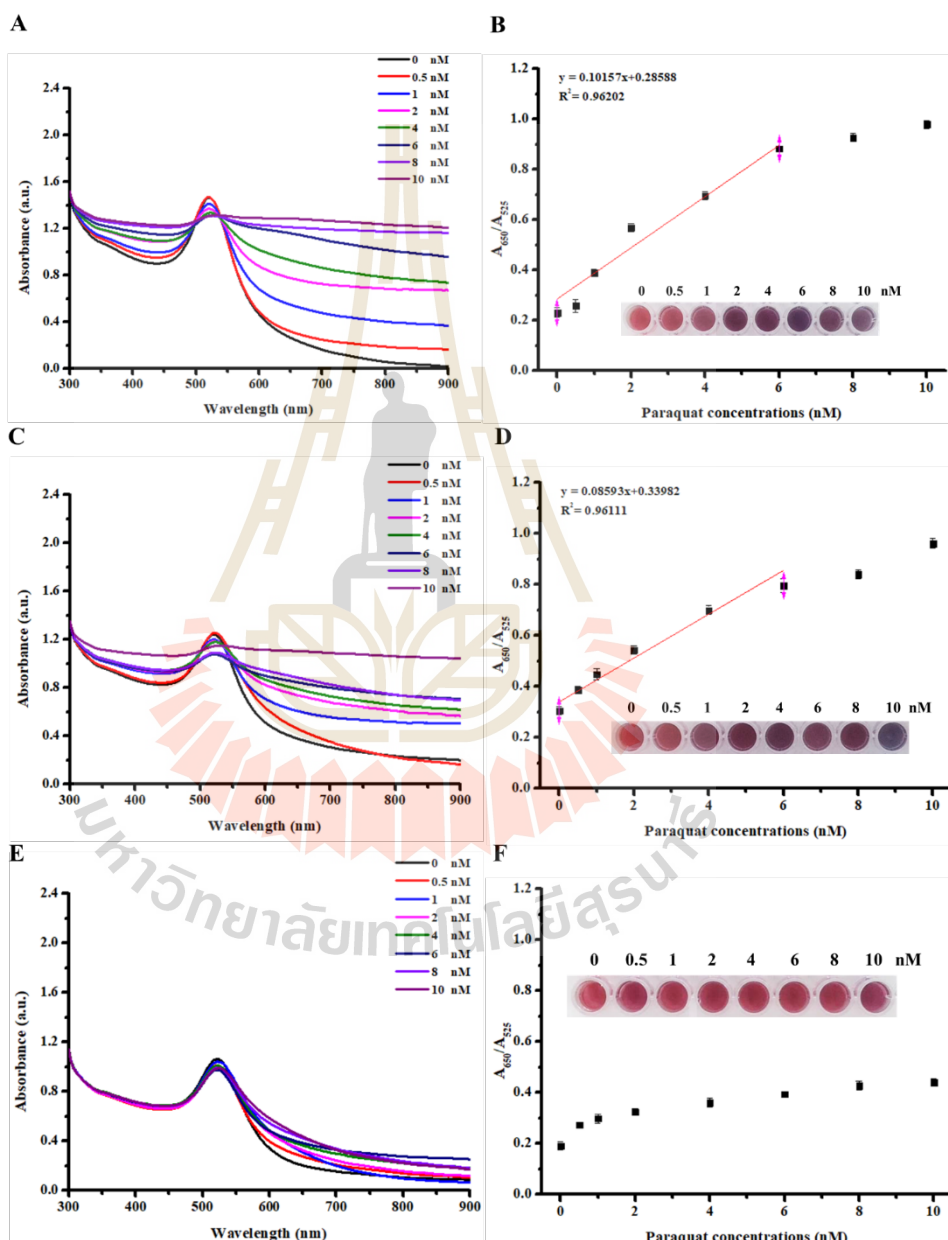
10. Effect of different concentrations of aptamers with linear structure (P3-L3, P3-L4, and P3-L5) (A) and branched structure (P3-B3, P3-B4, and P3-B5) (B) to prevent the NaCl-induced aggregation of AuNPs



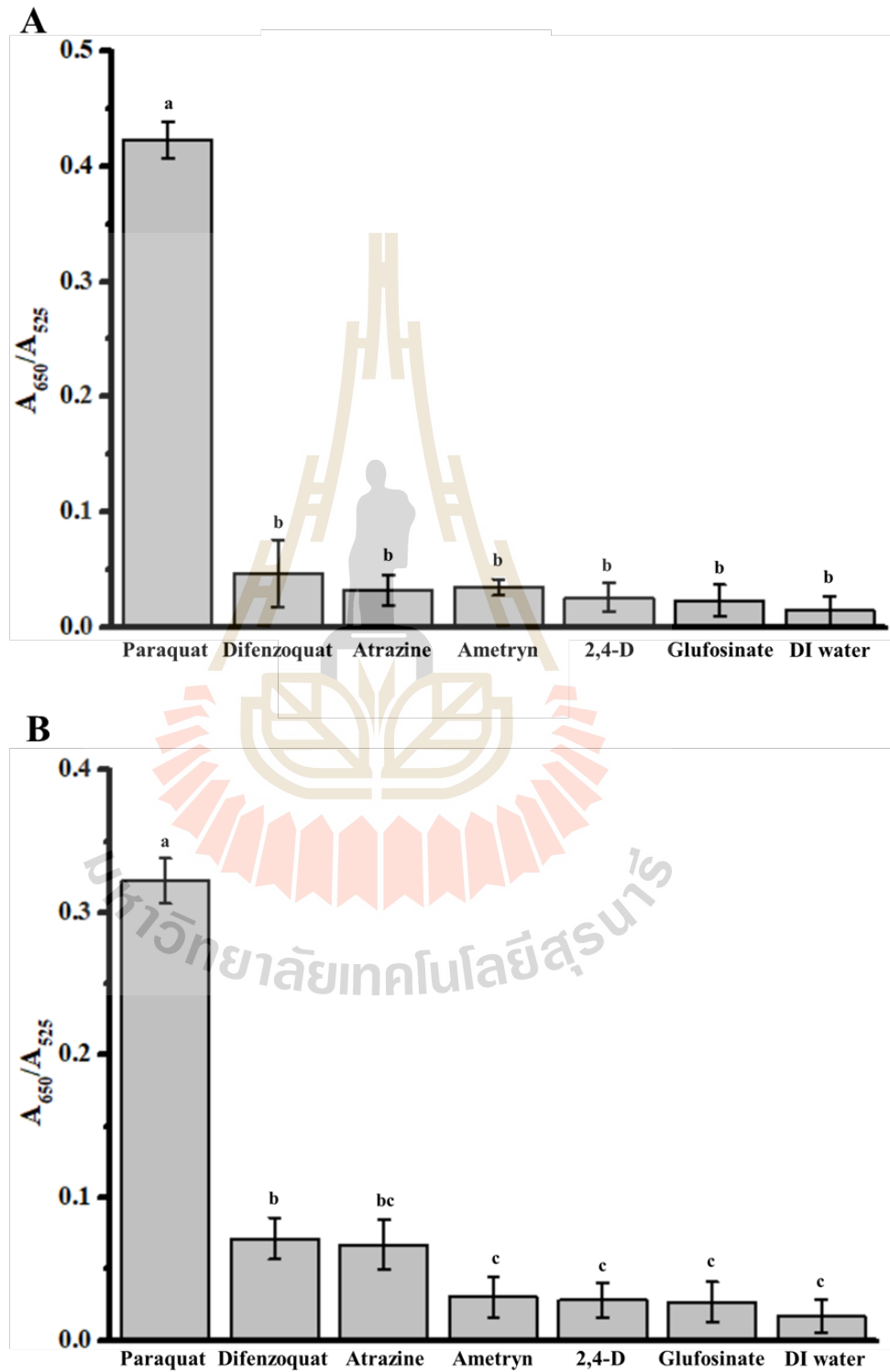
11. UV-Vis spectra of aptasensors based on linear aptamers (P3-L3 (A), P3-L4 (C), and P3-L5 (E)) and their linear relationship plots between A_{650}/A_{525} and paraquat concentration (P3-L3 (B), P3-L4 (D), and P3-L5 (F))



12. UV-Vis spectra in the presence of different paraquat concentrations of the P3-B3 (A), P3-B4 (C), and P3-B5 (E) aptamer-AuNP systems and their linear relationships between the A_{650}/A_{525} values and paraquat concentrations of these systems (B, D, and F, respectively)



13. Paraquat-selectivity of P3-L3 (A) and P3-B4 (B) aptasensors as compared with other herbicides



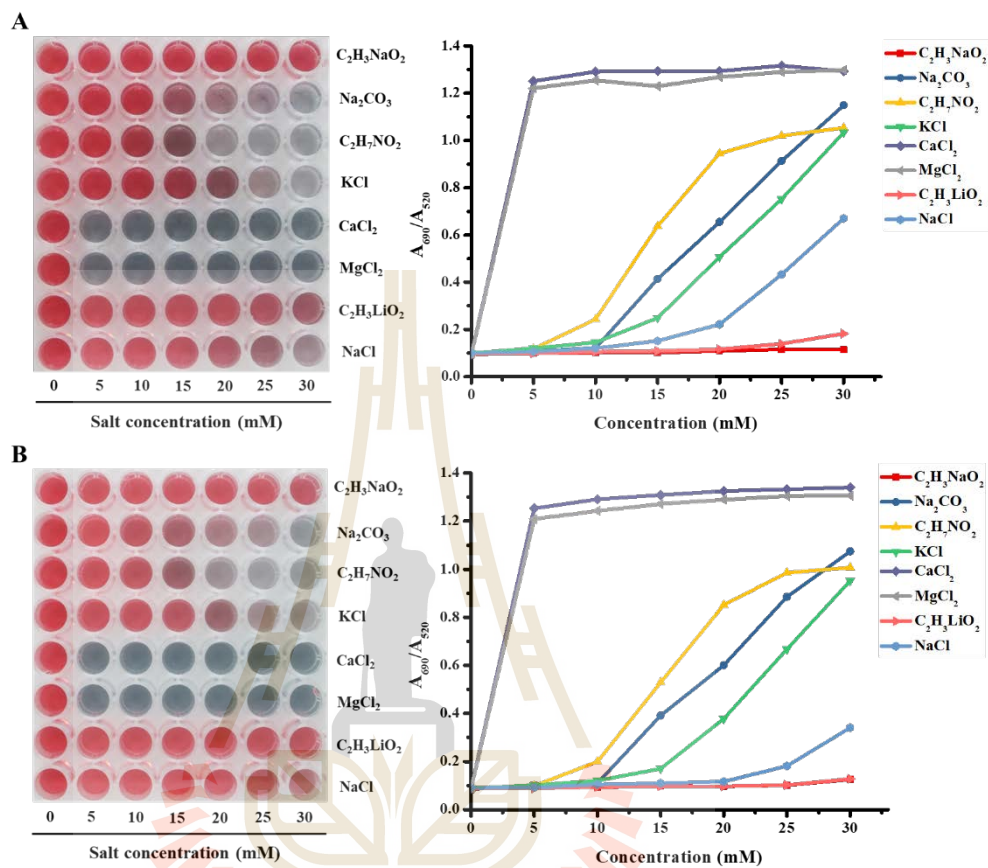
14. Determination of paraquat in spiked water by P2-L3 aptasensor (n=3)

Sample	Added (nM)	Found (nM)	Recovery (%)	RSD (%) ⁿ
Tap water	0.5	0.49	98.81	2.45
	2.0	1.93	96.56	4.76
	8.0	7.90	98.73	2.54
Pond water	0.5	0.53	106.13	4.19
	2.0	2.16	108.10	4.10
	8.0	8.34	104.23	4.21

15. Determination of paraquat in spiked water by P2-B4 aptasensor (n=3)

Sample	Added (nM)	Found (nM)	Recovery (%)	RSD (%) ⁿ
Tap water	0.5	0.51	102.3	4.42
	2.0	2.15	107.7	2.26
	8.0	7.95	99.4	4.81
Pond water	0.5	0.51	101.3	4.98
	2.0	2.13	106.5	4.51
	8.0	8.33	104.1	3.87

16. Effects of monovalent and divalent cations under the conditions with (A) and without (B) paraquat to enhance the sensitivity of detection



CURRICULUM VITAE

1. Personal information

Name: Pakawat Kongpreecha

Date of birth: January 1, 1996

Place of birth: Prachuap Khiri Khan, Thailand

2. Education

2018 – 2020

MSc in Environmental Biology

Suranaree University of Technology, Nakhon Ratchasima, Thailand

2014 – 2017

BSc in Biology (Honors Program, First Class Degree Honor)

Suranaree University of Technology, Nakhon Ratchasima, Thailand

3. Publication

2021. Pakawat Kongpreecha, Sineenat Siri. Simple colorimetric screening of paraquat residue in vegetables evaluated by localized surface plasmon resonance of gold nanoparticles. *Biotechnology and Applied Biochemistry*.

4. Conference Presentations

2019. Kongpreecha P, Siri S. Investigation of the paraquat residues in some vegetables using the developed assay based on gold nanoparticles. International Conference on Materials research and Nanotechnology 10-12 June 2019, Rome, Italy. *Poster Presentation*.

2018. Kongpreecha P, Siri S. Colorimetric detection of paraquat using citrared-capped gold nanoparticles. NanoTech Poland International Conference & Exhibition & 1st Symposium on Polydopamine 6-9 June 2018, Poznan, Poland. *Oral Presentation*.

5. Awards

2018:

The 1st place in SUT Hackathon #5

2017:

The honorable mention award in SUT Stratup Camp #10

6. Grants and Fellowships

2014 - Present

The Development and Promotion of Science and Technology Talented Project (DPST) scholarship.